NASA CONTRACTOR
REPORT

NASA CR-1605

NASA CR-1

C. 1

SPACE GEODESY ALTIMETRY -
PULSE COMPRESSION RADAR STUDY

Prepared by
RAYTHEON COMPANY
Sudbury, Mass.
for

NATIONAL AERONAUTICS AND SPACE ADMINISTRATION • WASHINGTON, D. C. • JULY 1970

NASA CR-1605

SPACE GEODESY ALTIMETRY - PULSE

COMPRESSION RADAR STUDY

Issued by Originator as Report No. R69-4346

Prepared under Contract No. NASw-1709 by
RAYTHEON COMPANY
Sudbury, Mass.

for

NATIONAL AERONAUTICS AND SPACE ADMINISTRATION

EXECUTIVE SUMMARY

The objective of this study is to determine what if any role compression might play in satellite ocean altimetry. This role is found in implementing high accuracy. Accuracy improvement is achieved by increasing the peak RF power delivered by the transmitter. When 10 cm accuracies are sought, the peak power requirements reduce the MTBF of the transmitter tube from 5000 to 500 hours and its DC to RF conversion efficiency from 25% to 2%. Pulse compression provides a method whereby peak power requirements can be reduced by a factor of 100 and the deterioration of efficiency and reliability eliminated. The studies are done by both parametric analysis and specific hardware configuration studies. The one major uncertainty in the design of precision satellite altimeters is a lack of experimental back scatter data at vertical incidence.

Conclusions

a. In calm weather, the short pulse system 10 ns will provide a greater measurement accuracy than a long pulse system 50 to 100 ns, such as configured in SGAS study. Air and space flight test data are required to evaluate how this performance may deteriorate at higher sea states.

b. When the system is designed as a short pulse system to provide the 10 cm system accuracy required for oceanographic geodesy, pulse compression will permit a system to be designed that has substantially improved power efficiency and reliability with less size and weight, than can be attained with a non-pulse compression system.

c. Range sidelobes contribute insignificant error to pulse compression, less than 1 cm error.

d. Systems designed for 3-5 meter accuracy do not require sufficient peak powers to necessitate pulse compression.

Recommendations

a. Pulse compression should be seriously considered for the Sea Sat A program, the final decision pending the evaluation of the results of both the Aircraft Experiment Program and the GEOS C Radar Experiment.

b. The radar altimeter system for the GEOS C satellite should not necessarily be a pulse compression type of radar. Gaining experience with pulse compression by using it in the GEOS C radar altimeter would be desirable. But there may be reasons for transmitting simple, unmodulated pulses in GEOS C that would outweigh the value of the experience gained.

c. Aircraft and Satellite Flight tests be conducted that encompass:
- Specific referencing of pulse shape data to the height above the ocean to an accuracy comparable to that which is sought by the altimeter.
- Evaluation of the capacity of the system to measure sea state as such data may be of inherent value in correcting sea state bias error.
- Evaluation of different possible processors;this involves developing breadboards of different configurations.

d. In support of this flight test program study and hardware development, work is required for:
- dispersive delay line

- pulse processing circuitry
- study of adaptive processor

e. There are key long lead development items that need to be developed and space qualified for this program.   They are:

- Shadow grid TWT
- Solid State RF Source
- Lithium Niobate Dispersive Delay lines

ACKNOWLEDGEMENTS

FOREWORD

This report contains the results of the Space Geodesy Altimetry Study Pulse Compression Modification awarded Raytheon Company under Contract No. NASW-1709 Mod 1 by the Geodetic Satellite Program Office, Office of Space Science and Applications, National Aeronautics and Space Administration. The study was conducted by the Equipment Division of Raytheon Company, under the direction of Mr. Myer Kolker as Program Manager with Dr. Charles J. Mundo, Jr. as Program Scientist.

Successful implementation of this effort was due largely to Mr. Jerome D. Rosenberg, Manager, Geodetic Satellite Programs, NASA, OSSA. Mr. Rosenberg provided the necessary guidance and direction during the study, assisted by Dr. Martin J. Swetnick, Chief Scientist, Geodetic Satellite Programs.

The primary objective of this study was to provide the information for use in evaluating what role pulse compression should play in the geodetic radar satellite altimetry program operating in the 1971-1972 time period over the oceans.

ABSTRACT

A study was conducted to establish the applicability of pulse compression to Satellite Altimetry. Parametric trade offs were made and experimental results presented. The study concludes that if 10 cms measurement accuracy is to be achieved a pulse compression system can achieve it with less size, weight and power than can a system that relies solely on a short pulse for its accuracy.

TABLE OF CONTENTS

TABLE OF CONTENTS (cont'd)

LIST OF ILLUSTRATIONS

LIST OF SYMBOLS

A^2	power attenuation of two-way radar path
BW, B	bandwidth
C	velocity of propagation
C	channel capacity
D	dispersion ratio
E	received pulse energy
F	receiver noise figure
G	antenna gain
L	system losses
N	received noise power $= N_o B$
N_o	white noise spectral density $= kT_e$
N_e	clock count
N(f)	nonwhite noise spectral density
P_{AV}	average power
P_{PK}, P_t	transmitter peak power
S	received signal power $= E/T$
$(S/C)_{d\ell}$	single pulse SCR
$(S/C)_i$	signal-to-clutter (SCR) after integration
$(S/N)_{d\ell}$	single pulse SNR
$(S/N)_i$	SNR after integration
T	temperature
T_e	effective receiver temperature
SCR	signal to clutter power ratio
SNR	signal to noise power ratio

a	measure of pulse duration
f	doppler frequency
f_c	clock frequency
f_r	PRF
h	Boltzmann's constant
k	satellite altitude
n_i	number of pulses integrated
$\hat{t}$	pulse length
v	satellite velocity
x, y, z	Cartesian coordinates
θ	depression angle
θ_e	effective beamwidth
μ	transmitter duty factor
σ^2	a priori range variance
σ_o	ocean cross section at vertical incidence
$\sigma(f)$	target spectrum
σ_{hB}	bias error
σ_{hQ}	quantization error
σ_{hr}	refractivity error
$\sigma(\tau, f)$, $\sigma(\theta, f)$	target scattering function
τ	delay time
ϕ	azimuth angle
td	maximum time between correlated pulses
σ_t	clock error
σ_{hn}	noise error
σ_{hc}	circuiting error

SECTION 1

INTRODUCTION AND SUMMARY

C. J. Mundo

1.1 Brief Statement of the Objectives

The objective of the Space Geodesy Altimetry-Pulse Compression Radar Study is, to provide the information for use in evaluating what role pulse compression should play in the Space Geodesy Altimetry program; and further what steps must be taken if it is desirable to initiate a pulse compression program. Pulse compression is a technique wherein peak power requirements can be reduced without loss of resolution.

In order to accomplish this objective we have pursued the selection of a method of pulse compression which, within the constraints of hardware available by 1972, best meets the altimeter performance goals of the Space Geodesy Program.

A tradeoff comparison is made between the selected pulse compression system and conventional radar approaches to this problem. The reference radar system design for this study is that given in Raytheon's Space Geodesy Altimetry Study Final Report.

This study should not be construed as a pulse compression system design, but rather an evaluation of the impact of pulse compression upon the general question of radar altimeter designs. To draw realistic conclusions, some parts of the system were designed in detail.

This study is a continuation of the Raytheon Space Geodesy Altimetry Study (SGAS) and in many cases draws material directly from that study without the courtesy of quotation in that it is a continuation of that study. The radar that was developed in that system for a comparison with laser altimeters was not an optimized radar altimeter system. In-house studies

and hardware developments, that are in progress at Raytheon, have lead to changes in our concepts about this radar system. Some of which are reflected in this study.

1.1.1 Background

The ultimate goal of the satellite altimetry program is to provide an altimeter that can measure the dynamic topography of the ocean to an accuracy of 10 cms or better. This is a goal that will make this instrument of great value to

> The Geodesist
>
> The Oceanographer
>
> The Solid Earth Scientist

However it appears to be neither necessary in terms of science nor sound in terms of technology development to attain this goal in a single step. Rather it should be achieved in three or more steps each of which will contribute to

- Providing improved measurement data for the scientist to better model the earth.

- Providing a better understanding of the problems that are involved in building an instrument that measures the mean sea level of the ocean.

The rationale for the selection of a particular instrument configuration will vary at each step along the way. Such differences do not constitute inconsistancy but rather represent a carefully developed program.

In the GEOS C phase of the program the primary goals will be:

- The 3-5 meter accuracy required for the geodesist to improve his models of the geoid.

1-2

- Sample radar signal returns from the ocean at satellite altitudes that will enable the system designer to better understand what he can expect to happen to a pulse when it is reflected by the ocean from such altitudes.

The sample radar returns are important for designing later systems, so it is essential that this data be generated as soon as possible if it is to reflect in later phases of the program. It would also be desirable to have this data uncomplicated by the problems of possible interaction between surface effects and the range ambiguity function of the radar pulse. Further it is critical that the GEOS C program be implemented as early as possible and in a manner that will insure a minimum risk in obtaining adequate data and providing the concept.

This study is primarily concerned with radar altimeters for later phases of the program, where the concern is one of achieving the ultimate accuracy.

1.2 Assumptions

The following assumptions served as a basis for this study:

a. Flight capabilities assumed for the approximate time period 1971-1972.

b. Approximate altitude of spacecraft: 500 - 800 nmi.

c. The fundamental mission of Geodesy is to measure mean sea level, not to measure ocean sea state conditions. Although the results of this study may be useful to oceanographic sea state research, the primary purpose of the study concerns the specific area of satellite Geodesy altimetry related to mean sea level or geoid determination.

d. No specific mission was defined; e. g., unmanned and manned

spacecraft could be considered.

e.   The specific geodetic requirements were the same as those which were defined by Raytheon with NASA concurrence in the SGAS study.

f.   Only parameters immediately related to pulse compression and transmitter need to be varied. Such factors as antenna configuration and altitude stabiliation are not necessarily varied in these design studies.

g.   Implied in most studies on radar altimetry is a model about the ocean surface and its statistical distribution about the nadir. The implications of this model are only understood in a very limited sense and need further investigation, particularly with regard to the signal surface interaction. Error analyses, that have been performed here, have many implications pertaining to symmetries (height distribution as a function of range) about this nadir. It might be concluded, therefore, that studies of this type are only useful in a context of evaluating the range measurement capabilities of the system. The model used assumes that a processor can be configured which matches the convolution of the transmitted impulse on the scattering function of ocean surface.

1.3 The Rationale of this Study

The general organization and flow diagram for this study is shown in Figure 1-1. The input to this study is the parent SGAS program. In that program, a set of specifications were developed and a conventional radar altimeter designed to these specifications. Specifications of the parent study provide the design goals for the pulse compression study and the radar design as a basis of comparison against which the pulse compression system can be judged. This study compares possible hardware implementations for pulse compression and selects the most appropriate for the Geodesy altimeter.
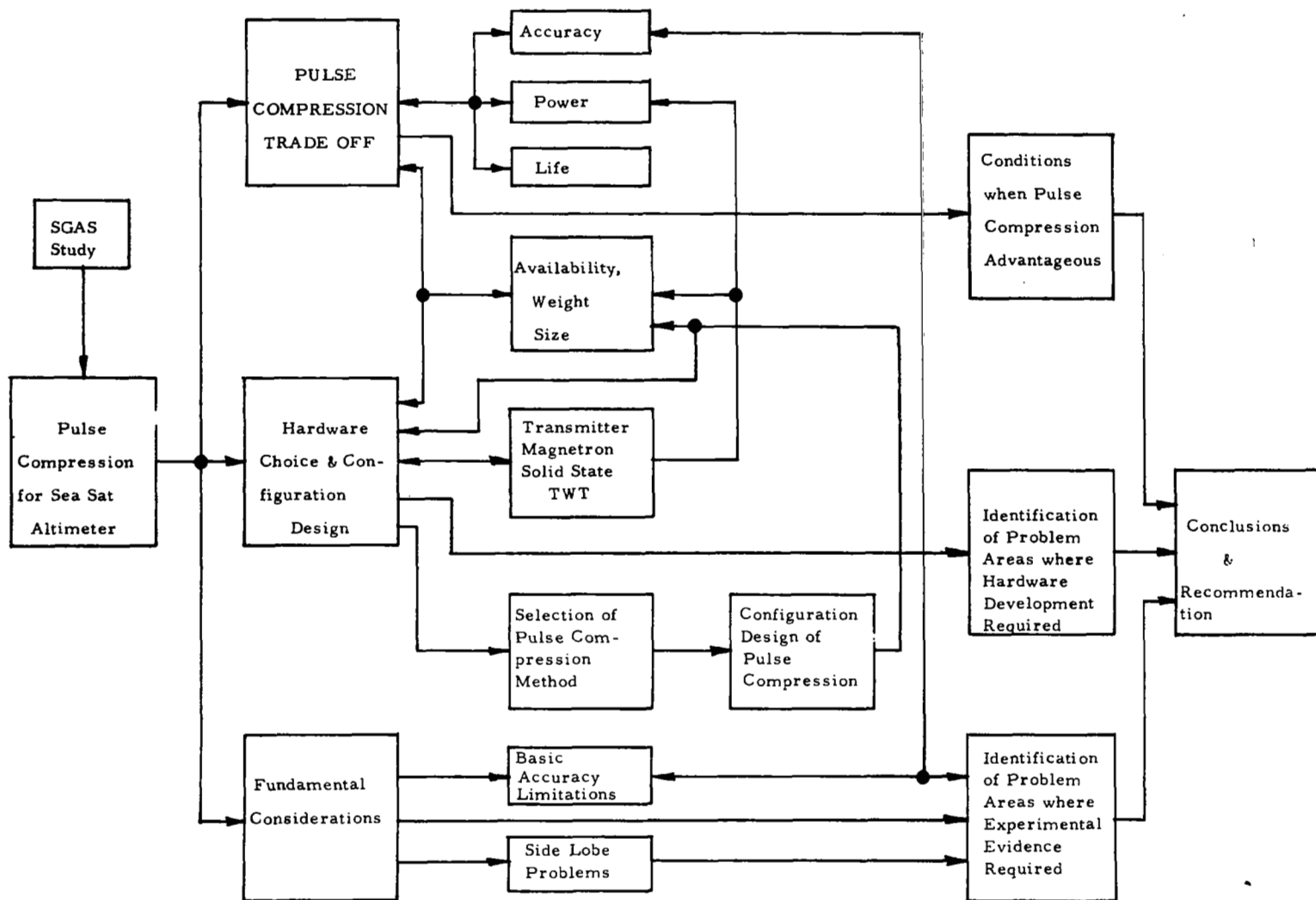
Figure 1-1. Study Flow Diagram

The supporting hardware modification required for pulse compression is examined and a configuration selected for comparison with SGAS radar altimeter.

In parallel with these hardware studies, systems studies trade-off were made to ascertain the variation of performance characteristics that could be expected from pulse compression relative to the conventional systems, with a longer pulse length and a short pulse length. Specific results of these studies are presented in Tables 1-1 and 1-2. These tables show, for the three systems respectively, a comparative description of the hardware characteristics and their expected error performance. The error analysis, indicates there is little difference between the short pulse uncompressed and the short pulse compressed in terms of capability of achieving a given accuracy. The advantage of pulse compression appears only in the hardware implementation of the system.

A trade-off comparison was made between the two systems to establish whether a pulse compression development program is justified.

1. 4 Conclusions

The objective of this study is to establish whether or not pulse compression has a role in satellite altimetry and what that role is. Pulse compression can permit the system designer to attain shorter effective pulse length with less peak power than would be required without pulse compression.

The 10 cm accuracy requirement of the Sea Sat program necessitates an effective pulse length of 10 ns. This effective pulse length can either be achieved directly through a short pulse 10 ns long or through compressing a 1 μs coded pulse to 10 ns. Implementing the direct approach leads to the following problems:

Table 1-1

Candidate Radar Altimeter System Design Specifications

System	SGAS Study	Short Pulse	Pulse Compression
Source Power Required	43 watts dc*	70 watts dc	29 watts dc
Overall System Weight	20 kg (45 lb)	20 kg	18 kg
Overall System Volume	10, 000 cm^3 (. 35 ft^3)	10, 000 cm^3	9, 000
Accuracy	< 50 cm	10 cm	10 cm
Attitude Stabilization Accuracy	± 3°	±0. 3°	±0. 3°
Antenna			
Diameter	. 75 meters (2. 5 ft)		
Thickness	≈ 1 cm		
Aperture Shape	Circular		
Aperture Illumination	Uniform		
Type	Slotted Array	Same	Same
Beamwidth	2. 3° (40 milliradians)		
Gain	38 dB		
Weight	2 kg (est.)		
Antenna Pattern	sin θ/θ		
Sidelobe Level	13 dB		
Transmitter			
Type	Coherent, Gated Amplifier	TWT	TWT
Frequency	X-band	X-band	X-band
Pulse Peak Power	1 kw	100 kw	1 kw
Pulse Length (Transmitted)	50 ns	10 ns	1 μsec
Pulse Length (Compressed)			10 ns
Pulse Rise and Fall Times	10 ns	7 ns	5 ns
Pulse Repetition Frequency	100 KHz (at 1000 km - altitude dependent)	1000 Hz	1000 Hz
Average Power	5 watts	1. 0 watt	1. 0 watt
Conversion Efficiency ***	22%	2 %**	15%
Receiver			
Noise Figure	8 dB (conservatively)	8 dB	8 dB
Bandwidth	20 MHz	100 MHz	100 MHz
Bandpass Characteristic	Synchronous Single Tuned	Hetrodyne	Pulse Compression
Receiver Delay	150 ns	30 ns	5 μsec
Detector	Coherent Synchronous	Square Law	Square Law
Processor			
Type	Two-Stage Delay Differencing		
Processor Delay	75 ns	Same	Same
Output Waveform	Ramp Doublet (ideal)		
Timing Sensor	Pulse-Time Discriminator		
Altitude Tracking Circuit			
Type	Phase (altitude) Locked prf Oscillator		
Tracking Bandwidth	. 157 Hz	Same	Same
Tracking Time Constant	1 second		
Altitude Counting Circuit			
Type	Digital Frequency Meter (prf count)	Coincidence Counter	
Reference Oscillator Stability	10^{-8}	10^{-9}	10^{-9}
Reference Oscillator Frequency	10 MHz	10 MHz	10 MHz
Data Storage	**Remarks**		
Altitude Counts			
Time Signals			
Temperature	(Diagnostics)		
Voltage	(Diagnostics)	Same	Same
Signal Strength	(Sea-State Indication)		
Bias Delay Altitude	(Bias Error Correction)		
Radiometer Signal	(Refractivity Correction)		
Estimated Stored Data Rate	350 Kilobits per hour		

* This result based upon analysis in Section 3. 4 and does not agree with
the overly conservative results in parent study.
** 50 watts to Filament
*** Figure 2-3

Table 1-2

Error Summary

Error Item	SGAS Radar Errors	
	Estimated with Data Corrections	Estimated Error with Either Short or Compressed Pulse System
1. Receiver Noise	.009 m	.01 m
2. Sea Clutter	.04 m	.01 m
3. Sea State	.01 m	.01 m
4. Refractivity	.1 m	.05 m
5. Integration	0	0
6. Bias	.2 m	.05 m
7. Waveform Variations	.1 m	.05 m
8. Amplitude Variation	.05 m	.01 m
9. Digital Counting	.1 m	.05 m
10. Multipath	0	0
11. Range SL	NA	.02 m
12. Altitude Rate	0	.015 m
13. Attitude	0	.02 m
Total (rss)	.26 m	.11 m

- Transmitter efficiency 2%
- Electromagnetic Interference with other satellite equipment
- Transmitter life >500 hrs.

Pulse compression overcomes these difficulties. The detailed trade-off analysis that substantiates these facts are presented in Section 2.

As a result of Section 2, Figure 2-4, it can be concluded there are three classes of errors:

- Pulse length dependent
- Independent of pulse length
- Experimental evidence is required to evaluate.

The errors which depend upon pulse length can be reduced to a point where they are not the limiting factor for achieving 10 cm accuracy by reducing pulse length from 50 ns to a 10 ns pulse. The errors that are independent of pulse length are the limiting lower bound on system performance so that it can be concluded that there is little pressure to pay the price that is required to reduce pulse length beyond the lower limit of 10 ns.

One important caveat must be placed upon these conclusions; that is, there is inadequate evidence as to what effects sea state will have on scattering the pulse energy whose length is comparable to, or shorter than, the wave height. Hence, if we are trying to measure mean sea level when wave height $H_{1/3}$ exceeds 2 meters, experimental evidence is required to predict what is measured by the altimeter. We can thus conclude that:

- In calm weather, the short pulse system 10ns will provide a greater measurement accuracy than a long pulse system 50 to 100 ns, such as configured in SGAS study. Air and space flight test data are required to evaluate how this performance may deteriorate at higher sea states.

The studies in Section 2 and 3 examined the efficiency, reliability and weight implications of pulse compression, and as a result it can be concluded that:

●   When the system is designed as a short pulse system, to provide the
10 cm system accuracy required for the oceanographic geodesy,
pulse compression will permit a system to be designed that has
substantially improved power efficiency and reliability with less size
and weight, than can be attained with a non-pulse compression system.

Range sidelobes have repeatedly been raised as objection to pulse
compression. We have calculated these effects in Appendix H and it can be
concluded that:

●   Range sidelobes contribute less than 1 cm error to pulse compres-
sion.

The question of how general are the conclusions relevant to pulse com-
pression for Satellite Altimetry must be asked. Altimeters require large in-
creases in peak power requirements to achieve the 10 cm accuracies sought.
If lesser accuracies are sought, the peak power drops. As a result one should
expect the necessity for pulse compression to be reduced. The reduction of
accuracy requirements introduce magnetrons as a plausible candidate for the
transmitter tube. The trade off in favor of pulse compression disappears
for accuracies of 50 cms or greater. Therefore it can be concluded

●   The GEOS C 3 to 5 meter accuracy requirement does not
favor the use of pulse compression.

This study is based upon a highly idealized model corresponding to
relatively low sea states. The risk that is involved in the precision altimetry
program is sufficiently high that a comprehensive aircraft and satellite flight
test program to confirm this model should be developed. Such a program
is now in progress at NASA's Wallop's Island Facility. This program should
be extended in scope to provide a sound foundation for the Sea Sat precision
satellite altimeter. In particular, the following items should be covered.

- Specific referencing of pulse shape data to the height above the ocean to an accuracy comparable to that which is sought by the altimeter.

- Evaluation of the capacity of the system to measure sea state as such data may be of inherent value in correcting sea state bias error.

- Evaluation of different possible processors;this involves developing breadboards of different configurations.

In support of this flight test program study and hardware development, work is required for:

- dispersive delay line
- pulse processing circuitry.
- study of adaptive processor

The lithium niobate delay line gives chirp pulse compression a material advantage over other short pulse systems. Other dispersive delay lines were considered and found to have sufficiently greater power and weight requirements to move the margin of favorable balance away from pulse compression to a straight short pulse system. It is recommended that a development program be funded for evaluating and space qualifying the lithium niobate surface dispersive delay line that meets the requirements of the Sea Sat pulse compression system. This development program should include the associated pulse compression circuitry.

It should be pointed out that the lithium niobate dispersive delay line is a development that has come into being since the earlier satellite radar altimeter studies were made.

The pulse processor is the key to determining mean sea level within the wave structure; both study and development work is required here.

In addition there are key long lead development items that need to be developed and spaced qualified for the Sea Sat Program per se. They are:

- Shadow grid TWT
- Solid State RF Source
- Lithium Niobate Dispersive Delay lines

The argument for pulse compression is that high accuracy systems must be short pulse systems. The unsuitability of magnetrons and the inefficiency and short life of high power TWT's imply the requirement for a low power TWT, with pulse compression to attain these goals.

We have conducted a market survey of available TWT's and find that there is no proven TWT available on the market that meets the requirements. However, tube manufacturers could easily design a TWT to meet these specifications. We therefore recommend that such an effort, which will take one year, should be initiated immediately to fit into the GEOS-D flight development program.

Solid state devices may possibly replace the TWT at a 1 kw level in the time frame of the Sea Sat program as discussed in Appendix G. If so, they would provide a further weight saving. Progress in the development of solid state technology should be watched to establish a possible role they might have in this program. At this time, these devices are a high risk item, but should the risk become smaller, it is recommended that funds be provided for evaluation and space qualification.

Finally there are two general recommendations that can be made:

- Pulse compression should be seriously considered for the Sea Sat A program, the final decision pending the evaluation of the results of both the Aircraft Experiment Program and the GEOS C Radar experiment.

- The radar altimeter system for the GEOS C satellite should not necessarily be a pulse compression type of radar. Gaining experience with pulse compression by using it in the GEOS C radar altimeter would be desirable. But there may be reasons for transmitting simple, unmodulated pulses in GEOS C that would outweigh the value of the experience gained.

SECTION 2

NOTE: References to Appendices commencing with R refer to Appendices in the Raytheon Space Geodesy Altimetry Study, NASA CR-1298, March 1969

SECTION 2

PULSE COMPRESSION TRADE OFF

C. J. Mundo

2.1 Introduction

In this section, we will establish the operational performance conditions
under which pulse compression can be shown to have advantages over systems
without pulse compression.

Pulse compression is a technique that permits the system designer to
gain the benefits of a short pulse and high peak power with a long pulse at a
lower peak power level. The operational performance parameters that lead to
a choice between different configurations have been developed in Section 5
of the parent SGAS study and are presented in Table 5-3 of that study.

We shall approach this problem by identifying which of the parameters
called out in that study are most sensitive to this decision and analyze these
factors. Subsequently, it will be shown that the other parameters do not upset
this conclusion. The sensitive operational parameters are the accuracy, life
and power requirements of the system. The system accuracy requirement
of 10 cms for the Sea Sat Program necessitates high peak power, short pulses
and freedom from jitter in the transmitted RF pulse. These factors dominate
the selection of a source of radio frequency power and in turn lead to the
criteria for the use of pulse compression.

Identification of the conditions under which pulse compression will be
used centers around the selection of the transmitter. The 40 cm error due to
jitter rules out magnetrons and CFAs. In addition, magnetrons suffer from
a limited life (under 500 hours). Solid state devices are not compatible with
even the compressed pulse power level requirements at this time.

TWT's can meet the 10 cm accuracy requirement in that they are less
susceptible to jitter than magnetrons, and can provide the short pulses and
high peak powers required. However, the TWT's can be shown to operate

more efficiently and for a longer life if they are operated at a higher duty factor than is possible when short high peak power pulses are used. See Figure 2-1. Pulse compression provide this improved duty factor and as a consequence greater efficiency and life when accuracies greater than 50 cms are sought.

The remainder of this section will be devoted to discussing the details of the accuracy, power, and life trade offs and justifying the conclusions that are presented here.

2.2 Decrease in Altimeter Instrument Errors by Shortening the Pulse Length

Our studies indicate that accuracy can be improved, possibly to an accuracy of 0.1 meter with pulse lengths of 10 ns. Improvements beyond this point will be limited by:

- Tropospheric refractivity
- Equipment complexity
- Timing reference base
- Sea State

Figure 2-2 shows the improvement that could accrue from reduced pulse length. The long pulse system represents the performance results that could be expected from the Sea Sat system that was investigated in the Raytheon SGAS study. The short pulse system is the result of modifying the SGAS system to provide short pulses such as pulse compression would. The changes involved are primarily in the receiver and transmitter.

2.2.1 Errors Attributable to Pulse Compression

A comparison of the error allocation in the SGAS system and the short pulse system is shown in Table 2-1 which is derived from Table 4-1 in the SGAS study. Four new errors not present in the SGAS system must be considered if pulse compression is used to achieve the short pulse. They are:
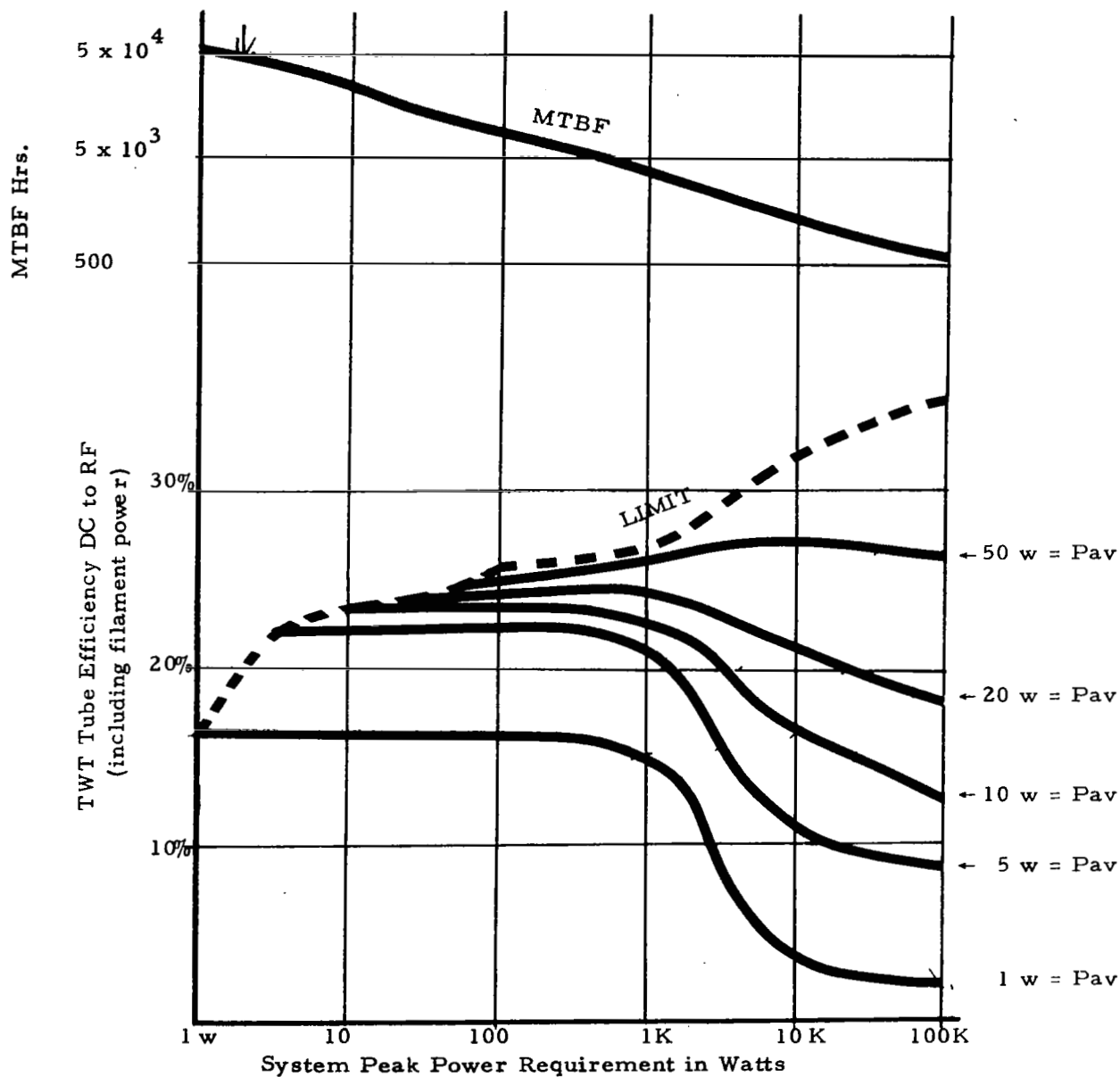
Figure 2-1. TWT Efficiency & Tube Life
for Different Power Levels
(Generated from data provided by Dr. D. Winsor of Raytheon
Power Tube Division)

*Composite of errors
that are linearly de-
pendent on pulse length
6 Bias
7 Wave form variation
8 Amplitude variation

*Composite of errors
that are independent of
pulse length
4 Refractivity
9 Digital counting

Sea Clutter Error

Receiver Noise Error

Magnetron System Accuracy

⊗ Short Pulse 10 ns

⊚ Long Pulse 100 ns

Altitude Error in Meters

0.1

0.01

0.001

TWT

RSS Short Pulse System

TWT

RSS Long Pulse System

1 ns   10 ns   100 ns

Length of Compressed Pulse in Nanoseconds (*Use with Table 2-1)
Figure 2-2.   Accuracy Improvement Resulting from Shortening Pulse
at Constant P$_{av}$

Table 2-1

Error Summary

	Error Item	SGAS Radar Errors	
		Estimated with Data Corrections	Estimated Error with Either Short or Compressed Pulse System
1.	Receiver Noise	.009 m	.01 m
2.	Sea Clutter	.04 m	.01 m
3.	Sea State	.01 m	.01 m
4.	Refractivity	.1 m	.05 m
5.	Integration	0	0
6.	Bias	.2 m	.05 m
7.	Waveform Variations	.1 m	.05 m
8.	Amplitude Variation	.05 m	.01 m
9.	Digital Counting	.1 m	.05 m
10.	Multipath	0	0
11.	Range SL	NA	.02 m
12.	Altitude Rate	0	.015 m
13.	Attitude	0	.02 m
Total (rss)		.26 m	.11 m

- Range Sidelobes
- Altitude Rate Error
- Attitude Error
- Errors Associated with Hardware

The error from the range sidelobes will represent a bias. The errors associated with the hardware are discussed in paragraph 3.2.3.

2.2.1.1 Range Sidelobe Error

The range sidelobes will cause a reduction in the altitude measured
by reflecting energy off the surface before the main pulse. These sidelobes
have maximum energy 30 dB down from the main pulse and can be considered
to add in a random manner. The total expanded pulse is 1 μsec long so that
there are 50 range side lobes 10 ns long ahead of the main pulse, so that
an excess of energy of 0. 7% is the maximum that might be expected to weight
the leading edge of the pulse in an early direction by less than .07 ns or
0. 01 meters. A precise error estimate can be determined by convolving
the surface scattering function (Appendix F) on the pulse ambiguity func-
tion. This accuracy estimate would be somewhat improved by range lobe
weighting consideration.

2.2.1.2 Attitude Error

In pulse compression, attitude errors cause a different illumination
of the surface scattering function than the scattering function for range side-
lobes. This can be determined by deriving the surface scattering function
associated with the particular pointing angle of the antenna. The error gen-
erated would be a function of the ratio of the stabilization error to the antenna
beam width. When this ratio is less than 10% , the range distortion is
comparable to that found in the range sidelobe case. It is apparent, that to
take full advantage of pulse compression either the power must be increased
or stabilization must be provided. The 0. 3° of the SGAS study is adequate.
[An attractive approach which requires more study, is to use the radar re-
turns to control beam steering of the antenna.]

2.2.1.3 Altitude Rate Error

A much more serious error than that arising from the sidelobes, is
the error that arises from a velocity displacement, i. e., altitude rate within the

main lobe of the ambiguity function. Fortunately, this error can be readily corrected by offsetting the frequency of the transmitted pulse or computing a correction for the return data.

The maximum expected altitude rate is 300 m/sec which would yield a doppler of 20 KHz/sec. Then the range error expected from altitude rate, $E\pi$, is given by:

$$E\pi = f_d \frac{\hat{t}e}{BW_{pc}}$$

$$= 3 \times 10^8 \times \frac{20,000}{100 \times 10^6} \times 10^{-6} \qquad (2\text{-}1)$$

$$= 0.06 \text{ meters}$$

2.2.2 Other Error Considerations

In addition to the errors that are specifically related to pulse compression, the errors that were discussed in the SGAS study apply to this system. A review of Section 4 and its appendices in the SGAS study would prove of value to the reader. First let us call to the readers attention that the errors will depend upon the nature of the processor that is used to locate the signal. To insure that the two studies are comparable, the SGAS type of processor has been used in considering the analysis of errors in this study. These errors can be broken down into three categories:

- Independent of pulse length
- Dependent on pulse length
- More investigation is required

2.2.2.1 Errors Not Pulse Length Dependent

The errors that are not dependent upon pulse length present a particular problem because they establish an ultimate limit on system performance. In this section, it is shown how these errors can be reduced to a point where

they are compatible with 10 cm system accuracy. These errors are caused by atmospheric refractivity and timing errors.

Changes in Atmospheric Refractivity

Changes in refractivity (propagation velocity) in both the ionosphere and the troposphere have been considered. These errors are one of the limiting factors on shortening the pulse length, because they do not decrease as the pulse length is shortened. Frey, Harrington, and Von Arx[2] show that for the ionosphere at X-band, day to night variations in range "error" (delays) of 2 to 10 cm can be expected. Since a portion of this delay is predictable, it appears that at X-band, uncorrected ionospheric residual errors can be made negligibly small.

Troposphere data is taken from Barton[3], Chapter 15, and from the Handbook of Geophysics[4] Chapter 9. Mean delay through the troposphere corresponding to a refractivity (N) of approximately 300 amount to a range delay at vertical relative to that in vacuum of about 2 meters, which can be used as a corrective factor. Extreme variations in N at sea level amount to about ±50 and represent altitude errors (uncorrected) of about 0.3 meters (see Appendix R-I).

Corrections for variations in N require information on synoptic weather conditions including water vapor content, temperature, and pressure would reduce this error to 0.1 m. A further improvement can be made if water vapor and temperature data (the most significant parameters) can be obtained by the use of satellite-borne radiometer operating at about 23 GHz, where moisture absorption and reradiation is prominent. This condition should provide better than 5 cm accuracy. Relationships between radiometer signal strengths and N have not been determined in this study, but can probably be obtained by further study. Further weather information may be obtained from ships at sea, weather satellites, and from ground weather stations where they exist.

Assuming probable operation at much less than the extremes of ±50 in N, and with at least partial correction being possible with use of extensive weather data, Thayer[5] estimates troposphere altitude errors in the vicinity of 0. 05 meter:

$$\sigma_{hr} = 0.05 \qquad\qquad (2\text{-}2)$$

In addition to the errors resulting from pulse delay, errors could arise from atmospheric distortion. Figures 2-3[6] and 2-4[7] indicate negligible distortion of the pulse in transit to a 10 GHz signal.

Altitude Counting Errors

Altitude counting errors are likely to be one of the most serious factors in the error budget in that they are not proportional to pulse length and are not improved with decreased pulse length. Altitude counting, referenced to a secondary frequency standard, is subject to three error sources: (1) that resulting from inaccuracy or instability in the reference oscillator, (2) that resulting from quantization, and (3) that resulting from vehicle altitude changes during the counting interval.

The reference oscillator stability requirements are related to altitude accuracy requirements by the error form:

$$\frac{dh}{c} = \frac{df_c}{f_c} \quad \text{(counting oscillator stability error)} \qquad (2\text{-}3)$$

Requirement for less than 0. 05 meter error in 1000 km therefore, dictates a frequency stability of the same ratio, or better than 1 part in 10^8. To eliminate this error source entirely requires that stabilities of at least 10^{-9} and preferably 10^{-10} be attained. Good crystal oscillators with oven controlled crystals are presently capable of this accuracy.

$$\int_{s_1}^{s_2} N_e^2 ds = 50 \times 10^{12} \text{ Electrons/cm}^2$$

τ = Pulse width
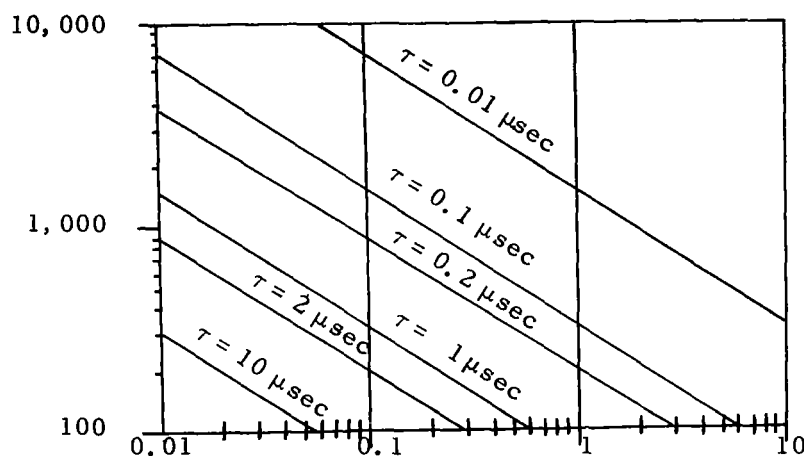
Figure 2-3. Pulse Shape Distortion for Propagation Through the Ionosphere, two-way Transmission Path
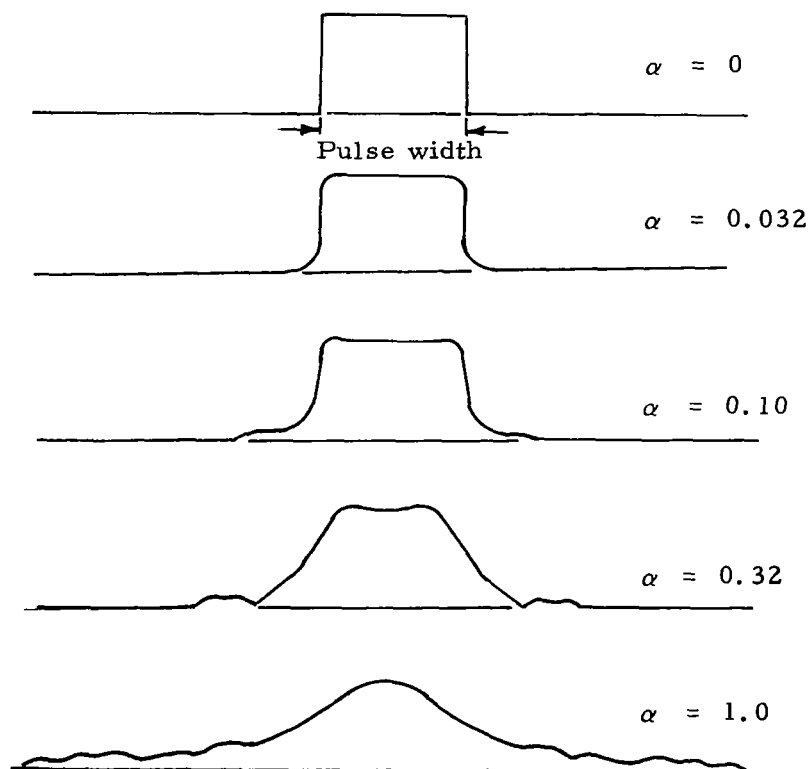
Figure 2-4. Pulse Shape Distortion due to Dispersion in a Waveguide (after Elliott)

Quantization problems become more serious as resolution is increased because of the demand for faster counting rates. An accuracy of 10 cm would demand counting rates greater than 1GHz. This is sufficiently beyond such techniques of MECL logic that a new approach is needed. Coincidence counting techniques will probably solve this problem.

If the vehicle changes altitude during the counting interval, the final altitude count corresponds to some previous altitude because of counting lag. The correction for this effect is simplified by the fact that orbital velocities are essentially constant over the 1-second counting intervals. On the basis of constant velocity, analysis (see Appendix R-E) shows that the actual altitude at the end of the count is given by combining these three counting errors, an error of

$$\sigma_{hc} = .05 \text{ meter (expected counting error)} \tag{2-4}$$

should be attainable.

2.2.2.2 Pulse Length Dependent Errors

The pulse length dependent errors obviously afford the opportunity of improving accuracy by decreasing pulse length as shown in Figure 2-2.

Receiver Noise Error

The received pulses are processed to generate a doublet waveform whose zero axis crossing point is used as a timing reference. When the idealized waveform is perturbed by receiver noise, some timing uncertainty results in the axis-crossing instant of the timing waveform. This timing uncertainty corresponds to an altitude uncertainty which can be estimated as follows. (Receiver noise in the presence of the axis-crossing ramp is shown in Figure 2-5 below.)
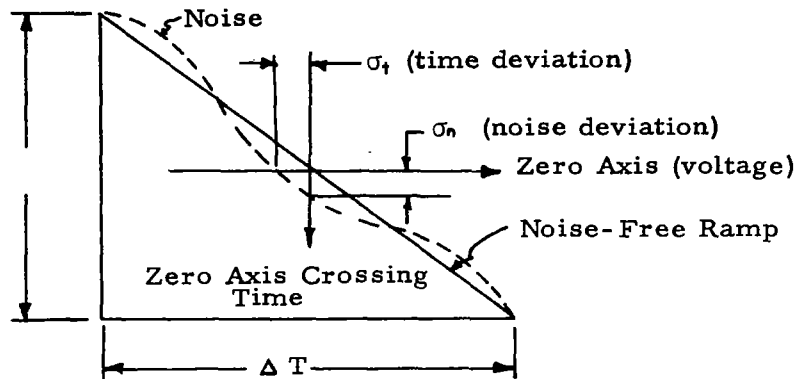
Figure 2-5. Receiver Noise in Presence of Axis-Crossing Strip
(from SGAS study)

From the figure above, the following proportion is apparent:

$$\frac{\Delta v}{\Delta T} = \frac{\sigma_n}{\sigma_t} \tag{2-5}$$

Solving for the time uncertainty (σ_t) due to noise gives:

$$\sigma_t = \sigma_n \frac{\Delta T}{\Delta v} = \frac{\Delta T}{v/\sigma_n} = \frac{\Delta T}{\sqrt{S/N}} \tag{2-6}$$

The corresponding altitude uncertainty due to noise is:

$$\sigma_{hn} = \frac{c \, \sigma_t}{2} = \frac{c \, \Delta T}{2 \sqrt{S/N}} \tag{2-7}$$

From the doublet waveform diagram (Figure A-6 of Appendix R-A), it can be seen that:

$$\Delta T = 50 \text{ ns} = \text{pulse length of transmitter} \tag{2-8}$$

and from Appendix R-B

$$\sqrt{S/N} = 2\sqrt{(S/N)_i} = \text{peak-to-peak signal to rms noise amplitude} \tag{2-9}$$
$$\text{ratio after integration}$$

2-12

The range equation analysis (see Appendix R-B, Section B. 1) for the worst case parameters in Table B-1 results in an altitude uncertainty of:

$$\sigma_{hn} = .0086 \text{ m altitude uncertainty versus noise.} \tag{2-10}$$

Let us next look at how the signal to noise error is changed if the average power is maintained the same but the length of the pulse is reduced. The signal to noise ratio is given by:

$$\frac{S}{N_i} = n_i \frac{P_{Pk}}{BW_{comp}} \ c \ \hat{t}_{comp} \ \frac{G^2 \lambda^2 \sigma_o}{64 \pi^2 \ KTFL} \tag{2-11}$$

$$\frac{S}{N} = n_i \frac{P_{AV}}{n_i \hat{t}_{comp}} \ \frac{c \hat{t}_{comp}^2 \ G^2 \lambda^2}{h^3 \ 64 \pi^2 \ KTFL} \tag{2-12}$$

$$= \frac{P_{AV}}{h^3} \hat{t}_{comp} \ \frac{G^2 \lambda^2 c}{64 \pi^2 \ KTFL} \tag{2-13}$$

substituting in 2-7

$$\sigma_{hn} = \frac{2\pi}{G\lambda} \sqrt{\frac{\hat{t} h^3}{P_{AV}} \ c \ KTFL} \tag{2-14}$$

This error is plotted in Figure 2-2.

Clutter Error

Clutter results from the vector addition of random return from independent target points. When the number of point scatters is large, the detected amplitude of the reflected signals has a Rayleigh distribution and its bandwidth is the reciprocal of the transmitted pulse length. If the transmitted pulse is rectangular with length $\hat{t}$, its bandwidth is about $1/\hat{t}$ (cps) and the clutter waveform will have not more than about $1/2$ cycle of clutter per signal pulse length or over the rise time of the received signal. This

waveform will be somewhat coherent from pulse to pulse, but the phase will change at the doppler frequency rate, i.e., many times slower than the clutter signal frequency or pulse signal frequency.

Clutter introduces an altitude uncertainty similar to receiver noise error, and the altitude uncertainty can be reduced by integration. The altitude uncertainty due to clutter can be written as:

$$\sigma \, hc \;=\; \frac{\dfrac{c\hat{t}}{2}}{2 \, \sqrt{(S/C)_1}} \tag{2-15}$$

where $ct/2$ is the pulse time base (meters), and the factor of 2 in the denominator results from slope doubling by the delay-differencing circuits in the processor (SGAS study).

The signal-to-clutter term $(S/C)_1$ is the power ratio after integration, and can be estimated as follows:

$$(S/C)_i \;=\; (S/C)_{dL} \, n_i \quad \text{(assuming nearly matched filter processing)} \tag{2-16}$$

where $(S/C)_1$ is the signal to clutter ratio of signal waveform samples and is given as:

$$(S/C)_{dL} \;=\; \frac{\text{mean}^2}{\text{rms}^2 - \text{mean}^2} \;=\; \frac{\pi}{4 - \pi} \tag{2-17}$$

For Rayleigh distribution, the number of clutter samples (n_i) integrated is given by:

$$n_i \;=\; \frac{f_d}{2 \, BW_n} \tag{2-18}$$

where:

$$f_d \;=\; \frac{2v}{\lambda} \, \sqrt{\frac{ct}{h}} \tag{2-19}$$

$$\sigma h_c = \frac{1}{4}\sqrt[4]{\frac{t^3 c^3 h(4-\pi)^2 \lambda^2}{BW_n^2 4\pi^2 v^2}} \qquad (2-20)$$

This error is plotted in Figure 2-2.

Bias Errors

Bias errors can be defined as errors resulting from uncorrected, slowly-varying or fixed signal delays such as receiver delays, processor delays, transmitter and modulator delays, pulls other miscellaneous variable delays which may be temperature, voltage, or aging dependent. Delays tend to increase the apparent altitude and may represent one of the largest error sources unless corrections are provided.

This class of errors is inversely proportional to the bandwidth of the system, so that when the bandwidth of the system is increased to match narrower pulse widths, this type of bias is proportionally decreased. This error can be estimates as:

$$\sigma_{BW} = 0.2 \cdot \frac{20 \times 10^6}{BW} \sim 0.05 \text{ at } 10 \text{ ns} \qquad (2-21)$$

2.2.2.3 Experimental Investigation Required

Attaining 10 cm accuracy in an altimeter depends upon what happens to the pulse at the time it reflects from the ocean surface. There exist models to describe this interaction but there is not sufficient experimental evidence to distinguish between the models yet alone be unto itself an emperical model.

In Appendix R-A, it is pointed out that the effect of sea-state is (1) to round out the waveform somewhat in the vicinity of break points, and (2) to shift the ramp crossover point by an amount equal to the shift of the

centroid of the sea-state impulse response. (See also Appendix R-G.) Since the timing point, which is chosen as the zero axis crossing point in the processed doublet, is instrumented to be centered between breakpoints, the error of principal importance is the shift in centroid due to sea-state.

Elaborate theoretical analysis of the electromagnetic response of the sea surface at vertical incidence, under widely varying sea-state conditions, and backed up by extensive experimental data, is singularly lacking. However, computer-generated simulations obtained from Raytheon's Submarine Signal Division (see Appendix R-G) allows preliminary estimates of shift in centroid versus sea-state to be made. These data ignore possible effects of whitecaps and spray.

The data in the table of centroid shifts shown below indicate that for the processor assumed, (which Appendix R-A shows are the same magnitude as centroid shift due to impulse response), sea-state errors are negligible for winds of less than 20 knots.

Wind (Knots)	Approximate Shift in Centroid of Impulse Response
10	.01 m
20	.03 m
30	.07 m
40	.12 m
50	.20 m

The shifts indicated are too small to be significant for purposes of this study, and may well be the result of sampling errors because of limited empirical data. The shifts shown were downwards, toward wave troughs, which may seem paradoxical in light of the higher elevations in the crest direction. This elevation effect appears to be more than compensated for by the occurrence of a larger number of troughs and few high crests.

The only information that can be considered as conclusive is carefully instrumented experimental data. The forthcoming NASA sponsored Space Geodesy Altimeter Aircraft Experimental Program will give further empirical insight into this problem.

2.3 Power Requirements for Providing Improved Accuracy

Accuracy demands larger peak power unless pulse compression is used to spread the pulse in time. At this juncture we will show the specific relationships between peak power and accuracy and show how pulse compression reduces the peak power requirement. The key to more accuracy is shortening the pulse width. This is clear from the error analysis. There are fixed errors such as: atmospherics, timing reference and sea state, which, in our current thinking, would limit us from trying immediately for better than 0.1 meters. The other errors, as seen from Figure 2-2, are pulse length dependent and decrease at least as fast as $t^{\frac{1}{2}}$.

For this decrease in pulse length, a price must be paid in terms of increasing peak power. This price is inversely proportional to the square of pulse length if S/N ratio is maintained constant.

Figure 2-6 can be used as a focus for thinking about this problem. It shows the requirements for power and the alternatives that pulse compression offers for providing it. The shaded area to the left represents a lower limit of peak power in a single pulse that must be available for efficient integration incoherently. This line is determined from the single pulse signal to noise ratio $(S/N)_{d\ell}$

$$\frac{S}{N}_{d\ell} = \frac{P_{PK}}{BW} t \underbrace{\frac{c\,G^2\,\lambda^2\,\sigma_o}{64\,\pi^2\,h^3\,KTFL}}_{K_o} \qquad (2\text{-}22)$$
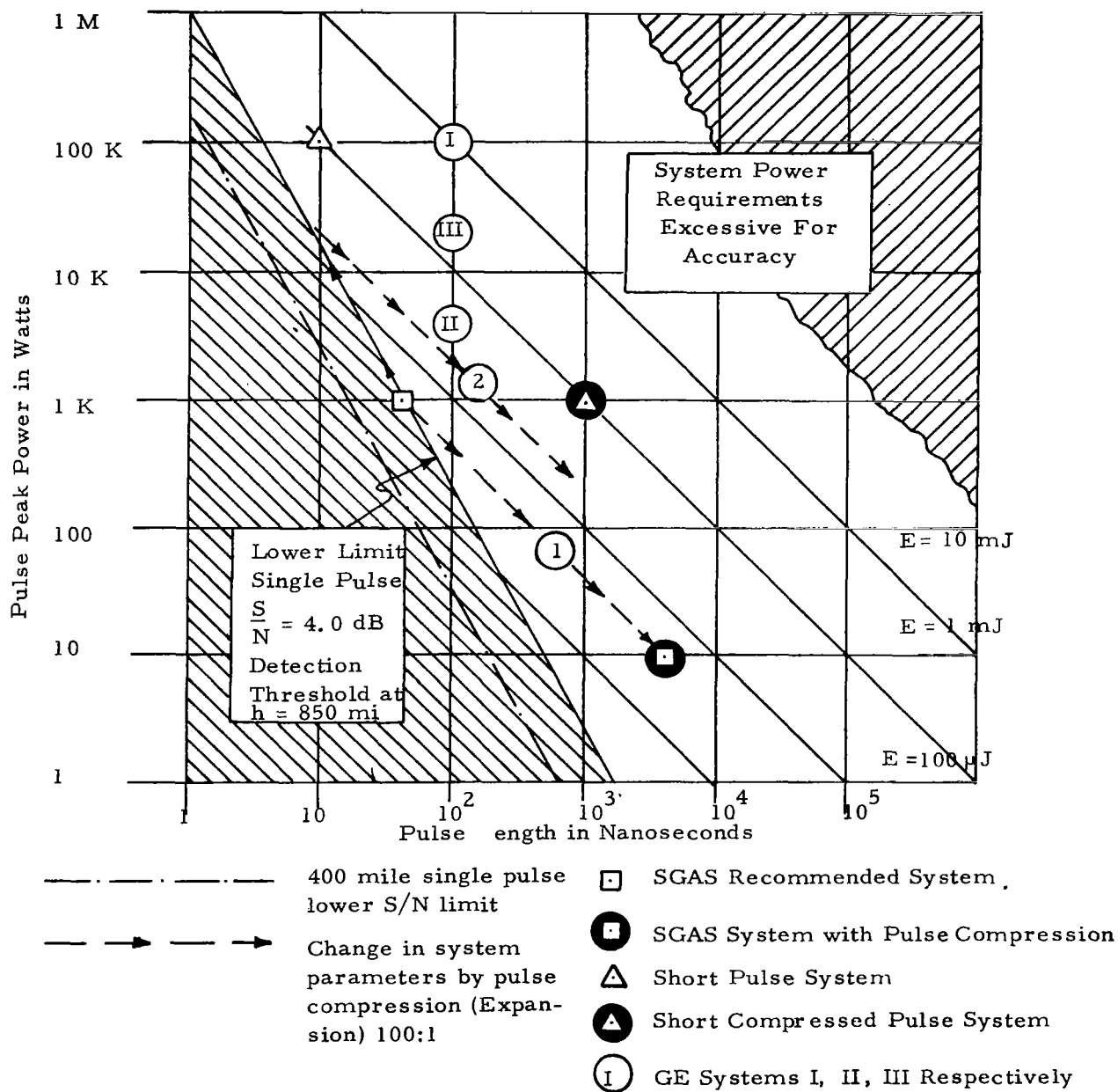
Figure 2-6. Time Bandwidth Power Allocations
For Geodesy Altimeter Systems

or for a matched filter system

$$\frac{S}{N}\,d\ell = P_{PK}\, \hat{t}^2\, K_o \tag{2-23}$$

$$\frac{S}{N}\,d\ell = P_{AV}\, \hat{t}\, K_o / f_r \tag{2-24}$$

The solid parametric lines represent contours of constant energy per pulse. The specific conditions for which this particular minimum power curve was derived is given in Table B-1 of the SGAS study.

Pulse compression added to a system would cause the point describing the system to be moved by a distance proportional to the compression ratio D along one of these isopower lines, E = const. The system that was configured for GEOS-D in SGAS study is represented by a point ▣ on the lower limit line. If the designer wished to shorten the pulse, say by a factor of 5 on this system, it would be necessary to increase the average power by a like amount in order that the system would not fall below the single pulse lower limit boundary. Hence, the peak power supplied to this system would be increased by a factor of 25 from 1 kw recommended in the SGAS report to 25 kw when the system has its pulse length shortened by 5. Now, if this system were to have pulse compression added to it, the pulse would be expanded in time along an isopower contour (②on Figure 2-1). The peak power could then be reduced by the compression ratio, a factor of 100 to 250 watts. This time expansion of the pulse length would not result in an improved signal to noise ratio nor a decrease in the accuracy of the system. The pulse could have been expanded before it was shortened (①on Figure 2-1). In this case, the final power could have been 10 watts. The signal to noise ratio would not have changed and the system accuracy would not have been improved beyond its initial value. The latter case suggests that under the constraint of maintaining SGAS accuracy, size and weight might possibly be reduced by going to a solid state transmitter. In summary, we can say for radar altimeters:

- Peak power increase is required to improve accuracy
- The more accurate system must incorporate broader bandwidth
- Pulse compression at a fixed signal to noise ratio and power can only be used to reduce peak power requirements.

2.4 Comparison of Pulse Compression with High Power RF Sources

What price must be paid if we attempt to use peak power alone to improve accuracy. There are three broadband microwave power tubes, Magnetrons, CFA, and TWT's. The Magnetron operated at the required power level has a short life expectancy, 500 hrs, and is subject to problems of both jitter and pulse stability. This uncertainty alone could amount to more than 2 ns (40 cms). The CFA is not subject to the short life problem but does have the jitter problem associated with magnetrons. However, it is a heavy device, approximately 50 pounds, and has a low power gain, 10 dB. As a consequence, it would have to be driven by a TWT that had a larger peak power rating than the TWT that could be used as a power output stage if pulse compression were to be incorporated into the system.

Let us turn to the use of a TWT as a power output stage. The problem here is that at low duty factors high power TWT's have low DC to RF conversion efficiency because of the large filament power requirements. This question of power efficiency is illustrated in Figure 2-1. The average power requirements of the radar altimeter will be under 10 watts.

If one examines the parametric curve for 10 watts, one sees that for TWTs with peak powers greater than 1 KW, the efficiency of the tube is low. For peak powers above 1 KW, the efficiency increases dramatically. Equally important as efficiency is the question of reliability. From Figure 2-1, it is also apparent that a decrease in peak power by a factor of 100 increases the MTBF by a factor of 8.

We can conclude therefore, that if we are seeking 10 cm accuracy, a TWT operated at a lower peak power with pulse compression appears to be a better alternative than any of the other RF sources, that are currently available, operated at higher peak power without pulse compression.

2.5 Comparison of Pulse Compression with Integration Techniques

Pulse compression provides a larger signal to noise ratio for a given expenditure of energy than any other type of system that spreads the energy in time. Two other systems are the coherent integration system used in the SGAS study and straight forward integration of incoherent pulses. The coherent integration of pulses is limited to less than the compression ratio of 100 by the doppler from satellite motion. The number of pulses that can be integrated coherently is determined by the number of pulses that can be squeezed into the maximum time t_d that the pulses are sufficiently correlated that they can be coherently integrated (Appendix D); and the maximum PRF $f_{r(max)}$ that the limitation of avoiding ground return from the previous pulse can be avoided (Appendix C).

$$N_a = t_d f_{r(max)}$$
$$= \frac{1}{650} \times 20,000 \tag{2-25}$$
$$= 33$$

The incoherent integration of pulses is limited by the fact that incoherent pulses contribute at a rate somewhat less than $N^{0.81}$ can easily amount to a loss of 8 dB.

2.6 Influence of Other Operational Parameters

Do the other operational parameters that have not been considered effect the trade-off conclusions? The answer is "no". We have considered accuracy power and life in reaching our conclusions. The only other parameters

of those enumerated in Table 5.3 in parent SGAS study that are relavent, are weight, volume and availability. The weight and volume of the pulse compression components are 200 gms and 100 cc respectively. The weight and volume saved in the modulator and the receiver would be about 2 kg and 1000 cc's respectively.

The availability is dependent upon the time required to package and space qualify components that are already available. This should be about one year.

SECTION 3

SELECTION OF A METHOD FOR PULSE COMPRESSION

H. Ward, A. McConchie, F. F. Reed, W. Glaven, C. Lorant

3.1 Summary

Pulse Compression can be accomplished in a number of different ways; the task that has been addressed here is the selection of a technique for pulse compression that is compatible with the stringent restraints on size, weight, reliability and freedom from adjustment that are imposed by satellite operation. The FM chirp surface wave dispersive delay line matched filter, offers the most promise as a result of these studies. Further design studies have been made on this system to develop it to a point that it can be compared with the short pulse system that was developed in the parent study.[*]

The initial tack that has been taken in this study is to select from systems listed in Appendix B six specific pulse compression implementations and to compare these approaches from the point of view of the practical applicability of the hardware involved and performance expectations. The consideration has been limited to those parts of systems that are directly concerned with pulse compression; the components for the initial expansion of the signal, the receiver, and the pulse compression components. The transmitter and processor will not be differentially effected by the various systems under consideration and hence have not been reviewed in the initial selection of approach.

The six systems that have been studied in detail are:

- FM[†] - Perpendicular Diffraction Dispersive Delay Line Matched Filter
- FM[†] - Surface Wave Dispersive Delay Line Matched Filter
- FM[†] - Correlation Receiver (serrodyne mixing)

---

[*] Space Geodesy Altimetry Study

[†] Continuously Swept.

- Discrete Coded - Binary Phase Coding (Barker Sequences)
- Discrete Coded - Staggered Spacing Pulse Groups
- Discrete Coded - Stepped Frequency Sequences

The advantages that hopefully could accrue from pulse compression are increasing the bandwidth of the system so that an improved altitude resolution capability can be achieved; and increasing the possible time bandwidth product so that lower peak powers can be realized. This decrease in peak power in turn hopefully would reflect in less weight and power consumption as well as improved reliability in the modulator transmitter parts of the satellite altimeter. Increasing the bandwidth, or in effect shortening the pulse to improve resolution, could undoubtedly improve accuracy materially at lower sea state levels; however, it has yet to be demonstrated that at higher sea states (e.g., 5 on Beaufort scale), where the effective pulse width is shorter than the wave height, a specific improvement would result. This latter question can only be answered when sufficient impulse transfer function data is available from the aircraft flight test.

Turning next to the possible reduction in peak power by increasing the time bandwidth product, the increased duration of the transmitted signal means that the average power required for detecting the signal return may be maintained while the peak power is reduced. If this peak power can be reduced from the present 1 kw to 5 watts, which is consistent with realizable $\tau \cdot BW = 200$, optimistically, a solid state transmitter now would become a possibility. This will result in less transmitter weight and longer life expectancy of the transmitter and modulator. There are currently available TWT's and magnetrons that could be used for pulsed application, that have life guarantees on the order of 500 hours, while solid state devices could be expected to provide a life in excess of 2000 hours. However, it should be pointed out that it is well within the state of the art to develop a TWT of comparable life

expectancy, although no such qualified tube is currently available. It will become apparent in the ensuing parts of the report that these improvements are paid for by increasing the basic complexity of the system.

The six systems that were specifically considered in this part of the study are compared in Table 3-1.

The accuracy goals of the parent study have been used to define the resolution requirements and, in turn, the minimum bandwidth requirements of 20 MHz. If an improvement in resolution can be shown to improve the accuracy performance of the system, the selected pulse compression system should afford the possibility of increasing the bandwidth to 100 MHz. The time bandwidth product or dispersion ratio of 100 is readily achievable by all of the systems that we have chosen to consider.

3.1.1 Comparison of Applicable Techniques

There exists a multiplicity of techniques for achieving coded trans-missions (Appendix B) many of these can be immediately eliminated either from practical implementation considerations or from bandwidth (and hence resolution) considerations. The methods outlined below can be considered as either phase coded systems or FM chirp systems. A chirp system can be implemented with a matched filter receiver using a dispersive delay device or with a correlation receiver using serrodyne mixing techniques.

3.1.2 FM Chirp Matched Filter Techniques

Of the two approaches noted above, the one in the most advanced state of development employs matched filter chirp techniques. The trans-mitted waveform for a chirp system can be generated actively, by sweeping a voltage controlled oscillator (VCO), or passively, by impulsing a disper-sive network. The systems shown in Figures 3-1 and 3-2 use a dispersive network to expand and to compress the pulse.

Systems Comparison

Table 3-1

System	Max. BW	Time Bandwidth or Disp. Prod.	Relative Size	Relative Weight	Remarks
Surface Wave Disp. Delay Line	100 MHz	200	1	1	Good resolution; high disp. prod., small, lightweight
Serrodyne Technique	200 MHz	400	1.3	1.3	Good resolution, high disp. prod., small, lightweight
Perpendicular Diff. Dis. Delay Line	100 MHz	200	3.5	5	Good resolution, high disp. prod., delay lines are large, and heavy
Discrete Frequency Sequences	20 MHz	N^2	0.5N+1	0.5N+1	Requires N matched filters, marginal resolutions
Barker Code (N = 13)	20 MHz	13	2.3	2.3	Requires tapped delay lines, marginal resolution, low disp. prod.
Staggered Spacing Pulse Groups	20 MHz	M^*	$\propto T^{**}$	$\propto T^{**}$	Requires tapped delay lines, marginal resolution, low disp. prod. unless M is large.

* M = Number of pulses in ensemble

** T = Duration of ensemble

Tx - Rx
Timing

1-1/2"x 1"x 1/2"
.3 Watt

1-1/2" x 1" x 1/2"
.6 Watt

9" x 4" x 3/4"

2" x 1" x 1/2"
.2 Watt

Tx
Timing → → Spectrum Generator → Diode Switch → Drive Amplifier → Perpendicular Diffraction Dispersive Delay Line → Post Delay Amplifier

3-1/2" x 1" x 1/2"
.25 Watt

3" x 1" x 1"
.2 Watt

From RF
Amplifier → Second Mixer → Pre-Amp.- Filter

Weighting Filter- Amplifier ← Diode Switch ← Tx-Rx Timing

Totals
35-3/8 Cu. Inch
1.9 Watts

Local Oscillator

1" x 3/4" x 1/2"
.1 Watt

1-1/2" x 1" x 1/2"
.25 Watt

To Transmtr.

Detector- Video Amplifier → To Processor

Figure 3-1. FM Chirp System with Perpendicular Diffraction Dispersive Delay Line

Tx - Rx
Timing

1-1/2"x1"x1/2"
.3 Watt

1"x1"x1/2"
.2 Watt

4"x 1"x 1/2"

1"x 1"x 1/2"
.2 Watt

Tx
Timing

| Spectrum Generator | Diode Switch | Drive Amplifier | Surface Wave Dispersive Delay Line | Post Delay Amplifier |

3-1/2"x1"x1/2"
.25 Watt

3"x 1"x 1"
.2 Watt

From RF
Amplifier

| Second Mixer | Pre-Amplifier Filter | | Weighting Filter Amplifier | Diode Switch |

Tx-Rx
Timing

Totals
9-5/8 Cu. Inch
1.5 Watts

Local Oscillator

.1 Watt

1"x3/4"x1/2"

Detector-Video Amplifier

To
Transmtr.

To
Processor

.25 Watt
1-1/2"x1"x1/2"

Figure 3-2. FM Chirp System with Surface Wave Dispersive Delay Line

There are various methods for achieving dispersive delay devices; only two, however, have sufficient bandwidth (at least 20 MHz) and time-bandwidth product (at least 100) to be of value in the application at hand. Perpendicular diffraction delay lines utilizing a quartz medium are readily capable of 20 MHz bandwidths and dispersion ratios of at least 100. Experimental models have been built having bandwidths approaching 100 MHz.

Range sidelobes would most probably have to be suppressed by the addition of a weighting function in the receiver or by transmitting a non-linear FM chirp. Sidelobe suppression by weighting the received signal would decrease the resolution of the radar by a factor of one and a half to two and also increase the power requirements for signal detection. Therefore, to achieve the same resolution as the present short pulse system, a bandwidth of considerably more than 20 MHz would be necessary. The requirement of increased bandwidth would also apply to a nonlinear chirp case.

Even though perpendicular diffraction delay lines show promise of sufficient bandwidth, their bulkiness (see Figure 3-1) and high loss (typically 50 to 60 dB) would make them unattractive for satellite applications.

A recent development at Raytheon's Research Division shows a great deal of potential for producing small, lightweight dispersive delay lines in the very near future[8]. These devices have interdigital arrays printed on lithium niobate and use surface wave rather than bulk wave techniques. Besides being small and lightweight, these delay lines would be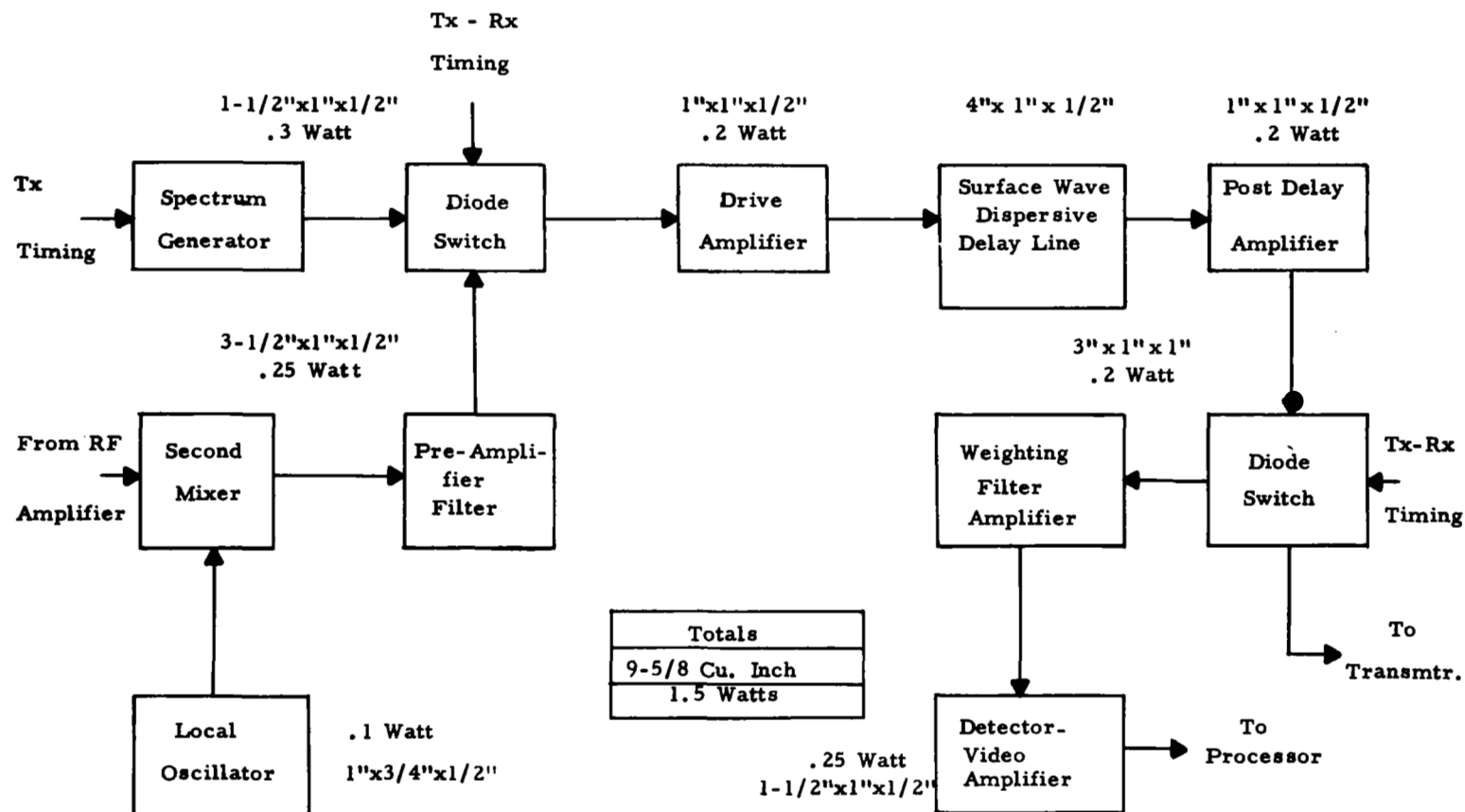 relatively inexpensive and highly reproducible and would have much less loss than bulk wave type devices. Typically, the surface wave lines have usable dispersive bandwidths of thirty to forty percent of their center frequency. The upper limitation on center frequency is dictated by present photolithographic

techniques; however, a line with a 300 MHz center frequency and 100 MHz bandwidth seems quite feasible. These new lines offer good possibilities for chirp systems much smaller (see Figure 3-2) than many which have been built to date.

3.1.3 Phase Coded Systems

A conceptual diagram of a phase coded pulse compression system is shown in Figure 3-3. There exists a veritable infinity of optimum and sub-optimum discrete coded sequences of which phase coded sequences are one group[9]. Most discrete coded waveforms can be disregarded either from the standpoint of poor sidelobe performance or from the standpoint of rather complex implementation. Another disadvantage that can be inferred from Figure 3-3 is that the tapped delay lines will constitute a size and weight problem.

The use of longer suboptimum codes to achieve higher compression ratios or the use of polyphase rather than binary phase codes to achieve better sidelobe performance does not alleviate the system problem, in that they would make the system prohibitively large and/or complex. In summary, the only sequences which show promise for the present application are the Barker sequences.

The maximum length, Barker sequence (N = 13), has a theoretical sidelobe level of approximately -23 dB; and therefore, a modest amount of weighting may still be necessary: Since it would be difficult to space the taps any closer than 50 nsec. The binary phase coded system would not provide any increased resolution over the short pulse system, but would only serve to reduce the transmitter peak power (by a factor of 13:1 with the maximum length sequence). In comparison with the other coding systems discussed here, the binary phase coded system would seem to be the least attractive approach because of the difficulties involved in operating the transmitter in a phase discontinuous mode.
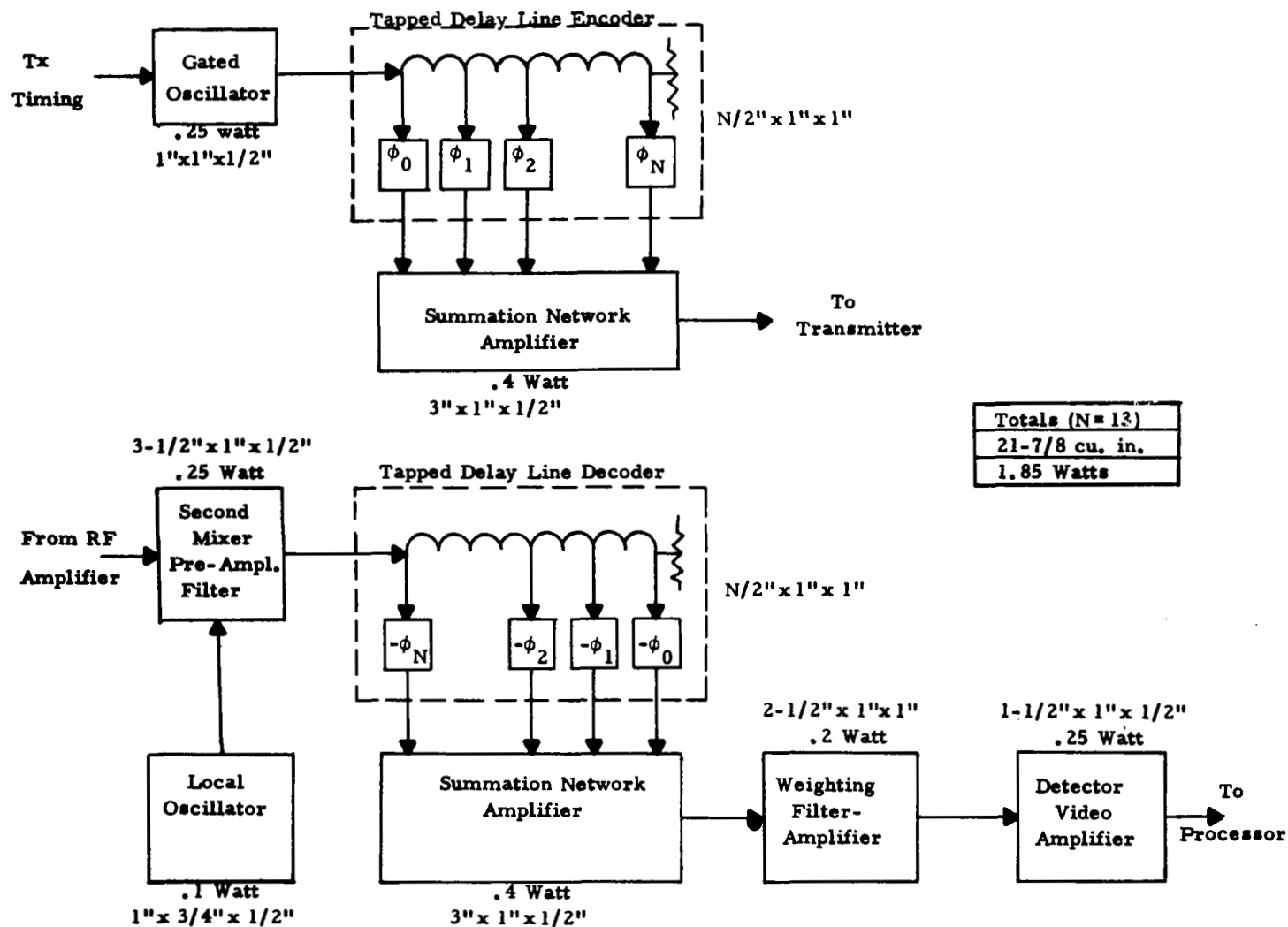
Figure 3-3. Phase Coded Pulse Compression

3.1.4 Serrodyne Techniques

A functional diagram of a serrodyne system is shown in Figure 3-4. This system represents a different approach than either an FM chirp matched filtered or a phase coded system. The transmitted waveform for the serrodyne system shown in Figure 3-4 is an actively generated chirp. The received waveform is mixed with a signal from swept local oscillator which tracks the transmitted signal with a fixed frequency offset which would be the center frequency of the IF receiver. Therefore, the waveform to be processed in the IF receiver would not be phase or frequency modulated; but the frequency of the signal would be a function of target range.

A serrodyne system compares favorably with a matched filter chirp system in terms of resolution and time-bandwidth product. If a 1 μsec pulse with a 100 MHz frequency sweep were transmitted, then the width of the filters in the filter bank would be 1 MHz. However, since the transmitted signal has a 100 MHz frequency deviation, a 10 ns error between the start of the receiver sweep and the time of the return would shift the IF frequency of the signal by 1 MHz. Therefore, this system would provide a 5:1 (50 ns:10 ns) improvement in resolution and a 20:1 (1 μs:50 ns) reduction in transmitter peak power.

One of the major contributors to the size of the serrodyne system is the filter bank. The number of filters required in the bank is uncertain at this point and as a consequence, the weight estimates may turn out to be somewhat low. A five-filter bank might be sufficient; however, the exact number depends on the time requirement for acquisition and the detailed configuration of the acquisition circuitry.

2" x 2" x 1-1/2"
.3 Watt

1" x 3/4" x 1/2"
.1 Watt

Tx - Rx →

Timing →

Swept Local Oscillator

IF Offset Mixer

→ To Transmitter

To Processor

1-1/2"x1"x1/2"
.25 Watt

Detector Video Amplifier

Totals
12-1/4 cu. in.
1.2 Watts

Local Oscillator

1" x 3/4" x 1/2"
.1 Watt

Filter Bank

IF Amplifier

Pre-Amplifier Filter

Second Mixer

From RF Amplifier ←

2-1/2"x1"x1"

1"x1"x1/2"
.2 Watt
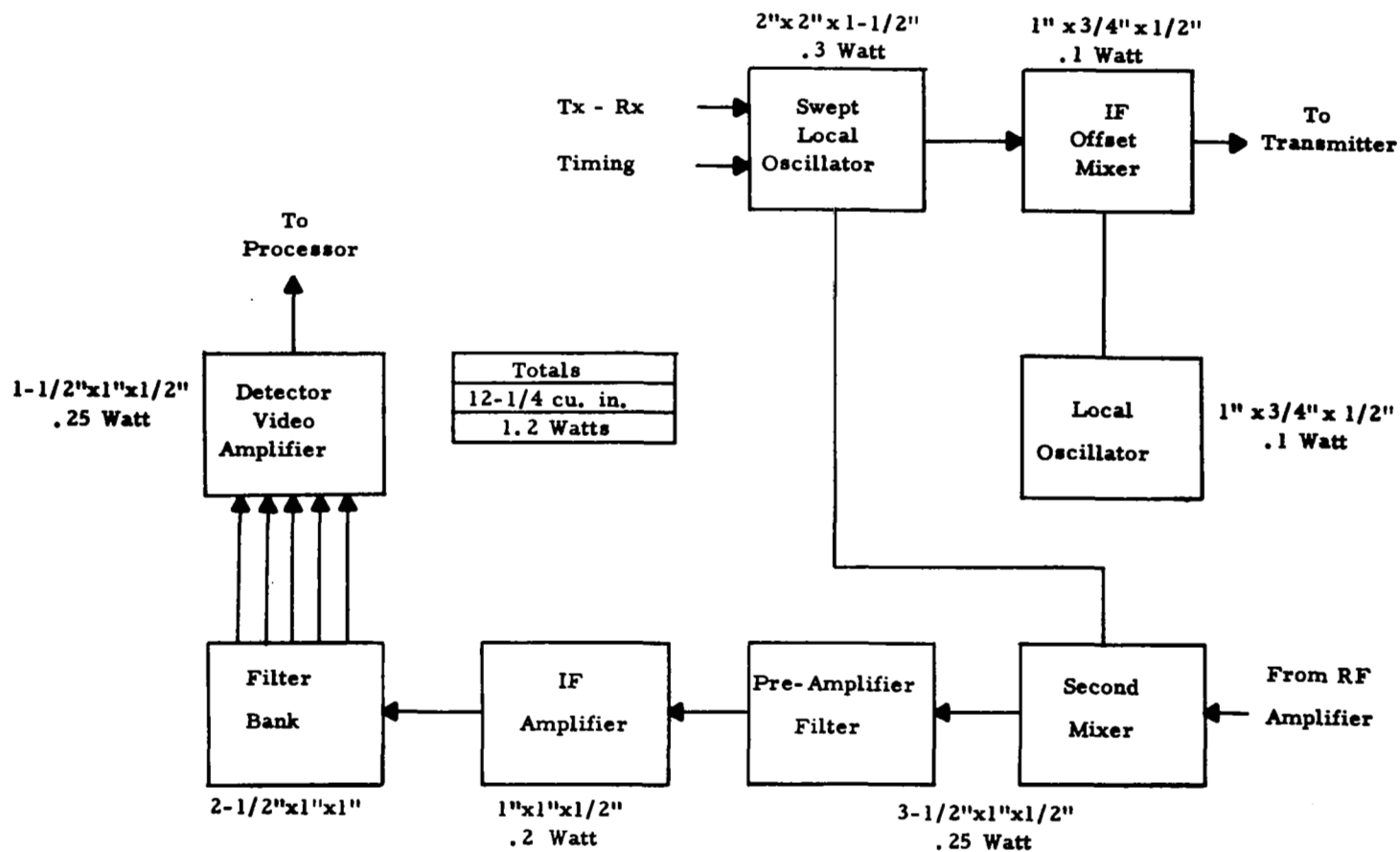
3-1/2"x1"x1/2"
.25 Watt

Figure 3-4.   Serrodyne Pulse Compression

3.1.5 Conclusions and Recommendations

Of the systems considered above, both the matched filter chirp system using surface wave dispersive delay lines and the serrodyne system seem to offer good possibilities for use in a satellite bourne radar altimeter. Both could quite readily provide a 20:1 reduction in transmitter peak power; and a three to five-fold increase in resolution seems feasible. The power required for both systems is approximately the same; but on the basis of size, the surface wave delay line approach has the advantage and should be the subject of further investigation.

3.2 The Design of a Pulse Compression Altimeter Radar for Space Geodesy

3.2.1 Introduction

The following section details the pulse compression configuration that was selected for incorporation in the radar altimeter to be used for space geodesy measurements from an unmanned space vehicle. A pulse compression system is being considered to provide the radar altimeter with increased range resolution capability in conjunction with decreased peak power requirements at a relatively small penalty in complexity, weight and volume relative to a conventional pulsed radar altimeter.

Section 3.1 covered the investigation of several applicable pulse compression techniques and described the rationale for selecting an FM chirp system employing surface wave dispersive delay lines as the candidate system for a more specific design investigation in the radar altimeter area. Provided herein is a detailed description of this system in terms of its physical design, its compatibility with the present radar altimeter designs and its performance characteristics.

3.2.2 System Considerations

3.2.2.1 The Impact of Pulse Compression on Various Altimeter Designs

When studying the possible use of pulse compression in the GEOS-D radar altimeter we considered the effect of pulse compression on the various radar designs. Aside from the pulse compression circuitry which would be added, a number of other changes must be made in the altimeter design and these are discussed below for the altimeters proposed by Raytheon and GE.

The portion of the radar most affected by pulse compression is the transmitter. Table 3-2 lists the parameters of the transmitters proposed by Raytheon and GE. The Raytheon design uses a traveling wave tube while the three GE designs all use magnetrons. Average power and pulse width remained nearly the same for all four designs as peak power and PRF vary considerably.

Since pulse compression will allow the receiver to compress the transmitted pulse by a factor of about 100 the altimeter can be reconfigured to reduce peak power or improve resolution. Since the four designs considered here use pulse widths ranging from 50 to 100 ns it would seem reasonable to divide the advantage gained by pulse compression between resolution improvement and peak power reduction. We will assume therefore that a 100:1 pulse compression ratio is used to produce a transmitted pulse of 1 microsecond and a compressed pulse of 10 nanoseconds. This improves resolution by a factor of 10. Table 3-3 lists the revised parameters.

The most important effect on the transmitter is the requirement that it
be an amplifier rather than an oscillator, therefore, a magnetron cannot be
used.

Changes in the other areas of the radar are needed to be compatible
with the shorter pulse at the receiver output. The receiver bandwidth and
signal processing speed will increase by a factor of 10. Bandwidth goes from
10 to 100 Megacycles and the sample spacing (if the processor takes time
samples of the receiver waveform) is reduced from 100 nanoseconds to 10
nanoseconds.

Timing is also more critical. Because of the shorter pulse width, resolution
is improved and the altimeters will obtain a more precise altitude measure-
ment. This in turn requires that the timing accuracy, height measurement
and data correction be more accurate by a factor of 10. Also more capacity
is needed in the data link which transfers the measured height information
to the ground.

Table 3-2

Altimeter Transmitter Parameters

(without Pulse Compression)

	Raytheon *	GE**#1	GE** #2	GE** #3
Transmitter Tube	TWT	Magnetron	Magnetron	Magnetron
Peak Power (radiated)	1 KW	100 KW	4 KW	20 KW
Pulsewidth	50 ns	100 ns	100 ns	100 ns
PRF	100 KHz	100 Hz	5000 Hz	1000 Hz
Average Power (radiated)	5 W	1 W	2 W	2 W
Energy/Pulse	50 μJ	10,000μJ	400μJ	2000μJ

* This represents the direct conversion of the SGAS System to pulse compres-
  sion to provide a direct basis for comparison. It is not the system that has
  been described in Table 1-1.
** GE Report, "Space Rated Radar Altimeter," Jan 1969, NAS 12-683.

Table 3-3

Altimeter Transmitter Parameters

(with Pulse Compression)

	Raytheon*	GE #1	GE #2	GE #3
Transmitter Tube	TWT	TWT	TWT	TWT
Peak Power (radiated)	250 W	100 KW	4 KW	20 KW
Pulsewidth	1 μs	1 μs	1 μs	1 μs
Compressed Pulse-width	10 ns	10 ns	10 ns	10 ns
PRF	100 KHz	100 Hz	5 KHz	1 KHz
Average Power (radiated)	25 W	10 W	20 W	20 W
Energy/Pulse	250 μJ	.1 J	4000 μJ	20000 μJ

3.2.2.2 Proposed Pulse Compression System

The main reason for considering pulse compression processing as part of the radar altimeter system is to achieve better altitude resolution or reduced peak power requirements relative to that provided with a conventional pulse radar characterized by the same transmitted average power and PRF, i.e., the same transmitted energy/pulse. This objective is to be met with the least cost in additional equipment.

The measure of effectiveness of a pulse compression system is its time bandwidth product or dispersion factor.

$$D = \hat{t}_e \ BW_{pc} \qquad\qquad (3-1)$$

where

---

* This represents the direct conversion of the SGAS System to pulse compression to provide a direct basis for comparison. It is not the system that has been described in Table 1-1.

t_e = expanded pulse width

BW_{pc} = PC bandwidth

Conventional pulsed systems can be considered as having D = 1. Thus the parameters in (1) are related to the pulse length $\hat{t}_o$ and bandwidth BW_o of a conventional pulsed system by

$$\frac{BW_{pc}}{BW_o} \frac{t_e}{t_o} = D \qquad (3\text{-}2)$$

Since resolution is proportional to BW, allocating D entirely to $\frac{BW_{pc}}{BW_o}$ i.e., keeping $\hat{t}_e/\hat{t}_o = 1$, results in channeling all of the enhancement derived through P.C. as increased resolution. Conversely maintaining $\frac{BW_{pc}}{BW_o} = 1$ results in stretching the transmitted pulse by the ratio D, consequently lowering the required peak power for the same per pulse energy by an equivalent factor. In any case, large dispersion factors permit a considerable improvement in resolution and/or decrease in transmitter peak power requirements.

The pulse compression system proposed to be implemented as part of the Space Geodesy Radar Altimeter and described in the following section is expected to provide a dispersion factor D = 100 resulting from a 1 μsec wide transmitted pulse linearly modulated over a 100 MHz frequency band centered at a 300 MHz I.F. This P.C. performance is obtained by utilizing a frequency scaled version of the dispersive delay line described in Figure A-3 of Appendix A.

In terms of the 50μsec/20 MHz operation specified for the radar altimeter without P.C., the adjunct of pulse compression capability, as described herein, could potentially enhance range resolution by a factor of 100/20 = 5, namely the altimeter resolution could be improved from 50 ns (7.5 meters)

to 10 ns (1.5 meters). In practice spectral weighting to reduce range side-lobes will limit the resolution to about 13 ns (2 meters). Moreover transmitter peak power requirements can be reduced by a factor of four if the same signal to noise ratio is to be maintained.

The P.C. system proposed herein can be considered a minimum risk design in that it involves presently practical state-of-the-art lithium niobate dispersive delay lines. It appears quite probable that in the next year or two dispersive lines with at least a fourfold increase in D (i.e., BW = 200 MHz, $\hat{t}_e$ = 2 µsec) may be made available. This would increase the altitude resolution capability to about 1 meter at a negligible weight and size penalty provided that sufficiently wideband RF circuitry is employed in the radar front end.

The increased altitude resolution possible with the addition of P.C. processing will significantly improve the accuracy of altitude measurements at low sea states in that the compressed pulsewidth can now be better matched to the altitude distribution of quasi calm sea waves (i.e., $\hat{t}_c c = h_p$ = 4 meters) where $\hat{t}_c$ = compressed pulse width and h_p = ave peak-to-trough height of sea waves). Furthermore, the system will now provide the capability of developing a multigate processor that could specifically match the returned signal to specific sea conditions.

Lowering the peak power transmitted will significantly improve tube life-time and power supply sizes using conventional microwave tubes (i.e., TWT's). The ultimate payoff in reliability as well as weight and size derived from the reduction in peak power would be the realizability of the transmitting function through solid state devices. This becomes practicable when peak power requirements are lowered to the one watt region. As has already been pointed out, this objective can be pursued if one is willing to forego improvement in resolution. Specifically, one may consider using a dispersive delay

3-17

line which yields a 5 μsec expanded pulse with a 20 MHz chirp sweep (see Figure A-5 in Appendix A). Now, the altimeter resolution is maintained at 50 ns, but the peak power requirement is reduced to 10 watts which is within striking distance for solid state implementation. As lines with D = 100 over 20 MHz bandwidth are realized, solid state implementation becomes even more realistic.

Use of the LiNb O_3 dispersive delay lines for P.C. provides the system with an unusual degree of performance, flexibility, effectiveness, and growth potential since lines with different dispersion and bandwidth characteristics could be mounted as they are made available at a negligible price in weight and size and without requiring major redesign of interfacing equipment.

3.2.2.3 Chirp Pulse Compression Using Dispersive Delay Lines

The heart of a P.C. system is the device or mechanism which implements matched (optimum) filtering. The selection of the system proposed was dictated by the remarkable weight, size, and cost advantages provided by presently developed ultrasonic wave delay lines using surface propagation on lithium niobate. By varying in a linear manner the spacing within each of two interacting interdigital electrode arrays, used for generating and detecting surface waves, the delay line becomes dispersive with a linear delay-frequency characteristic. Delay lines with such characteristics are ideally suited for linear FM (chirp) modulation/expansion of an impulsive input signal. Time compression of the signal through matched response upon reception can be readily instrumented by either utilizing the same two arrays in a conjugate configuration or, as is proposed here, to operate on the inverted spectrum (i.e., the time inverse) of the expanded signal (Figures 3-5). Background information on LiNi O_3 delay lines physical and performance characteristics is provided in attached Appendix A.

300 MHz   10.0 GHz

TRANSMITTER

Signal generated by   LO   PULSE TRANSMITTED
dispersive delay line   AND RECEIVED

                                         GHz   TRANSMITTER
                                         10.3

                            9.7   RECEIVER
100 MHz   GHz

                                         LO RECEIVER

Signal to the dispersive   100 MHz
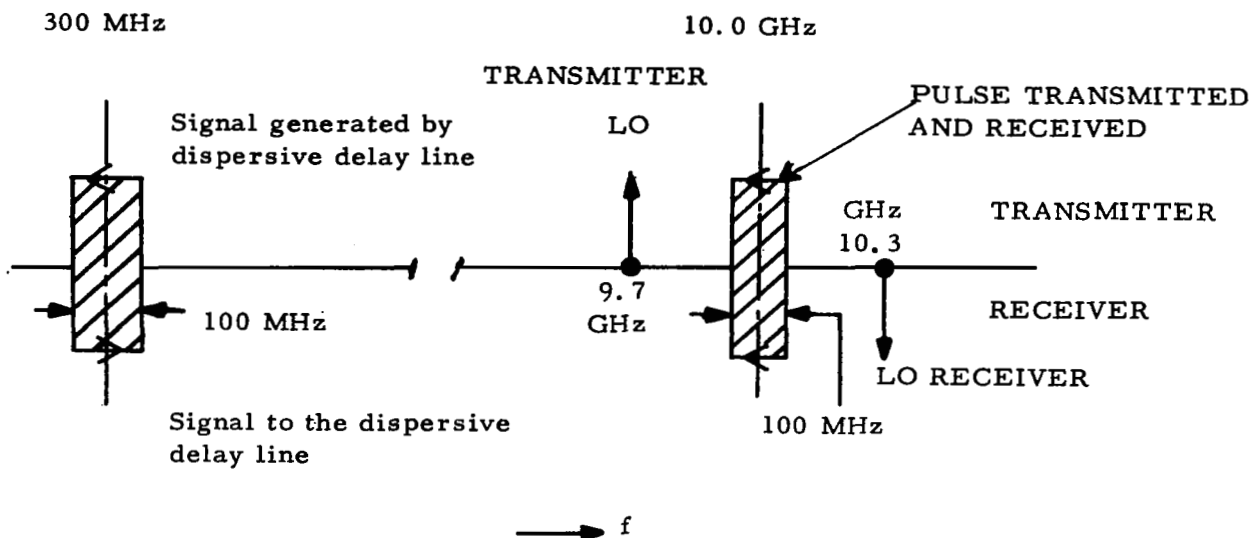delay line

⟶ f

Figure 3-5. Dispersion - Compression achieved by
Switching IF Sidebands

The delay-frequency characteristics shown display a variable fre-
quency ripple superimposed over the linear slope. This ripple is due to the
abrupt discontinuity in the time waveform as a result of the finite delay line
length and is characteristic of the Fresnel integral solution describing the
transform of a linearly frequency modulated square wave. Appendix A points
to the fact that the size of the ripple can be reduced by gradually tapering
off the degree of interdigital coupling near the array edges. In effect this
provides spectral weighting within the dealy line itself, rather than,
as is generally done, to control time sidelobes of the compressed pulse by
external weighting at the receiver. Since weighting within the delay lines
would result in amplifying a tapered waveform on transmission, with the
attendant loss in energy management, the proposed system will utilize un-
weighted lines. A filter will provide the necessary taper following the
collapsing operation.

3.2.3 Hardware Error Sources

There are new sources of error which are directly attributable to the
introduction of pulse compression. They might limit the performance of the
proposed P.C. system. They are caused by:

3-19

- Timing errors

- Errors due to temperature change

Timing errors have already been discussed in paragraph 3.2.2.1. System errors, such as range sidelobe, altitude rate error, and attitude error have already been discussed in Section 2.

3.2.3.1 Errors Due to Temperatures Changes

Temperature changes will induce errors by changing the delay frequency characteristic of the dispersive lines. Although there are no experimental results available about the effects on the lithium niobate lines to be utilized in the proposed P.C. system, there are indications that the interdigital spacing between array elements varies by 80 parts/10^6/°C. Since cyclic changes in temperature are expected to exceed the 1 sec integration time of the radar processor, temperature effects will be translated to altitude. Assuming temperature stabilities of the order of ±4°C within the temperature controlled part of the vehicle,

$$f_o = 300 \text{ MHz, and a center frequency delay of} \tag{3-3}$$

$$\tau_{max} = 5 \mu \text{sec}$$

one would expect delay shifts of ±.4 ns. The 0.4 ns uncertainty in time limits the maximum bias to 24% of the compressed pulse.

3.2.4 Pulse Compression Block Diagram

The Pulse Compression Receiver will interface with other components in the Radar System in the same manner that a pulsed CW receiver would.

Maximum signal and noise levels are shown on the block diagram of Figure 3-6. It should be noted that all noise levels are taken at a 100 MHz bandwidth except for the noise level after weighting which is 50 MHz.

The signal level before the preamplifier does not reflect the maximum signal energy that could be received, it only indicates the maximum signal handling capability of the complete receiver as shown at that point. With the use of AGC (40 dB) the dynamic range at the output of the receiver would be about 70 dB. Figures 3-8 and 3-7 show the AGC low and the power requirements needed to obtain a 28 dB output dynamic range.
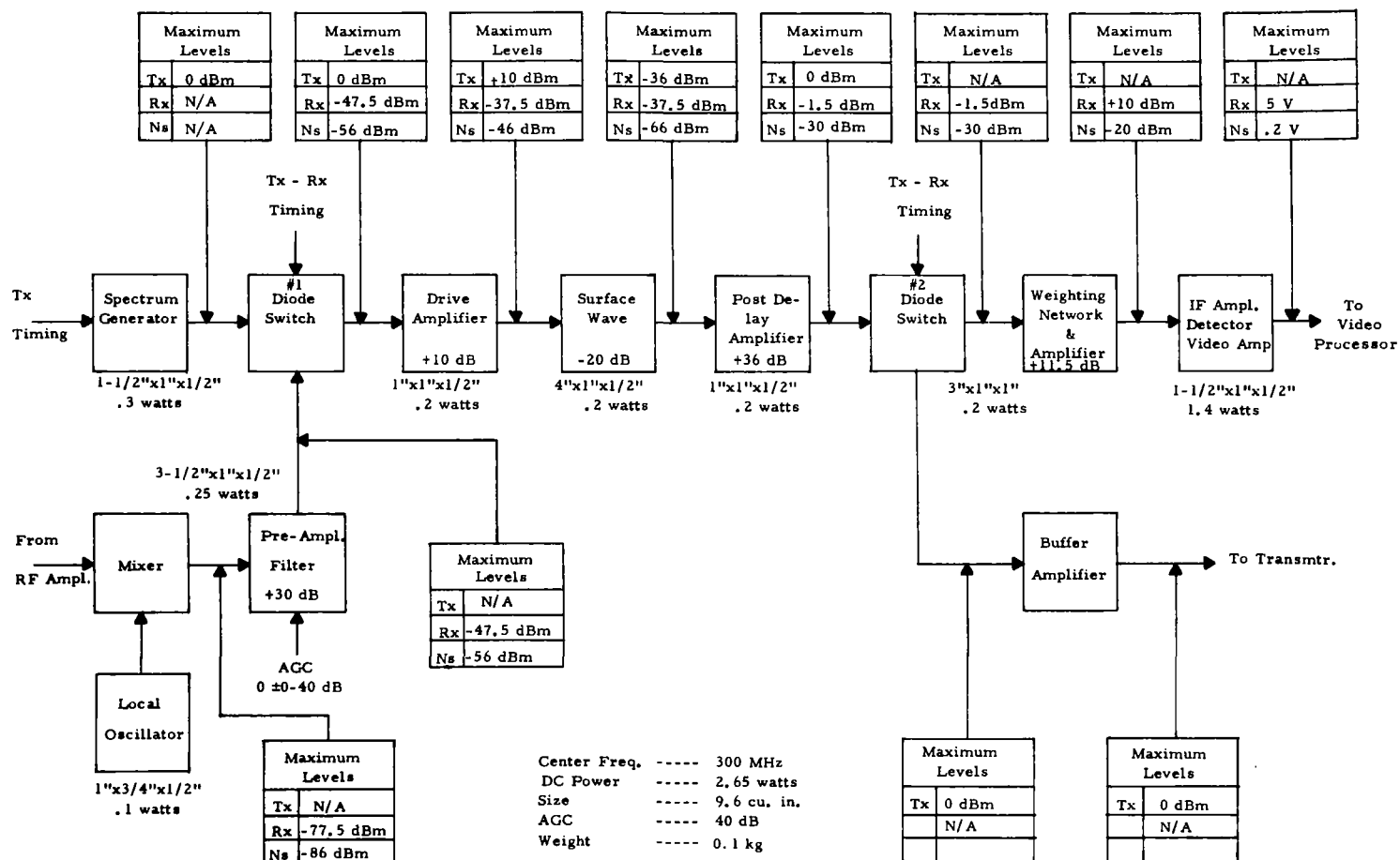
Maximum Levels tables across the top:

Maximum Levels		**Maximum Levels**		
Tx	0 dBm	Tx	0 dBm	
Rx	N/A	Rx	-47.5 dBm	
Ns	N/A	Ns	-56 dBm	

Maximum Levels

Tx	0 dBm
Rx	N/A
Ns	N/A

Maximum Levels

Tx	0 dBm
Rx	-47.5 dBm
Ns	-56 dBm

Maximum Levels

Tx	+10 dBm
Rx	-37.5 dBm
Ns	-46 dBm

Maximum Levels

Tx	-36 dBm
Rx	-37.5 dBm
Ns	-66 dBm

Maximum Levels

Tx	0 dBm
Rx	-1.5 dBm
Ns	-30 dBm

Maximum Levels

Tx	N/A
Rx	-1.5dBm
Ns	-30 dBm

Maximum Levels

Tx	N/A
Rx	+10 dBm
Ns	-20 dBm

Maximum Levels

Tx	N/A
Rx	5 V
Ns	.2 V

Tx - Rx Timing

Tx Timing → Spectrum Generator → #1 Diode Switch → Drive Amplifier +10 dB → Surface Wave -20 dB → Post Delay Amplifier +36 dB → #2 Diode Switch → Weighting Network & Amplifier +11.5 dB → IF Ampl. Detector Video Amp → To Video Processor

Tx - Rx Timing

1-1/2"x1"x1/2" .3 watts

1"x1"x1/2" .2 watts

4"x1"x1/2" .2 watts

1"x1"x1/2" .2 watts

3"x1"x1" .2 watts

1-1/2"x1"x1/2" 1.4 watts

3-1/2"x1"x1/2" .25 watts

From RF Ampl. → Mixer → Pre-Ampl. Filter +30 dB

Local Oscillator

1"x3/4"x1/2" .1 watts

AGC 0 ±0-40 dB

Buffer Amplifier → To Transmtr.

Maximum Levels

Tx	N/A
Rx	-47.5 dBm
Ns	-56 dBm

Maximum Levels

Tx	N/A
Rx	-77.5 dBm
Ns	-86 dBm

Center Freq. ----- 300 MHz
DC Power ----- 2.65 watts
Size ----- 9.6 cu. in.
AGC ----- 40 dB
Weight ----- 0.1 kg

Maximum Levels

Tx	0 dBm
	N/A

Maximum Levels

Tx	0 dBm
	N/A

3-22

Figure 3-6. Chirp Receiver Block Diagram

This graph shows the power requirements for the two IF stages that drive the Detector.

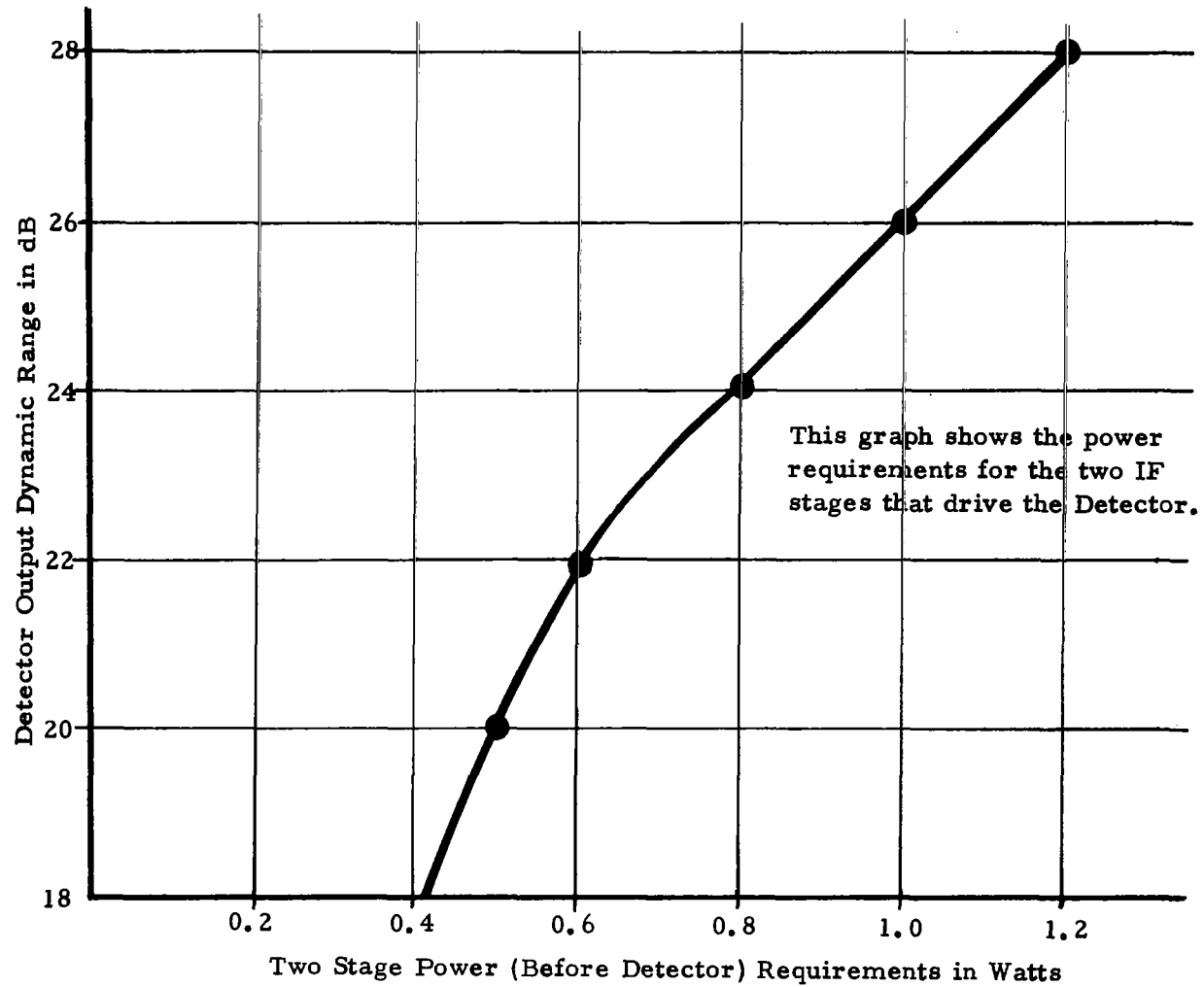Two Stage Power (Before Detector) Requirements in Watts
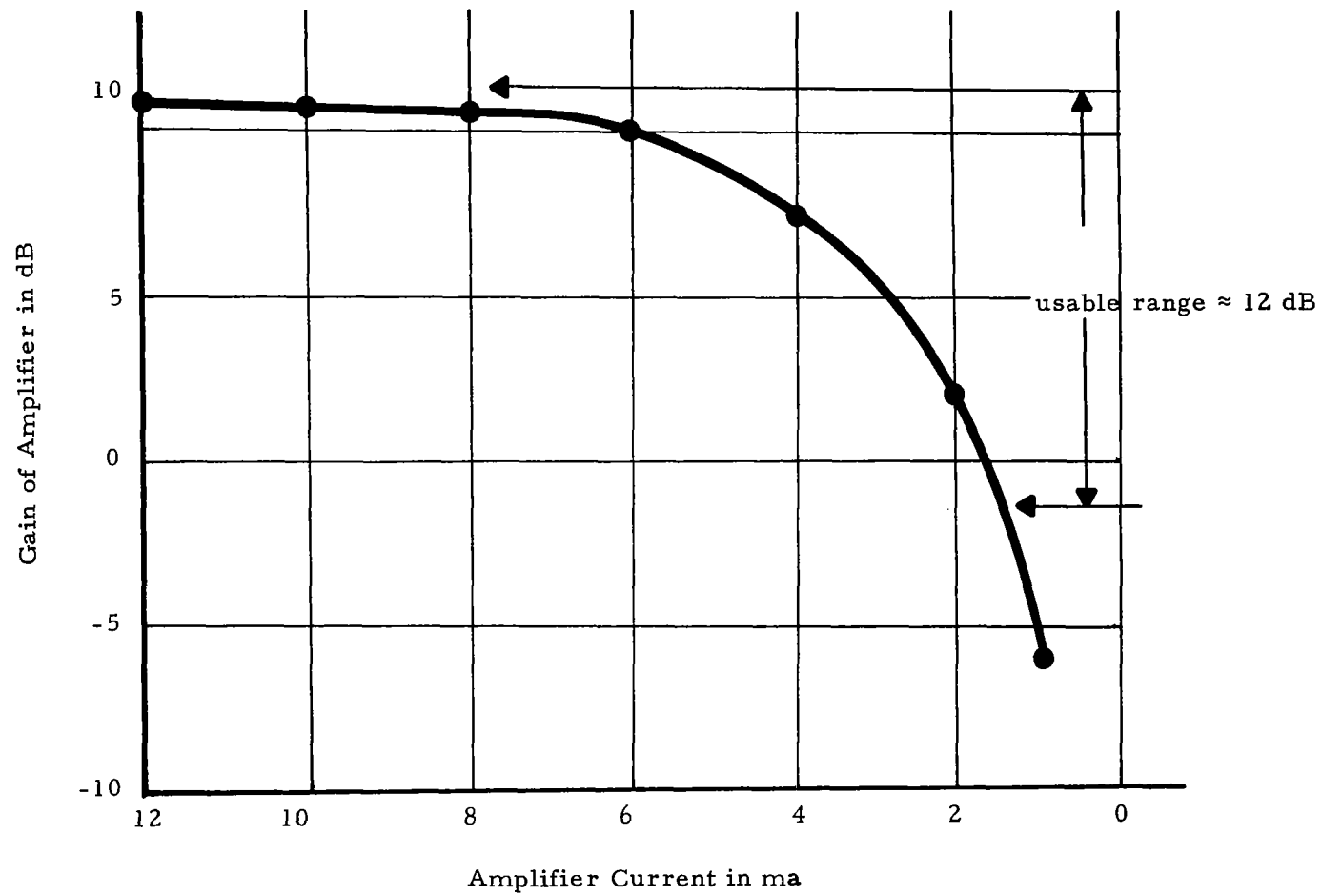
Figure 3-7. Dynamic Range Vs. Power

Figure 3-8.   Single Stage Gain Vs Current

3.2.5 Hardware Description

The local oscillator, second mixer, and preamplifier filter are not unique to a pulse compression system. The only requirement placed on these components by this chirp system is that the spectrum of the received signal must be inverted from that of the transmitted signal. This is accomplished by having the local oscillator at a higher frequency than the first IF and selecting the lower sideband out of the mixer.

The characteristics of each functional element in the pulse compression system has been determined and the results are presented in Figure 3-6. These are size, power gain and signal levels.

The spectrum generator receives a digital command at time zero in the transmit order and generates a pulse which is one cycle of 300 MHz. A modest amount of filtering may be necessary at the output of the generator to ensure that most of the energy delivered to the dispersive delay line is limited to its useful chirp bandwidth. This is required when the dispersive characteristic is double-valued. It is anticipated that the spectrum generator would have four active stages.

The drive amplifier and post delay amplifier are relatively straightforward devices, having flat amplitude and delay characteristics over the chirp bandwidth. The drive amplifier is a two stage device and its output must match the input impedance of the dispersive delay line. Similarly, the input of the post delay amplifier must match the output of the delay line. This amplifier requires four stages to achieve the necessary gain.

The diode switches select the appropriate input and output to and from the dispersive delay line and its associated amplifiers according to transmit-receive commands. The switches are diode bridge arrangements with a bridge for each IF input. A buffering stage and a control stage will be required for each bridge circuit.

The weighting filter-amplifier further amplifies the compressed IF waveform and reduces the range sidelobes to a level at least 30 dB below the main lobe level. The weighting function approximates a $\overline{N} = 34$ dB Taylor weighting and has a transfer characteristic proportional to within a linear gain factor.

$$H(F) = \text{rect } (\frac{F - 300}{100}) [1 + 0.69 \cos \frac{2\pi (F - 300)}{100}] \tag{3-5}$$

where F is in megahertz. Two active stages will be required to achieve the appropriate buffering and gain for the circuit.

The detector-video amplifier raises the level of the compressed, weighted IF signal for square law detection. Figure 3-7 shows the power required for certain values of instantaneous dynamic range. Two IF amplifier stages and two video amplifier stages will be required for this function.

The surface wave dispersive delay line proposed for this system has a 300 MHz center frequency with a dispersion bandwidth of 100 MHz and a dispersion time of 1 μsec. Typically, the insertion loss (CW) of a surface wave device is 15 to 20 dB; and temperature coefficient is 50 to 100 ppm/$^{\circ}$C. Assuming a center frequency delay of 1μsec, the temperature of the line must be controlled to 4 ° C to maintain less than .4ns range error. If a narrower dispersion bandwidth (and hence less resolution) can be tolerated, lines built at lower center frequencies are capable of dispersion times of 5 μsec or greater. A 5 μsec pulse would reduce the peak transmitter power required to 10 watts which is very close to the power capability of solid state C-band transmitters.

3.3 Transmitter Implications of Pulse Compression - F. F. Reed

3.3.1 Introduction

Our basic problem is to determine whether or not there is any advantage in using pulse compression in a satellite altimeter from a transmitter point

of view . For example, if the 1 kw short pulse system is used; could the existing source be utilized in a pulse compression system and would there be any advantage (i. e., a reduction in size, weight or modulation requirement of the source) in changing the peak power level of the system? In addition, could solid state sources be considered? This section attempts to examine this problem and serves as basis for the conclusions that are drawn about RF sources of power.

3.3.2 Klystrons

Klystron tubes do not in general, have sufficient bandwidth for pulse compression, using a predispersed signal, or phase coded techniques. This however would find application if the serrodyne technique were to be implemented.

3.3.3 Magnetrons and CFA's

Magnetrons and CFA's are the highest efficiency sources of RF power. They fail in meeting the system accuracy requirements because they lack adequate pulse stability and freedom of jitter to function effectively at accuracy levels of 1/2 meter and less. Life would also mitigate against magnetrons.

3.3.4 TWT Considerations

Assume for the moment that a 1-5 kw, short pulse (50 ns) system would be used initially with later conversion to pulse compression if possible. The TWT used for this system would most likely be an outgrowth of a proposed Raytheon development program .

Conversion to a "chirp" pulse compression system would require approximately 1 μsec pulses and a 200-300 MHz instantaneous bandwidth. Discussions with Dr. Winsor at Raytheon Power Tube Division indicate that the proposed tube can easily accommodate this bandwidth and pulse duration, lending

itself nicely to a chirp system. Phase linearity data is not presently available. This tube will have a projected electron efficiency of 25% or 30% operating with a depressed collector, excluding the power consumed by the heater. Expected operating lifetime for this tube will be in excess of 10,000 hours.

Now, consider the ramifications of changing the system power level. An increase to a 10 kw system could complicate matters severely. While the electron efficiency could be maintained at the 25 - 30% level, other complications would most certainly arise in the circuits providing power and modulation to the tube because of the higher voltages involved. This would necessitate an increase in the size and weight of these components as well as the increased size of the tube itself, being probably twice as large as a lower powered version. In addition, a driver stage would be required since the maximum gain expected in a tube of this type would be roughly 50 dB. It would seem, then, that since pulse compression would improve the performance of a lower power system, there would be little advantage in considering a higher power level.

Opposed to this, a system power level on the order of 50 - 400 watts peak might be considered. Clearly at these power levels there would be a saving in size and weight, the drawback however, is that the efficiency of the tube would be lower. The electron efficiency is dependent on the I/V ratio of the beam. Given the perveance obtainable in existing tubes, the low power tubes operate at a lower I/V ratio than tubes at the 1-5 kw level resulting in efficiencies of 10-20% for tubes in the 50 - 400w range. This lower efficiency would have to be weighted against any size and weight reductions that might take place. The operating life of the low power tube should be essentially equal to, or slightly greater than the higher power version.

Indications are that future TWT development effort will be concentrated in size reduction and lifetime improvement rather than increased efficiency, the efficiency being limited by certain complex constraints of the beam-field interaction in the tube. There should be significant improvements in operating life. Five to ten thousand hours are within reality now; Raytheon Power Tube Division is currently working on a 45,000 hour L-band tube; and Eimac is marketing a 1 watt, 50,000 hour MTBF design (although not guaranteed) for airborne service.

One last concern of a TWT system was that of feed through noise generated by the TWT in the absence of an RF pulse. Dr. Winsor indicates that control grid modulated tubes have residual beam current on the order of microamperes, concluding that noise feed through should not be a problem and that there should be no need to gate the collector supply.

It seems clear that the present technology favors continuation of the proposed 1-5 kw system since this gives the most efficient tube design and could be used in to a chirp system with little difficulty. Some modulator revisions might be necessary to accommodate the longer pulse width, but if the rise-time requirements could be relaxed, some saving in complexity might be possible here.

3.3.5 Applicability of Solid State Sources

The consideration of solid state sources for this application may require some reconsiderations in system design. Here a much lower power level (roughly 10 watts peak) would have to be considered with a corresponding increase in pulse width[9]. It would be desirable, if possible, to consider some kind of solid state amplifier which could be more or less substituted for the TWT. The only existing device which could be used in this application is the avalanche diode, operating as a reflection amplifier. In this mode the device

operates much like a tunnel diode amplifier but at a much higher power level. Considering that pulse width up to 10 μsec might be required, the device must have CW ratings roughly equal to the pulse power requirements if it is to operate satisfactorily. Existing, commercially available, X-band diodes can generate 1 watt cw as a fixed tuned oscillator at 5 to 7% efficiency, with operating life projected in excess of 15,000 hours. Experimental X-band devices have produced 4 watts CW at Bell Laboratories. Based on this, an avalanche amplifier with power output on the order of 10 watts could be expected to be developed in the near future. Raytheon, Bedford has a solid state, 3 stage, S-band amplifier (here using hybrid Gunn devices rather than avalanche diodes because of the lower frequency) with 20 watt peak power output in a 20 μsec pulse width. The unit has 7 dB gain per stage over a 120 MHz band at 3 GHz. The one major drawback to these devices would be their efficiency per stage would have an overall efficiency of 8%, much lower than any available TWT. However, the operating potentials would be much lower and the need for a modulator non-existent, producing a considerable saving in size and weight of these components, not to mention the size of the amplifier (about 3 in^3) compared to a tube. In light of this a development program in this area as a follow-up to a TWT system should be considered in spite of the lower efficiency.

The other solid-state approach that might be used is a frequency multiplier chain. This would require a different configuration, probably a serrodyne arrangement shown in Figure 3-9. Here we could have an S-band high power oscillator driving a times 4 multiplier. Assuming 50% oscillator efficiency and 20% for a broadband quadrupler, overall circuit efficiency would be comparable to the avalanche diode system. At this time, multiplier diodes are available to provide 1-2 watts output at X-band, but even a higher power diode would be limited in the drive power available from current S-band transistors. Also, most high power device development is being concentrated
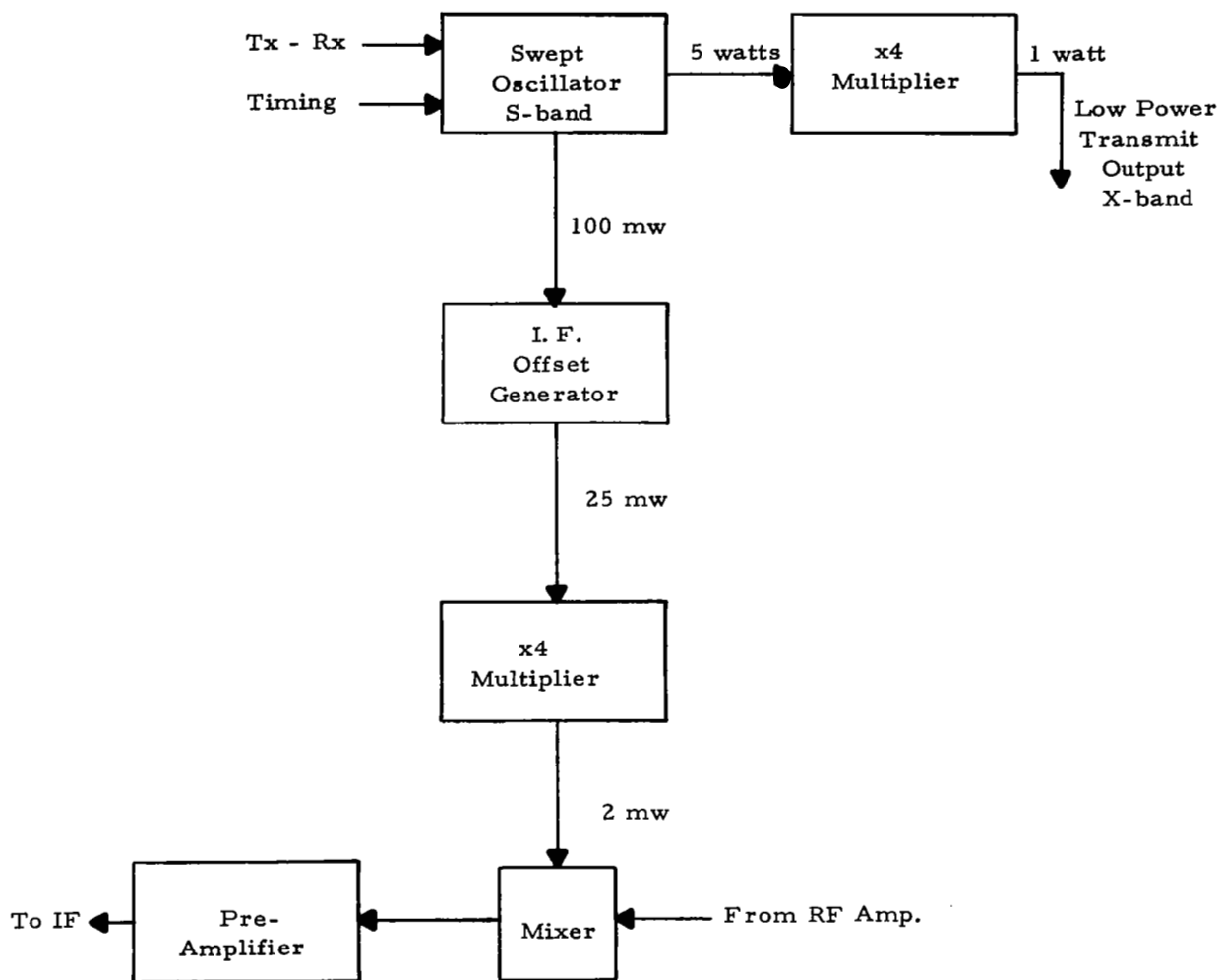
Figure 3-9. Serrodyne System Using Frequency Multipliers

on avalanche diodes rather than varactors. In addition, this system is more complex, requiring two multipliers and a sidestep generator making it less desirable than the avalanche diode amplifier.

3.3.6 Conclusions

On the basis of present information, it would seem best to go ahead with a 1 kw TWT system whether or not pulse compression is considered, leaving provision for converting to a pulse compression system at a later date.

Solid state devices presently are incapable of generating the required peak power unless used in a multiple diode array, but considering the present development effort in this area, a follow-up program for a 10 w avalanche diode amplifier might be considered.

3.4 Explanation of the Power Budget

To provide a basis for direct comparison between radar altimeter designs, it is necessary that a commonality exist in the design assumptions. To provide this commonality, we have reinterpreted the SGAS system power allocation based upon power efficiencies shown in Figure 2-1.

The three systems that are compared in Table 3-4 are all referenced to the SGAS computation for adequate S/N on a single pulse basis. This point $\boxdot$ is identified on Figure 2-3 as SGAS recommended system. On this same figure, the other two systems are also shown: The short pulse (10 ns) system $\triangle$, the compressed pulse system $\bullet$. Here the peak power of the short pulse system has been increased by a factor of 100. This increase is to provide adequate single pulse signal to noise ratio when one pulse is shortened (an extra factor of 4 is included that does not change conclusions). The pulse compressed system is then established by expanding this narrow transmitted pulse by a compression ratio of 100:1 relative to the short compressed pulse system. Each of these systems integrates a number of single pulses f_r to further improve S/N and to improve the signal clutter ratio of the

limit defined by the speed of the vehicle. The average power is then given by

$$P_{AV} = P_{PK} f_r \hat{t}$$

The efficiencies of these systems and hence the DC power requirements can be established from the curves of Figure 2-1 using the peak and average power requirements of each system. The receiver modulators and processors for the three systems are assumed to require 20 watts.

TABLE 3-4

	PRF	P_{PK}	P_{AV}	Efficiency	DC Transmitter Power
SGAS System	100,000	1 kw	5 w	22%	23
Short Pulse System	1,000	100 kw	1 w	2%	50
Short Compressed Pulse System	1000	1 kw	1 w	15%	7

3.5 Complete System Incorporating Pulse Compression

A system block diagram for the pulse compression altimeter is shown in Figure 3-10. A comparison of this diagram with Figure 4-1 of SGAS study will clarify the specific changes that are introduced by incorporating pulse compression into the system. One area that represents a substantial change from the SGAS system is the receiver. The receiver will become a broadband 100 MHz heterodyne receiver. The processor does not need to be changed to incorporate pulse compression.
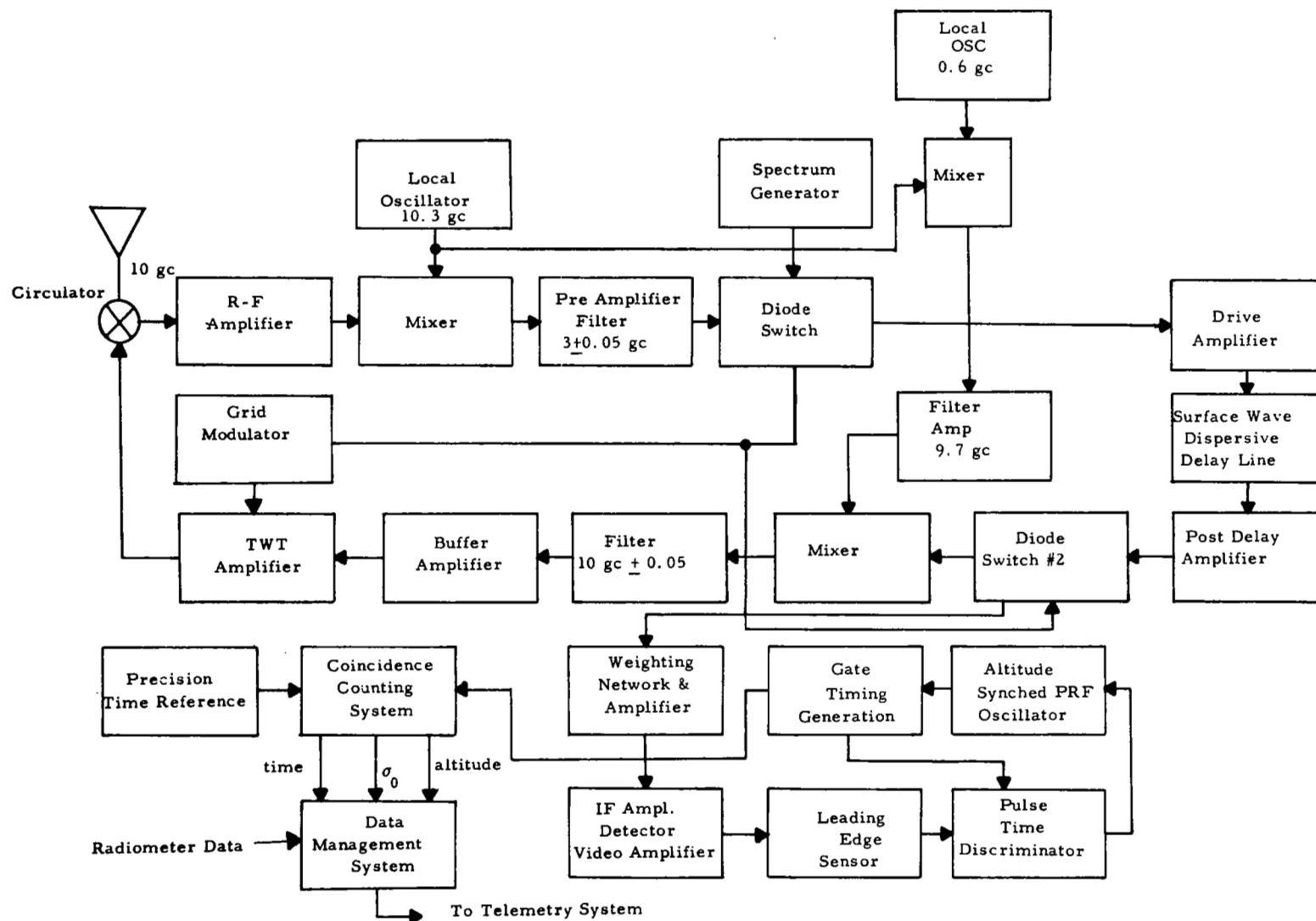
Figure 3-10. Radar System Block Diagram for Pulse Compression

SECTION 4

THEORETICAL ACCURACY LIMITS FOR SATELLITE ALTIMETRY

(T. Berger)

4.1 Accuracy Limitations

We have investigated the hardware and system considerations that limit
the accuracy of space altimeters. The question then arises are there any
limitations that nature imposes which would prevent us from measuring to this
accuracy.

There are two factors here:

- Ocean surface interaction
- Channel capacity limitations

The question of ocean surface interaction has already been identified as a
problem that requires experimental evidence to answer.

The second question which is treated in this section will tell us the
limitations that the channel has for ranging; enable us to compute the effect
of sidelobes (Appendix H); and suggest design possibilities for processing
systems.

The channel capacity analysis indicates an adequate channel capacity
for 10 cms. accuracy. The range sidelobes are also shown to make no
significant contribution (Appendix H).

Considerations from informations theory are brought to bear on the
problem. Specifically, Goblick's capacity bound is calculated for idealized
models of the satellite altimetry problem. This yields theoretical limits on
the range accuracy and information gathering capabilities of satellite altimeters
which suggest realistic system performance goals. Signal design techniques
for achieving these goals also are briefly discussed. In the course of the
analysis the range-doppler spread function (scattering function) of the radar
altimetry channel is derived which has applications in several related programs.

The scattering function that is developed here is used directly in estimating the error that is caused by range sidelobes. The theory that is developed here will ultimately contribute to a model that will result in a more credible model for predicting clutter effects on altimeter measurements.

4.2 The Satellite Altimetry Problem

A radar altimeter onboard an orbiting satellite surveys the ocean surface from an altitude of approximately 1000 km. System constraints impose limitations on certain crucial parameters such as average power, peak power, beamwidth, bandwidth, etc. The objective is to configure the altimetry system subject to these constraints such that the maximum possible accuracy is obtained in the measurement of the distance from the satellite to the mean ocean level at the nearest point on the surface.

In what follows we compute the capacity of the two-way radar channel in the satellite altimetry problem under various sets of idealizing assumptions. In each case this fixes the maximum rate at which information about the ocean surface can be extracted by a satellite altimetry system and hence, via Goblick's capacity bound, leads to a theoretical limitation on the ranging accuracy of the altimetry system. In particular, the capacity bound is computed for the following three channel models:

    a)   Ideal bandlimited additive white Gaussian noise (AWGN) channel

    b)   AWGN channel with a linear filter to simulate ocean impulse response

    c)   Fading dispersive, or "deep," channel with range-doppler scattering function and AWGN.

4.3 Goblick's Capacity Bound

A bound on radar ranging accuracy based on information theory considerations has recently been derived by Goblick[10]. The idea is to calculate an effective capacity for the two-way radar channel which depends,

naturally, on the peak power, average power, bandwidth, etc. If this effective channel has a capacity of C nats*/sec and is used for T seconds, then at most CT nats of information can be received. If the a priori distribution for the range is assumed Gaussian with mean h and variance σ^2, then Shannon's rate distortion theory[11] implies that the mean squared range error, ε^2, after time T satisfies

$$\varepsilon^2 \geq \sigma^2 \exp(-2CT).$$ (4-1)

It should be stressed that the lower bound to ε^2 provided by (1) may be far from attainable in practice. The reason for this is that it may not be possible to devise a signaling scheme which extracts information from the channel at the maximum possible rate all of which is expressly relevant to reducing the variance of the parameter of interest. We shall discuss this matter in greater detail subsequently.

4.4 Ideal Bandlimited AWGN Channel Model

As our first approximation we shall assume that the radar channel can be modeled as an additive white Gaussian noise (AWGN) channel with bandwidth B and one-sided noise spectral density $N_o = kT_e$ where T_e is the effective temperature of the receiver. The total energy E received during time T determines the signal-to-noise power ratio at the channel output, namely

$$\frac{S}{N} = \frac{E/T}{N_o B} = \frac{E/N_o}{BT}.$$ (4-2)

The capacity of the channel thus is given by Shannon's familiar formula[12]

$$C = B \log\left(1 + \frac{S}{N}\right).$$ (4-3)

---

* 1 Nat = $\log_2 \cdot$ Bits $\simeq 1.4$ Bits

It follows from (1) and (3) that after the radar channel has been used for T seconds we must have

$$\varepsilon^2 \geq \sigma^2 \exp\left[-2BT \log\left(1 + \frac{S}{N}\right)\right]$$

$$= \sigma^2 \left(1 + \frac{S}{N}\right)^{-2BT} \tag{4-4}$$

Goblick[10] refers to (4) as the "capacity bound" on radar ranging accuracy.

We see from (4) that a time-bandwidth product of BT=1 (uncompressed pulse) implies that the RMS range error is reduced by a factor of at most $\left(1 + \frac{S}{N}\right)$ from its a priori value of σ.

To illustrate the application of (4), let us use the parameter values listed in Table 4-1 which describe the radar altimeter proposed in[13]. The calculations done in Appendix R-B of[13] show that typical and worst-case S/N values for this system at the end of an essentially linear power ramp response of duration 50 ns are 91 (or 19.6 dB) and 2.5 (or 4 dB), respectively. The average signal power of the ramp response is only half of its peak value, so typical and worst-case average S/N values are about 45 and 1.25.[†] Assuming that $\sigma = 50$ m is representative of current knowledge of the geoid, we see from (4) that reception of a single, uncompressed pulse by this system cannot reduce the RMS range uncertainty to less than about 1m under typical conditions and 15m under worst-case conditions.

Let us now consider how system performance improves as the number n of pulses received increases. There is no theoretical reason why the next pulse shouldn't be able to reduce the range variance by the same factor as

---

[†] A more precise analysis will be carried out in the next section.

Table 4-1

Parameter	Typical Value	Worst Case Value	Remarks
P_t	1 lW	1 kW	Assumed transmitter pulse peak power
G	38 dB	38 dB	.76 m antenna-uniform illumination
λ	3 cm	3 cm	X-band, 10 GHz
σ_o	20 dB (10 knots wind)	10 dB (20 knots wind)	
c	3×10^{10} cm/sec	3×10^{10} cm/sec	
t	50 ns	50 ns	Transmitted pulse length assumed rectangular
h	1000 km	1300 km	
k	1.38×10^{-23}	1.38×10^{-23}	watts/°K/Hertz bandwidth
T_e	1690°K	1830°K	
B	20 MHz	20 MHz	
L	2	3	Propagation, mismatch, and microwave losses

did its predecessor, so the capacity bound clearly goes to zero exponentially as n increases (equivalently, as T increases in (4). However, in order to achieve such a "vernier effect," the system must be adaptive. If it continues to use the same pulse it used initially rather than to capitalize on the knowledge gained from the last measurement in order to optimally select the next transmission, the exponential decrease in range variance certainly will not be achieved. However, equipment limitations, especially in satellite-borne systems, often preclude the use of extensive adaptive circuitry, so the same waveform, selected with regard to the initial uncertainty, continues to be used after this uncertainty has been reduced. In such cases the RMS range error decreases only as the square root of the number n of (coherently) integrated

pulses. For example, with n=100 the bound on the accuracy achievable by the system discussed above becomes 0.1 m typically and 1.5 m in the worst case. The latter accuracy is marginal for the contemplated application.

It is of interest to calculate the variation of the capacity bound as a function of the BT product for a radar pulse with fixed energy E. Toward this end substituting (2) into (4) gives

$$\varepsilon^2 (BT) \geq \sigma^2 (1 + \frac{E/N}{BT})^{-2BT} \tag{4-5}$$

It follows that

$$\varepsilon_\infty^2 \triangleq \lim_{BT \to \infty} \varepsilon^2(BT) = \sigma^2 e^{-2E/N_o} . \tag{4-6}$$

Hence, increasing the BT product by means of pulse compression techniques improves matters but cannot drive the range error to zero. For the numerical values cited earlier, the single pulse lower bound on the RMS range error in the limit of infinite BT is 2.7×10^{-9} m and 13 m for the typical and worst cases, respectively.

The capacity bound is especially useful when S/N (or E/N_o) is small because it exhibits a strong threshold effect that is known to occur in practice. (In the previous example in which we let BT become infinite, threshold clearly occurs somewhere between the typical and worst-case S/N values.) For high S/N the capacity bound is not very enlightening since the well-known[14] Cramer-Rao bound on the minimum variance unbiased estimator is tighter.

4.5 AWGN Channel with Surface Impulse Response

The above analysis ignored the fact that the received signal must be of the form of electromagnetic backscatter from the region illuminated by the radar. To a first approximation this can be taken into account by incorporating a linear dispersive filter in the channel with an impulse response that corresponds to the signal received after transmission of an ideal impulse. In the case of satellite altimetry the _power_ response to an impulse is known[13], p. R-A-8 to vary with time in a manner roughly proportional to $e^{-\alpha t}$ where

$$\alpha = 2.77 \, c/h\theta_e^2$$
$$\theta_e = 3 \, \text{dB effective beamwidth.}$$

The low-pass equivalent of the RF channel therefore has a power step response of the form $(1-e^{-\alpha t})$ which for small αt is essentially a linear ramp. In order for a linear filter to behave in this way, the square of its _amplitude_ step response must be a ramp. That is, if h(t) is the impulse response of the linear filter, then we require

$$\left(\int_0^t h(x)dx \right)^2 = A^2 t \qquad , \quad t << 1/\alpha \tag{4-7}$$

It follows that the desired impulse response is

$$h(t) = A/2\sqrt{t} . \tag{4-8}$$

With h(t) given by (8), we obtain the communication channel shown in Figure 4-1 as our model of the ranging channel. The input power is P_t and the attenuation A represents the losses in the two-way radar path, namely

$$A^2 = \frac{G^2 \lambda^2 \pi \sigma_0 h \epsilon}{(4\pi)^3 h^4 L} . \tag{4-9}$$

The parameters in (9) are defined in Table 4-1.

It is shown in Appendix E that the capacity of the channel of Figure 4-1 is

Input

(Power = P_t)

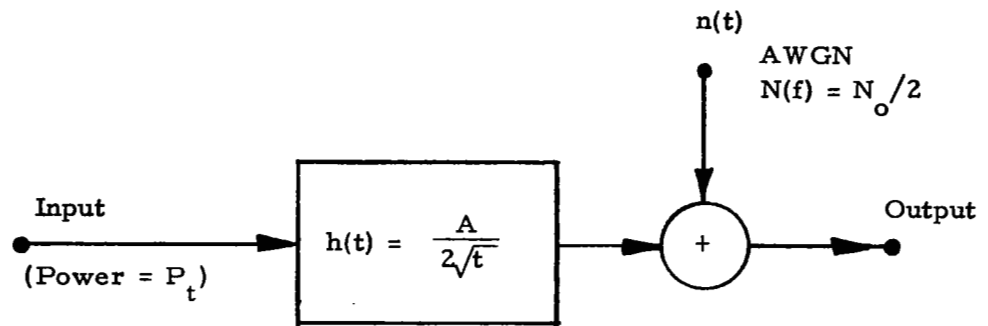$$h(t) = \frac{A}{2\sqrt{t}}$$

$n(t)$

AWGN

$N(f) = N_o/2$

Output

Figure 4-1.   Two-way Radar Channel Model with
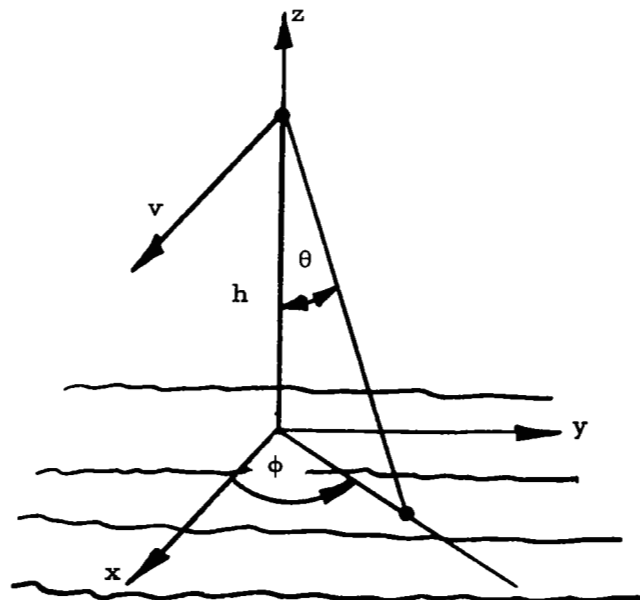Ocean Impulse Response and AWGN

Figure 4-2.   Backscatter Geometry

$$C = \sqrt{\frac{P_t A^2}{2 N_o}} \quad = \quad \left(\frac{P_t G^2 \lambda^2 \pi \sigma_o h c}{2(4\pi)^3 h^4 L k T_e} \right)^{1/2} \tag{4-10}$$

Plugging in the typical and worst case parameter values from Table 4-1 yields capacities of 1.4×10^8 and 2.32×10^7 nats/sec, respectively. When these are substituted into (1) with T=50 ns, we get single pulse RMS range accuracies of 0.001σ and 0.315σ in the typical and worst cases, or 0.05 m and 15m for an a priori standard deviation in range of 50 m.

4.6 Fading Dispersive Channel Model

A more refined model of the satellite altimetry radar channel takes into account the random nature of the backscatter from the dynamic ocean surface and the doppler shifts imposed by satellite motion. In particular, the two-way radar channel for the application in question is properly modeled as a fading dispersive channel, or so-called "deep" channel. The theory of deep channels was first applied to the problem of ranging to a surface by Price and Green in their fundamental studies of radar astronomy signal processing[15, 16]

A fading dispersive channel is described by a scattering function $\sigma(\tau, f)$ defined as follows. For any round-trip delay τ and doppler shift f, $\sigma(\tau, f) d\tau df$ equals the average signal power received per unit transmitted power with a delay in the interval $(\tau, \tau + d\tau)$ and a doppler shift in the interval $(f, f + df)$. It is assumed that when a sine wave is transmitted the in-phase and quadrature components of the received waveform are independent, identically distributed narrowband Gaussian random processes. This results in so-called "Rayleigh fading."

In the present problem the delay of the scattering facet at angle θ from the vertical and ϕ from the groundtrack depends on the propagation distance for a smooth sea plus the height of the local wave structure. (See Figure 4-2.) The doppler shift is determined principally by the satellite motion, the doppler caused by ocean wave motion being negligible in comparison.

The capacity of a fading dispersive channel having scattering function $\sigma(\tau, f)$ and AWGN of two-sided spectral density $N_o/2$ is [17], (Eq. 8.6.36), p. 438

$$C = \mu \int_{-\infty}^{\infty} \left[\frac{P_t \sigma(f)}{N_o} - \log \left(1 + \frac{P_t \sigma(f)}{N_o} \right) \right] df \qquad (4\text{-}11)$$

where

$$\sigma(f) = \int_{-\infty}^{\infty} d\tau \, \sigma(\tau, f) \qquad (4\text{-}12)$$

P_t = transmitter peak power

μ = transmitter duty factor = P_{av}/P_t

In Appendix F we show that $\sigma(f)$ for the two-way fading dispersive radar channel of Figure 4-2 is given by

$$\sigma(f) = \begin{cases} K_1 e^{-(\lambda f/2v\theta_e)^2} \displaystyle\int_0^{\sqrt{(2v/\lambda)^2 - f^2}} e^{-(\lambda z/2v\theta_e)^2} dz & \text{if } |f| \le 2v/\lambda \\ 0 & \text{if } |f| > 2v/\lambda \end{cases} \qquad (4\text{-}13)$$

where

$$K_1 = \frac{G^2 \lambda^4 \sigma_o}{2(4\pi)^3 h^2 v^2 L} \qquad (4\text{-}14)$$

The next step is to substitute (13) into (11) and integrate over f. The integral of $\sigma(f)$ is easily evaluated by changing to polar coordinates in the (f, z) plane. The result is

$$\int_{-\infty}^{\infty} \sigma(f)\, df = \int_{-2v/\lambda}^{2v/\lambda} \sigma(f)\, df = \frac{G^2 \lambda^2 \sigma_o \theta_e^2}{4(4\pi)^2 h^2 L} \left[1 - e^{-(1/\theta_\varepsilon)^2} \right] \qquad (4\text{-}15)$$

Since $N_o = kT_e$ we get

$$C = \frac{\mu P_t G^2 \lambda^2 \sigma_o \theta_e^2}{4(4\pi)^2 h^2 L k T_e} \left[1 - e^{-(1/\theta_e)^2} \right]$$

$$- \mu \int_{-2v/\lambda}^{2v/\lambda} \log \left[1 + \frac{P_t K_1 e^{-\left(\frac{\lambda f}{2v\theta_e}\right)^2}}{kT_e} \int_0^{[(\frac{2v}{\lambda})^2 - f^2]^{1/2}} e^{-(\frac{\lambda z}{2v\theta_e})^2} dz \right] df \qquad (4\text{-}16)$$

In most applications $\theta_e \ll 1$, so this detailed formula is well-approximated by

$$C \cong \frac{\mu P_t G^2 \lambda^2 \sigma_o \theta_e^2}{4(4\pi)^2 h^2 L k T_e} - \frac{2\mu v \theta_e}{\lambda} \int_{-\infty}^{\infty} \log(1 + K e^{-x^2})\, dx \qquad (4\text{-}17)$$

where

$$K = \frac{\sqrt{\pi}\, P_t v \theta_e K_1}{\lambda k T_e} \qquad (4\text{-}18)$$

The integral in (17) apparently cannot be evaluated in closed form, so a computer was used. Figure 4-3 shows the integral I(K) vs the parameter K. For $\theta_e = 2^o = 0.035$ rad, $v = 7.36$ km/sec, and the typical-case

4-11

target like that of the altimetry problem because most of the energy is far from the leading edge of the return. The number of pulses that can be coherently averaged in this scheme is reduced by the ratio of the beam-limited angle to the pulse-limited angle, but the power per return goes up roughly as the square of this ratio, so there is reason to hope for an improvement overall.

4.7 Summary and Recommendations

Three models for the satellite altimeter radar channel have been analyzed. Bounds on the range accuracy attainable have been calculated in each case. The analysis in all cases suggests that it might be possible to obtain rapid convergence of estimated range to true range by employing adaptive signaling schemes to achieve a "vernier" effect.

The "deep," Rayleigh fading channel model was analyzed in considerable detail. The scattering function was calculated and then used to determine the channel capacity. The typical and worst-case parameter values cited above yield capacities of 8×10^8 and 5×10^7 nats/second. The corresponding bounds on the RMS range accuracy for a 50 ns pulse and 50 m initial uncertainty are 2.1×10^{-16} m and 4.2 m, respectively. These accuracies can be improved by combining pulses that are sufficiently separated in time and/or space to experience independent Rayleigh fading. Approximately 1000 such independent pulses can be obtained with a single antenna during the one second interval that the target area is in the beam. This improves the above accuracies by a factor of $\sqrt{1000}$ so that, even with the worst-case parameters, an RMS error of less than 10 cm is not ruled out.

A more complete analysis should be undertaken in which the random space-time properties of the target field are explicitly considered and the theory of statistically optimum design and processing of signals is brought to bear on the problem. The groundwork laid by the radar astronomy studies of Price and Green[15,16] should prove very beneficial in this endeavor.

APPENDIX A

DISPERSIVE DELAY LINES USING ULTRASONIC SURFACE WAVES[*]

R. H. Tancrell, M. B. Schultz, H. H. Barrett,
L. Davis, Jr., M. G. Holland

The use of surface ultrasonic waves in place of bulk waves for UHF and microwave delay lines has generated a great deal of enthusiasm recently. We have attempted to demonstrate the utility of this approach by making dispersive delay lines designed to operate at 60 MHz with 20 MHz bandwidth. The devices have low insertion loss and the characteristics can be accurately predicted, but of more importance, devices of this type will be extremely simple to construct, low cost, and highly reproducible. For example, the devices discussed here were made by standard photolithographic techniques on polished surfaces of single crystal lithiumniobate.

Nondispersive delay lines using interdigital arrays on a piezoelectric surface have been described[18]. If the array periodicity is varied, dispersive time delay can be obtained[19]. A dispersive device, using two arrays, is shown schematically in Figure A-1. Each frequency component f can be thought of as being generated at the position along the array where the spacing is half an acoustic wavelength, $\lambda/2 = T = r/2f$, where r is the surface wave velocity and T the element spacing which varies with position. The high frequency waves travel a shorter distance and have less delay than the low-frequency waves; the total structure is dispersive.

When this symmetric device is used as a pulse expander or compressor[20], half of the operation is carried out in each array. Each array responds to the full frequency range of the input chirped pulse but provides only one half of the total time dispersion.

Consider a pulse with linear dispersion where the instantaneous frequency f changes at a rate $df/dt = a$. For a device to respond to this signal
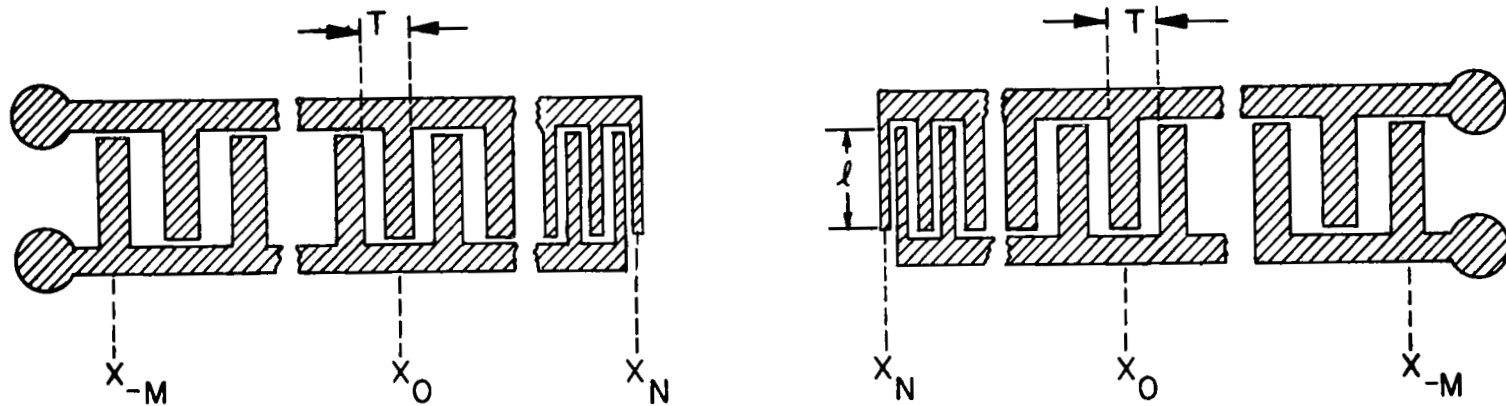
Figure A-1. Interdigital Arrays for a Dispersive Delay Line. The period
T of each array varies across each structure.

it must be designed so that the center position x_n of the nth element in the array is given by

$$x_n + \frac{rf_o}{2a} = \left\{ \left(\frac{vf_o}{2a}\right)^2 + \frac{m^2}{2a} \right\} \qquad -M \leq n \leq N. \qquad (A-1)$$

As shown in Figure A-1, x_o is measured from the central region of the array where the center frequency f_o is generated. The number of elements in the array $(N + M + 1)$ is chosen to achieve the desired bandwidth for a given a. Equation (A-1) is of the same form as that found for the transducer grating of the perpendicular diffraction delay line[21], but the conditions for the constructive and destructive interference between waves is different for the two devices. The operation of the perpendicular diffraction device is based on the fact that the energy from each element in the array radiates in two dimensions, whereas in the surface wave device the energy from each element in the array radiates only along one dimension of the surface.

Electrically, each interdigital structure can be represented as a parallel RLC circuit, with the resistive and inductive elements frequency dependent[18]. The resistance is minimum at the center frequency and is due primarily to the loading by the piezoelectric surface. It can be varied from device to device by changing the length 1 of the array elements. At the center frequency, the measured resistance of the various devices was between 50 and 180 Ω and the reactance was between 20 and 50 Ω capacitive, including leads and connectors. Broadband matching of each array to a 50 Ω line has been achieved by adding a shunt capacitor and a series inductor to the input capacitance to form a pi network.

The phase and amplitude characteristics of the surface wave device can be accurately predicted using a simple model. The model treats the edges of the teeth as sources of ultrasonic stress since the electric field gradient is largest there. The contribution from each tooth is added, with appropriate phase, to obtain the response of the entire structure. Computed

phase and amplitude characteristics are shown in Figures A-2 and A-3. The
derivative of the phase shift with frequency $(1/2\pi)(d\phi \; df)$ is plotted to illustrate
the dispersion of the device since this can be interpreted as the time delay
experienced by an RF pulse passing through the device. For comparison
measured phase and amplitude characteristics are also shown. The ripples
in the characteristic are due to the abrupt discontinuity in the comb structures
at their ends. These ripples can be reduced by gradually reducing the piezo-
electric coupling factor near the ends of the combs; for example, by reducing
the overlap region of the teeth near the comb ends. The results obtained,
both experimentally and theoretically, with a cosine-type weighting are shown
in Figure A-3. Clearly, the device characteristics show less ripple than
the unweighted case, but the experimental weighting is not yet completely
effective.

The device has been used to expand a short ~50-nsec pulse to ~ 1 μsec
and to compress a 1-μsec chirp[20] to about 50 nsec. The results were consistent
with a compression ratio of about 20 and the measured phase characteristics.
The conjugate filter has been made by interchanging the positions of the two
arrays shown in Figure A-1. Much higher compression ratios should be
possible with this approach. The interdigital arrays can be designed to gen-
erate and detect over a frequency range of 100 percent of the center frequency,
limited by third harmonic generation in the transducer[22]. The actual operating
3 dB bandwidth of the device will be less than 100 percent and could also be
limited by the generation of spurious bulk waves[21]. However, if weighting were
used to improve the phase characteristic, our calculations and experiments
indicate that the operating bandwidth could be decreased to about 40 percent
of the center frequency. This restriction still implies a bandwidth of about
100 MHz at a center frequency of 3MHz. The time dispersion of the device
is determined by the size of the interdigital array and so will, in fact, be
limited by the mask-making facility, but many microseconds should be easily
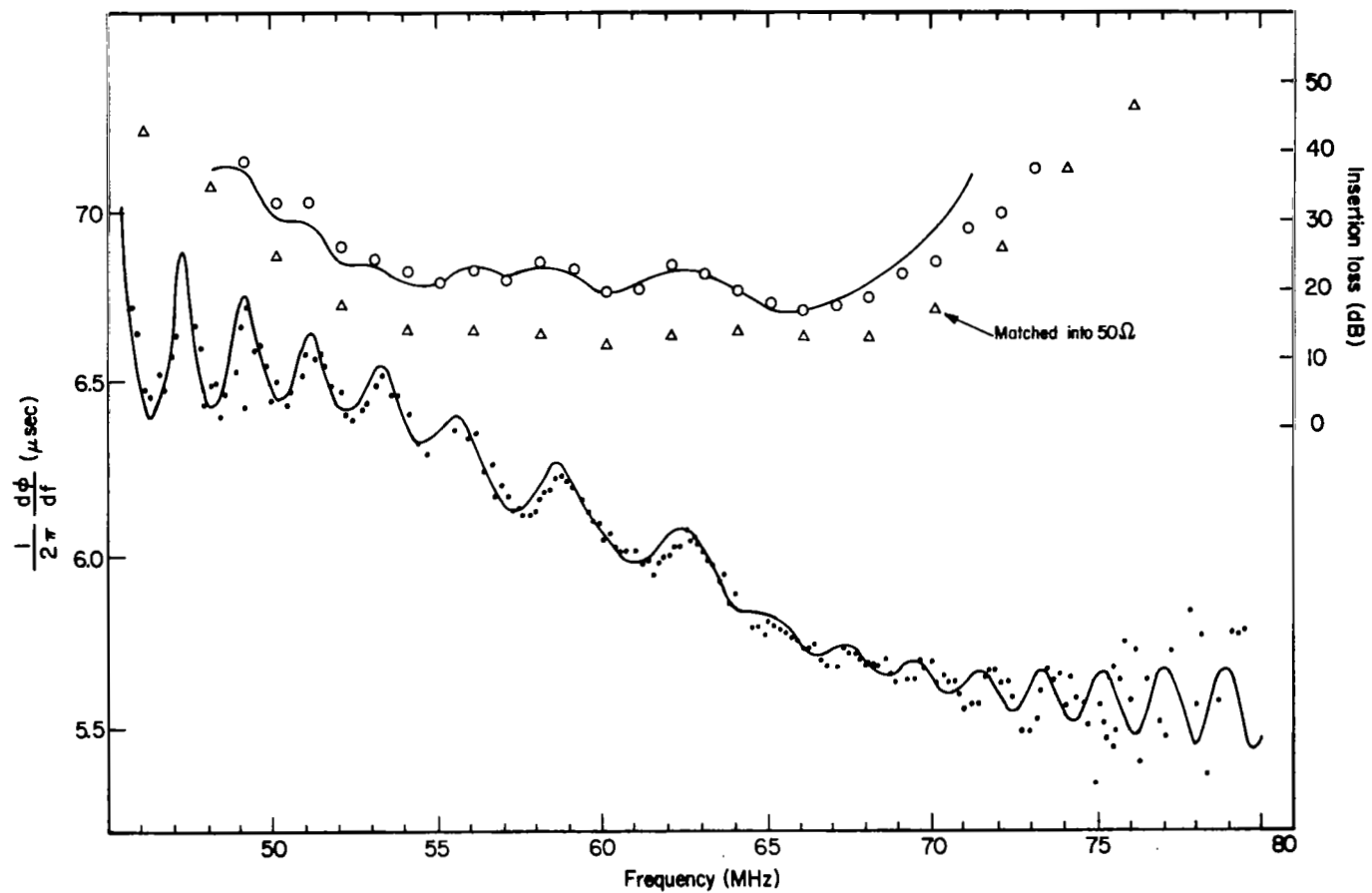obtained. Compression ratios of several hundreds thus appear feasible.

Figure A-2. Insertion Loss and Rate of Change of Phase (delay time)
as a Function of Frequency, $N+M+1 = 66$, $|\chi_N| = |\chi_{-M}|$,
$f_o = 60$ MHz, and $a = 20$ MHz μsec

Solid lines are computed curves. The computed insertion loss has
an arbitrary zero. The circles are data points taken with no matching.
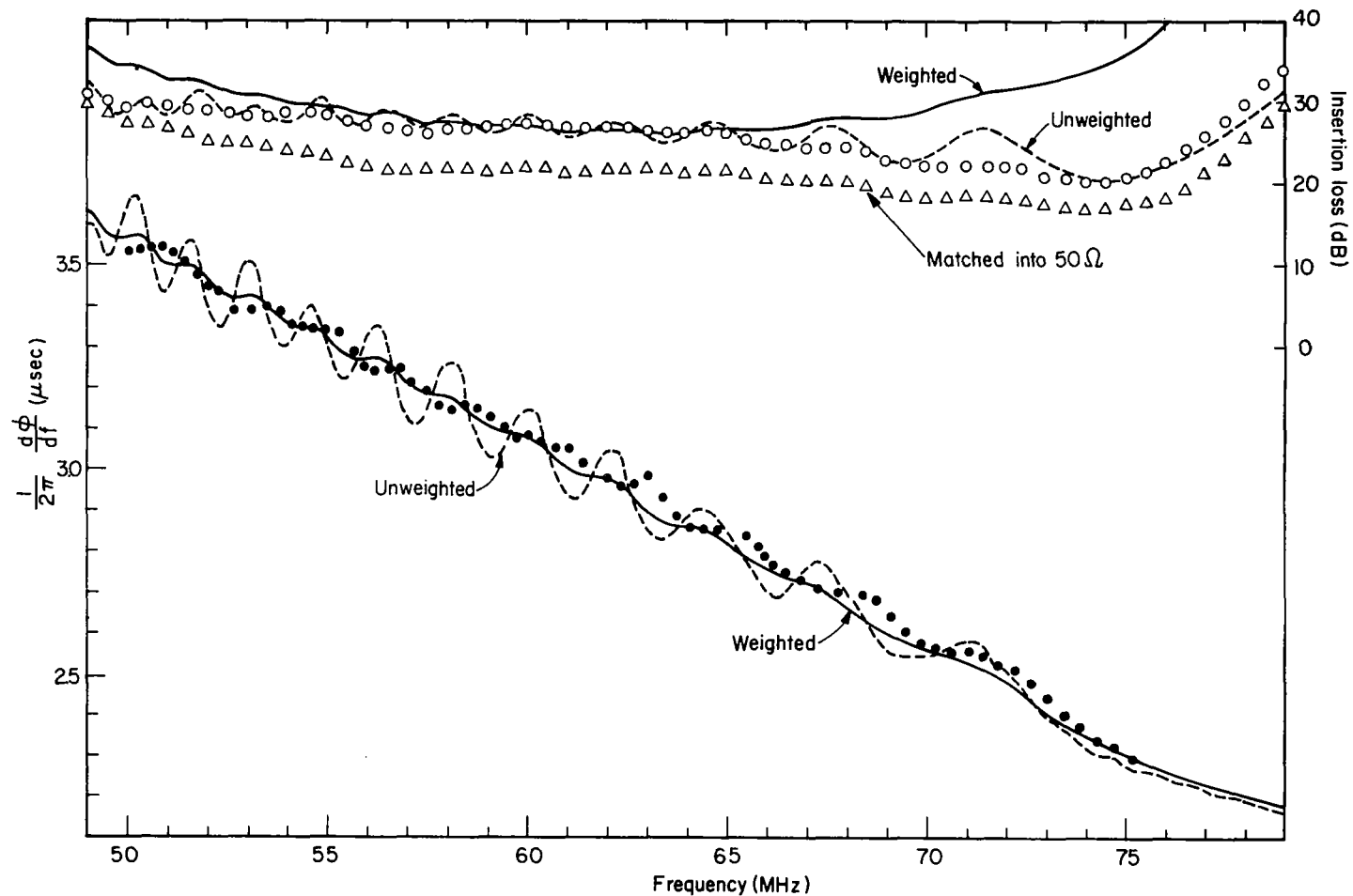
Figure A-3. Insertion Loss and Rate of Change of Phase (delay time) as a Function of Frequency. $N+M+1 = 120$, $|X_N| = |X_{-M}|$, $f_o = 60$ MHz, and $a = 20$ MHz/μsec

The dashed lines are calculated for an unweighted device. The calculated solid lines and the data points are for interdigital structures weighted by the function $A_n = \cos\left[\pi X_n/ X \cdot X \left(X_N - X_{-M}\right)\right]$ with X_n given by (1). The computed insertion loss curves have an arbitrary zero. The circles are data points taken with no matching.

The upper operating frequency of the device is presently ~400 MHz based on state-of-the-art of integrated circuit techniques, but could reach 1 GHz or higher in the near future. However, at a center frequency of 300 MHz this device should provide the bandwidth necessary for most presently foreseen signal and data processing needs. This capability, coupled with the predictability of the device characteristics, the low loss behavior and the ease of fabrication make this a useful improvement over existing bulk dispersive devices.
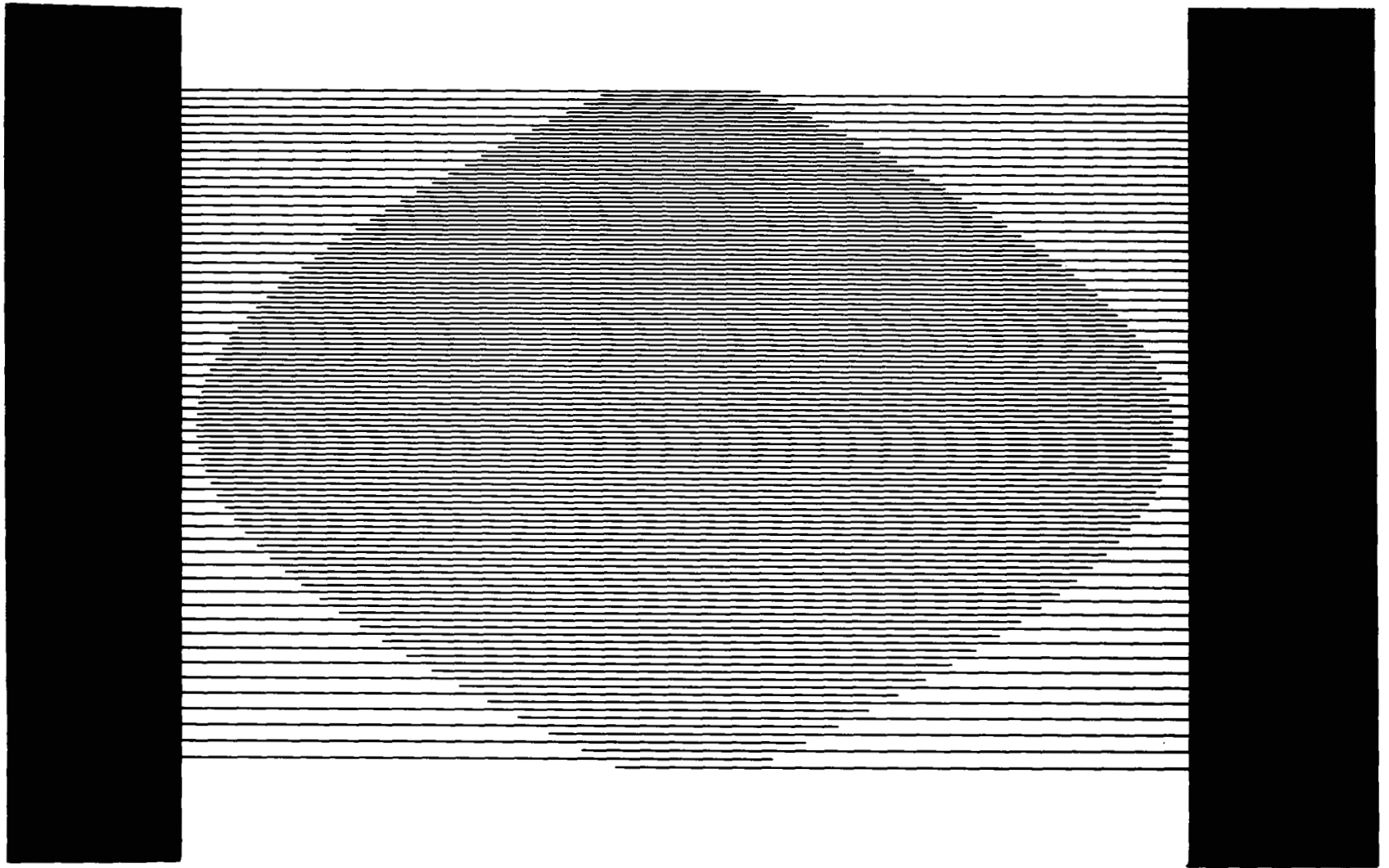
Figure A-4.   Cosine Weighting: Photograph of Mask Art Work

A series of curves showing the pulse compression performance charac-
teristics for two lithium niobate dispersive delay lines have been generated
by the Raytheon Research Laboratories. Curve A-5 was generated for the
following condition:

PULSE COMPRESSION CHARACTERISTICS

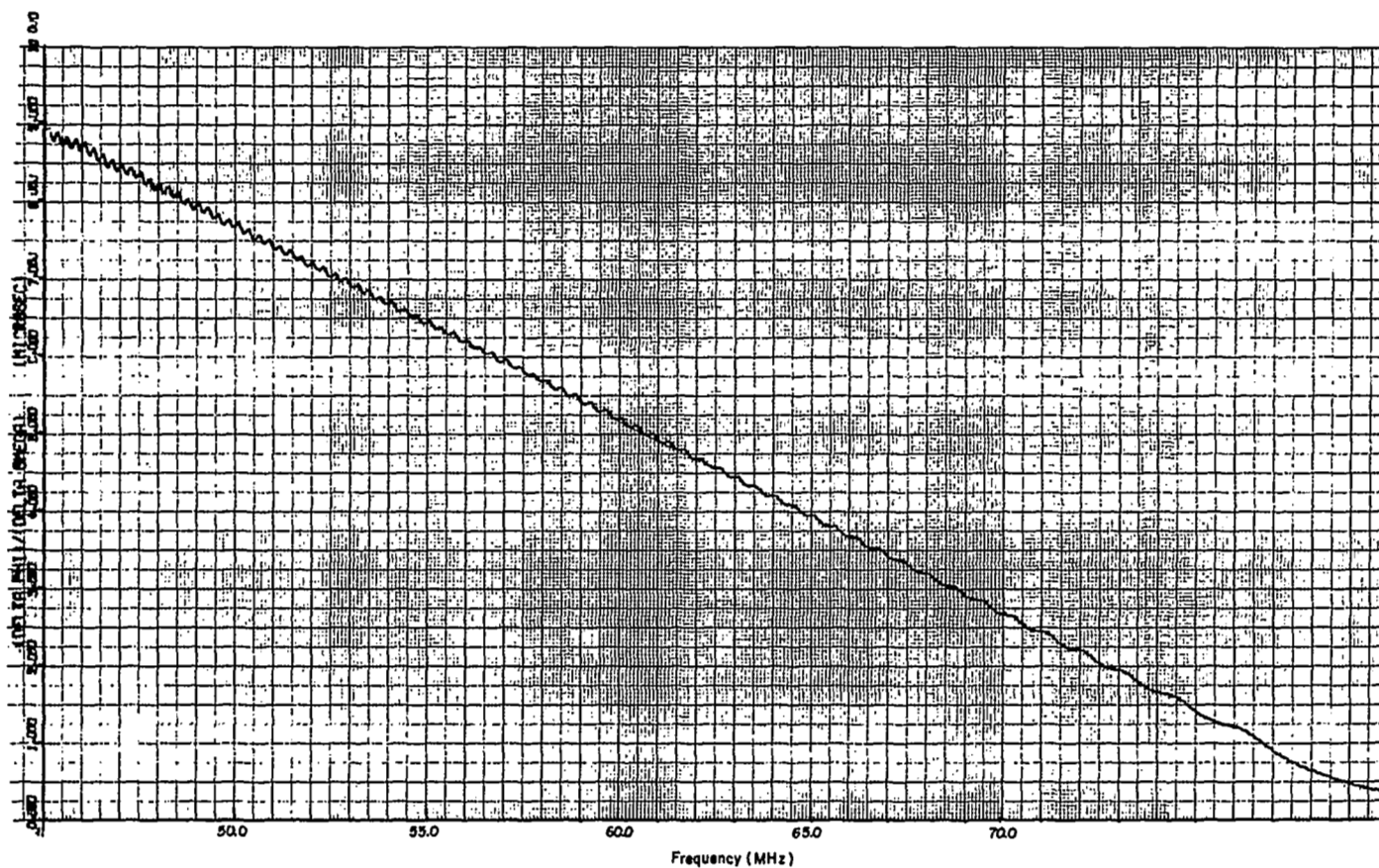60 MHz Center Frequency
5 μsec Dispersive Delay Time
20 MHz Bandwidth

Curves A-6, A-7 and A-8 were generated for the following condition:

PULSE COMPRESSION CHARACTERISTICS

300 MHz Center Frequency
2 μsec Dispersive Delay Time
200 MHz Bandwidth

Figure A-5. Computed Variation in Phase with Frequency ($d\phi/d\omega = \tau_d$) for a
Variably Spaced Interdigital Array Operating between 50 and 70 MHz
over a Delay Time of τ_d = 5 μsec. Each Array has 600 Teeth and is
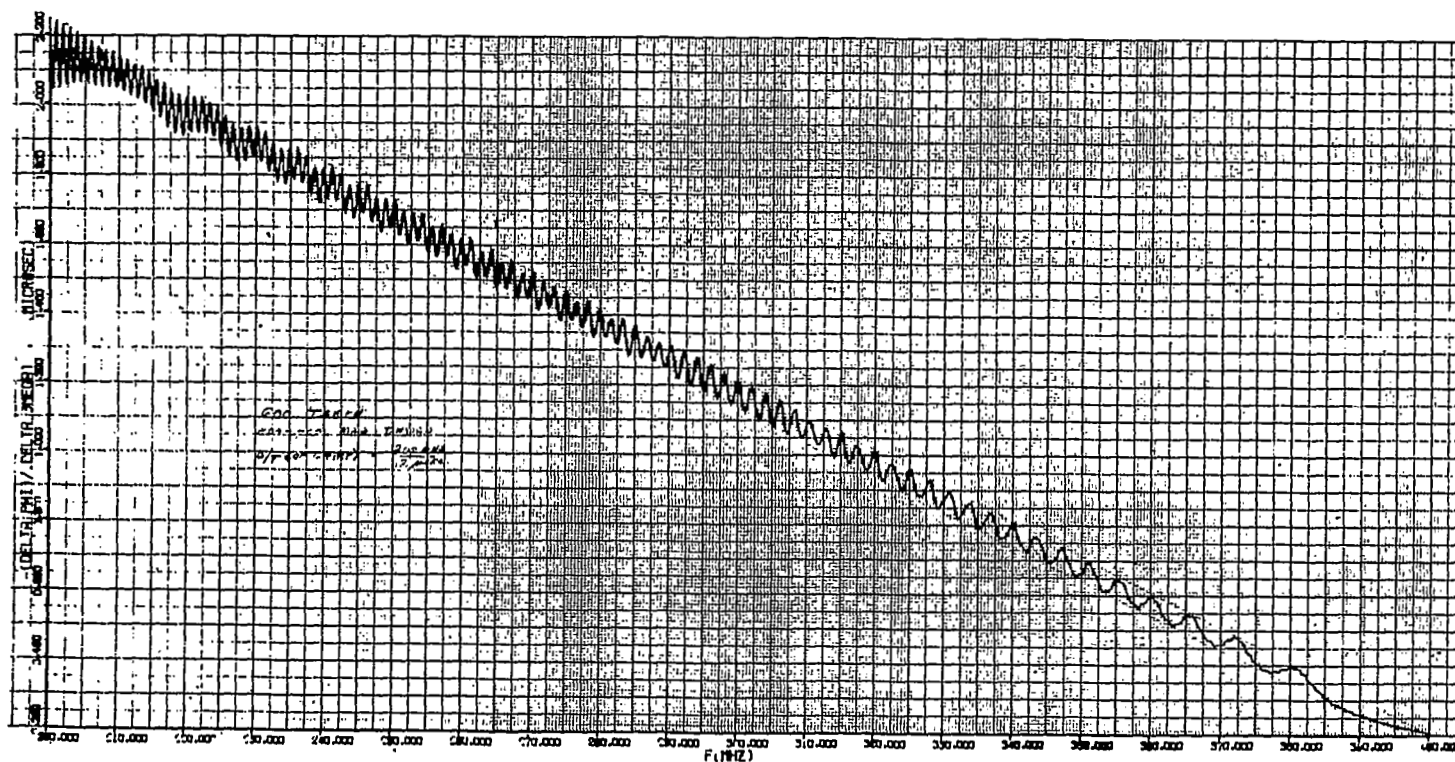1.2 cm long. This is a Direct Photograph of a Cal. Comp. Plot
from the Univac 1108.

Figure A-6. Variation in Phase with Frequency ($d\phi/d\omega = \tau_d$) for a Variably-Spaced
Interdigital Array Operating between 200 and 400 MHz over a Delay
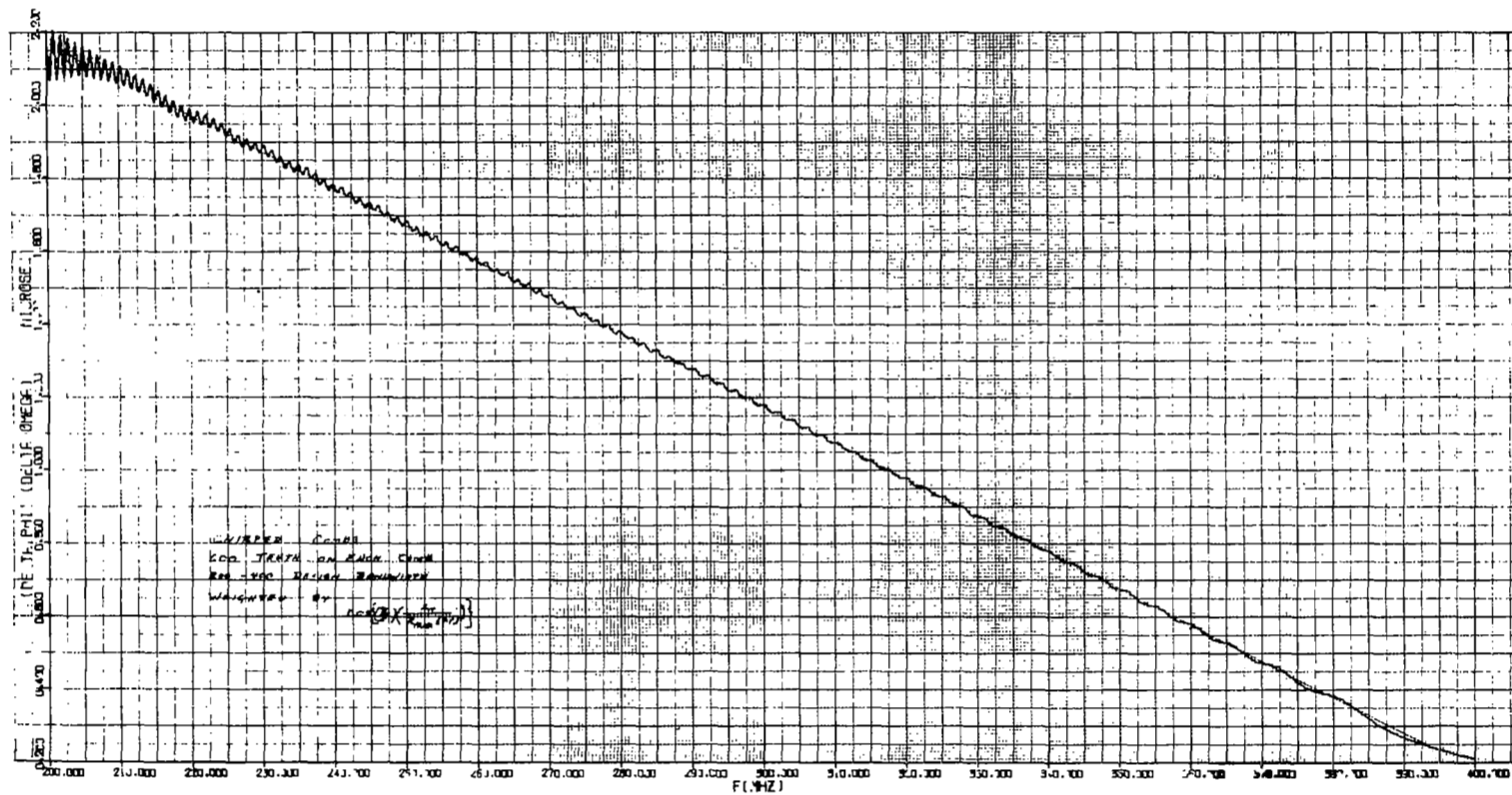Time $\tau_d = 2$ μsec Cal. Comp. Plot

Figure A-7. Same Array but Weighted with a Cosine Function. Cal. Comp. Plot
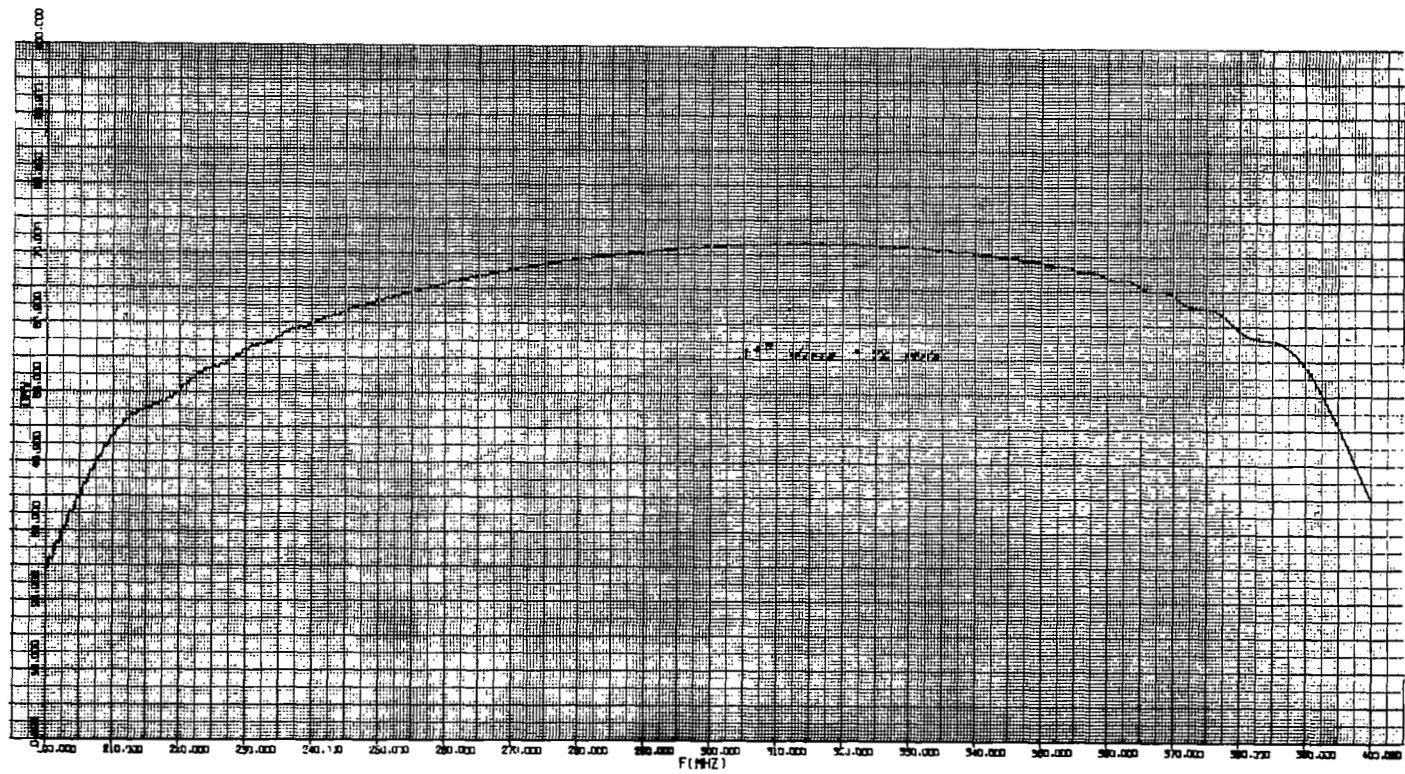
Figure A-8.   Insertion Loss (Arbitrary Zero) as a Function of Frequency for the
Weighted Array.   Cal. Comp. Plot

APPENDIX B
SYSTEMS INVESTIGATED

I. FM Chirp System

    A.   Correlation Receiver (Serrodyne Mixing Technique)

    B.   Matched Filter Receiver

        1)   Perpendicular Diffraction Dispersive Delay Line

        2)   Surface Wave Dispersive Delay Line

        3)   Dispersive Delay Line Using First Longitudinal Mode in a Strip

        4)   Lumped Constant Dispersive Delay Line

II. Discrete Coded Systems

    A.   Constant Carrier Pulse Trains

        1)   Uniform Spacing

        2)   Staggered Spacing

    B.   Binary Phase Codes

        1)   Tapped Delay Line Implementation

        2)   Shift Register Implementation

    C.   Polyphase Codes

    D.   Discrete Frequency Sequences

APPENDIX C

CHOICE OF PRF

H. Ward

The pulse repetition frequency, PRF, is set low enough to put the first ambiguous range return at an angle where it will be seen through the first null of the antenna pattern, as in Figure C-1.
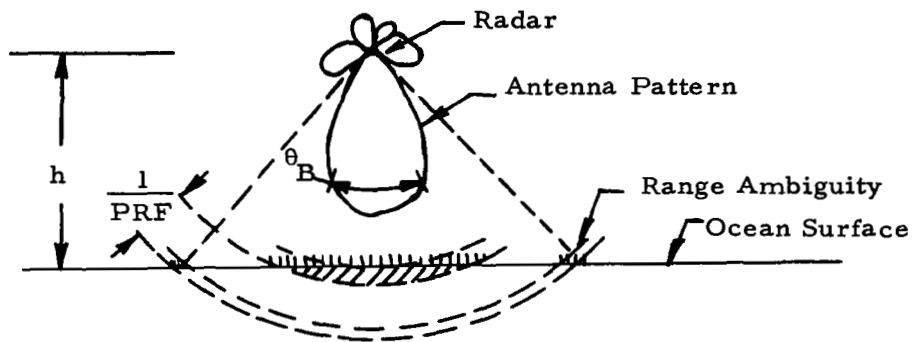
Range Return at an Angle
Figure C-1

Assuming a circular aperture with parabolic illumination, it can be shown that

$$\text{PRF (Hz)} \leq \frac{.58 \, C(m/s)}{h(m) \, \theta_B^2 \, (rad)} \quad .$$

The bound of this inequality is plotted in Figure C-2 for h = 1000 km and 1733 km.

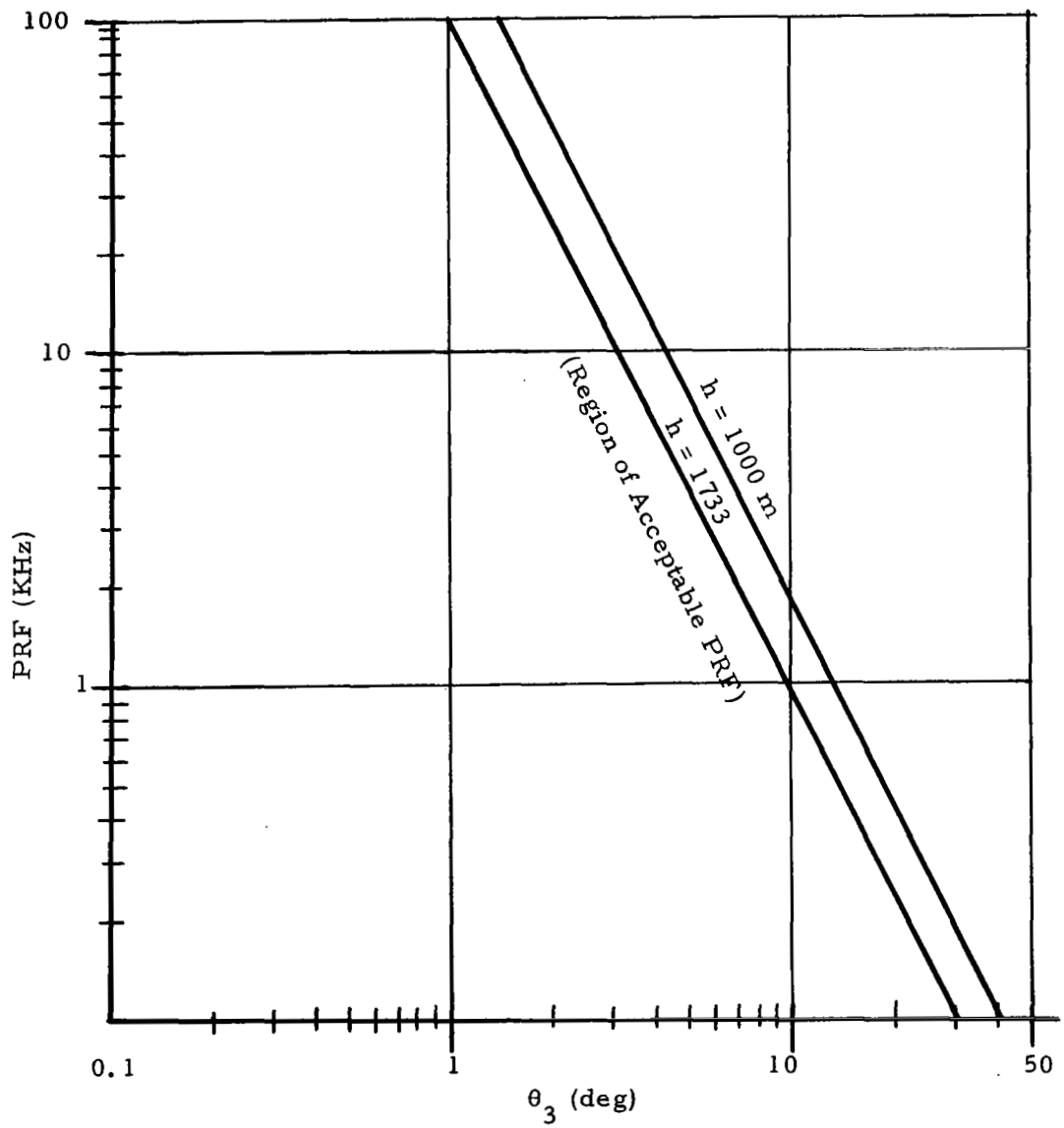Figure C-2.   PRF (Max) vs θ_B

APPENDIX D

PRF FOR INDEPENDENT SAMPLES

H. Ward

This appendix finds the rate that independent measurements are available. This is the reciprocal of the time required for the satellite to fly through one beamwidth of the pattern formed by the illuminated area of ocean surface radiating as an antenna. The diameter of the illuminated area is $D \doteq 2\sqrt{c\hat{t}h}$, where c = velocity of light, $\hat{t}$ = pulsewidth and h = radar height. Its beamwidth is λ/D. The time needed for the satellite to fly through this beam is $\frac{h(\lambda/D)}{v}\lambda$ where v is the satellite's velocity. The PRF for independent samples is therefore:

$$PRF = \frac{2v\sqrt{c\hat{t}h}}{\lambda h} = \frac{2v}{\lambda}\sqrt{\frac{c\hat{t}}{h}} .$$

Figure D-1 shows a plot of PRF versus pulsewidth for various values of wavelength, λ, and altitude, h. This PRF is the inverse of the decorrelation time
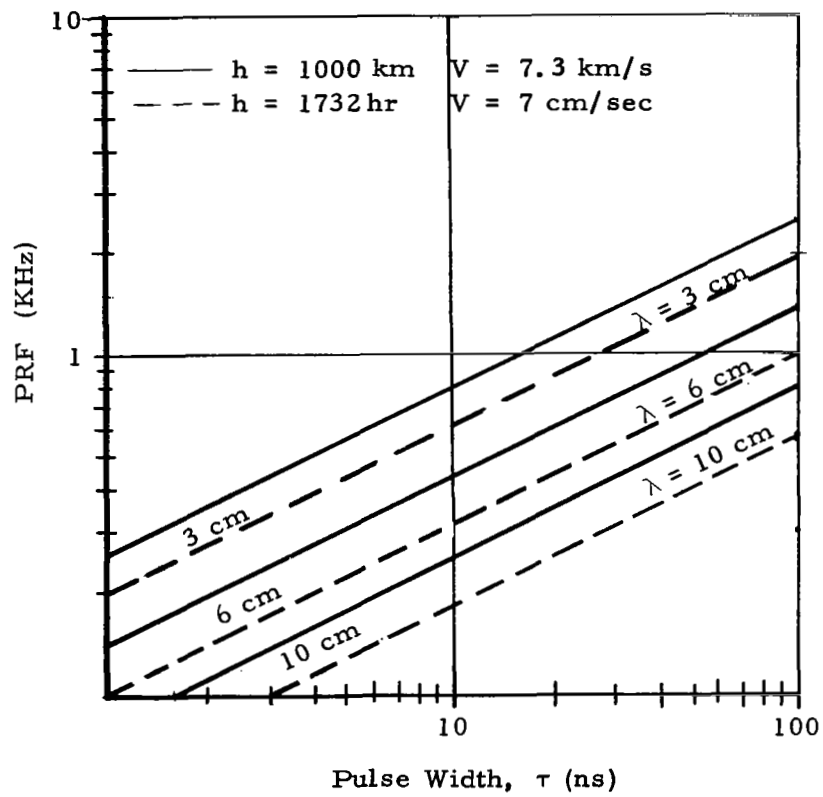
$$t_D = \frac{1}{PRF} .$$

Figure D-1. Maximum PRF for Independent Samples vs. τ

APPENDIX E

CHANNEL CAPACITY
T. Berger

Let us calculate the capacity of the channel of Figure 4-1. First we need the filter transfer function

$$H(\omega) = \int_0^\infty h(t) e^{-j2\pi ft} \, dt = (A/\sqrt{2}) \int_0^\infty t^{-1/2} e^{-j\omega t} \, dt$$

$$H(\omega) = (A/2) \, (\pi/|\omega|)^{1/2} \, (1 - j \, \text{sgn} \, \omega).$$

It follows from[17], Theorem 8.5.1, that the channel capacity C and input power P_t are related by the parametric equations

$$C(\gamma) = \int_{f: \frac{N(f)}{|H_1(f)|^2} \leq \gamma} (1/2) \log \left[\frac{|H_1(f)|^2 \gamma}{N(f)} \right] df$$

$$P_t(\gamma) = \int_{f: \frac{N(f)}{|H_1(f)|^2} \leq \gamma} \gamma - \frac{N(f)}{|H_1(f)|^2} \, df$$

where $H_1(f) = H(2\pi f)$ and $N(f)$ is the two-sided spectral density of the additive Gaussian noise. For a white noise channel we have $N(f) = N_o/2$, so

E-1

$$C(\gamma) = \int (1/2) \, \log \, (\gamma A^2/2N_o |f|) \, df$$
$$|f| \leq \gamma A^2/2N_o$$

$$= - \, (\gamma A^2/2N_o) \int_0^1 \log x \, dx = \gamma A^2/2N_o$$

$$P_t = \int_{|f| \leq \gamma A^2/2N_o} \left(\gamma - \frac{2N_o |f|}{A^2} \right) df = \gamma^2 A^2/2N_o$$

Hence, $\gamma = (2N_o P_t/A^2)^{1/2}$ and

$$C = (P_t A^2/2N_o)^{1/2}.$$

APPENDIX F

SCATTERING FUNCTION
T. Berger

Here we calculate the scattering function $\sigma(\tau, f)$ and power spectrum $\sigma(f)$ of the satellite altimeter radar channel. This is done by calculating contours of constant doppler frequency (isodops) and contours of constant round-trip delay (isodels). The returns from differential areas between closely spaced isodops and isodels then are weighted by the effective beam pattern and the fourth power loss in order to calculate the overall time-frequency dispersion of the transmitted signal.

We assume a flat earth, a purely horizontal satellite velocity vector, a radially symmetric beam pattern, a vertical beam axis, and a smooth (although Rayleigh fading) sea. Coordinates are established in Figure F-1 with the ground track traversing the x-axis. Ignoring relativistic effects[23], the instantaneous doppler frequency of the return from the facet at beam angle θ and ground plane polar angle ϕ is

$$f = \frac{2v \sin \theta \cos \phi}{\lambda} .$$

(F-1)

Since $x = h \tan \theta \cos \phi$, we have $\sin \theta \cos \phi = (x/h) \cos \theta$. Moreover $\cos \theta = h/\sqrt{h^2 + x^2 + y^2}$, so the isodop of frequency f is given by the equation

$$f = \frac{2vx \cos \theta}{\lambda h} = \frac{2vx}{\lambda (h^2 + x^2 + y^2)^{1/2}}$$
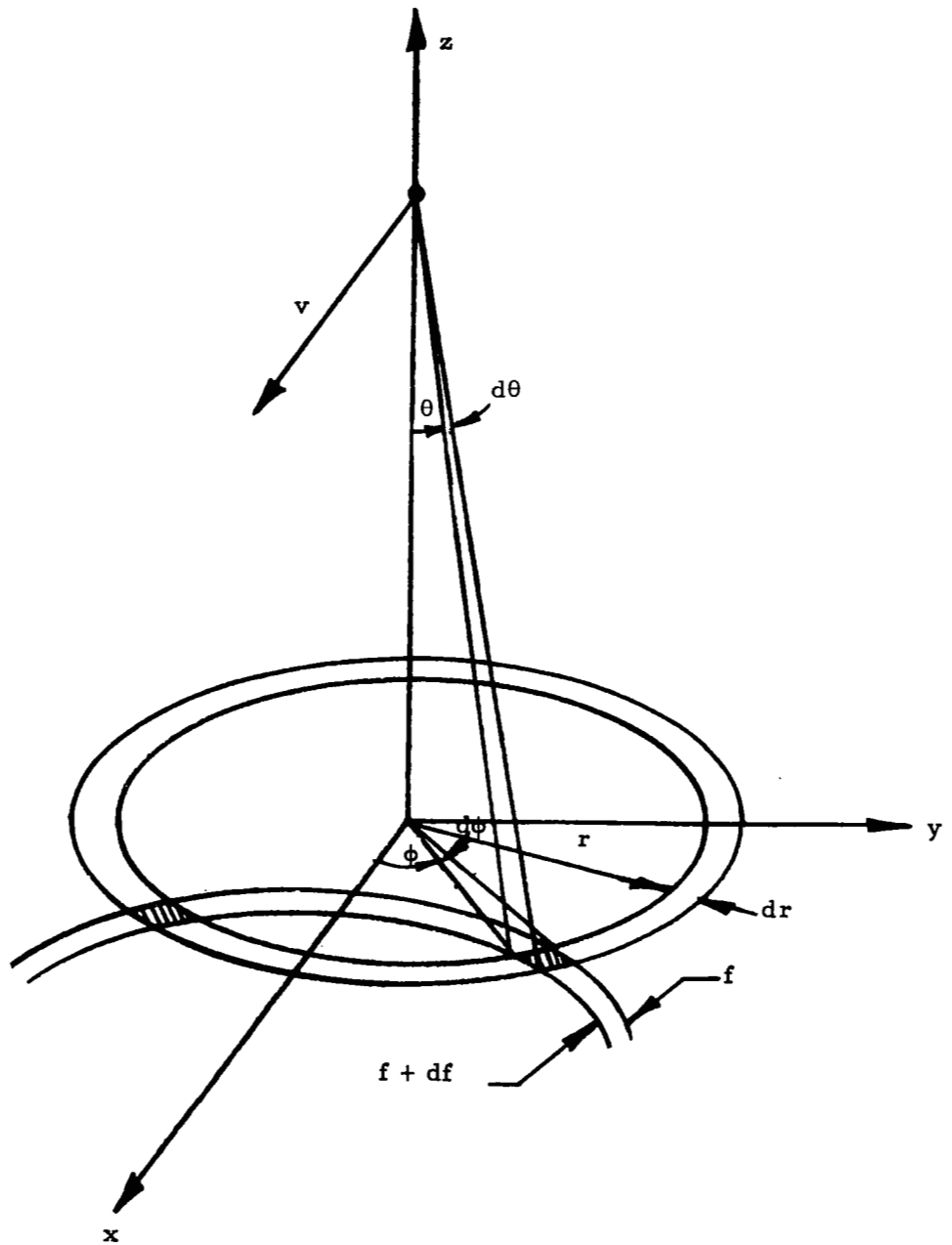
(F-2)

The isodops therefore are hyperbolas of the form

Figure F-1. Intersection of Isodops and Isodels

$$\left[\left(\frac{2v}{\lambda f}\right)^2 - 1\right] x^2 - y^2 = h^2 \tag{F-3}$$

The nonrelativistic[†] isodels clearly are circles corresponding to intersections of the ground plane with cones of constant half angle θ. The relationship between the round-trip delay τ and cone angle θ is found by noting that the range to points on the isodel corresponding to θ is

$$R(\theta) = h \sec \theta. \tag{F-4}$$

Hence

$$\tau(\theta) = \frac{2[R(\theta) - R(0)]}{c} = \frac{2h(\sec \theta - 1)}{c} \cong h\theta^2/c. \tag{F-5}$$

where τ is the minimum delay experienced along the beam axis and the approximation yielding the last member holds for small θ. Armed with (F-5) we shall work out results in terms of θ and then convert them to τ. Isodops for f and f + df are shown intersecting isodels for θ and $\theta + d\theta$ in Figure F-1. The differential area of intersection is

$$dA = 2r dr \, |d\phi| \tag{F-6}$$

where

$$r = h \tan \theta \tag{F-7}$$

is the ground plane radius of the θ-isodel. (The validity of (F-6), despite the fact that the isodels and isodops are not mutually orthogonal, follows from the fact that the two areas comprising dA are parallelograms for small enough df and dθ. The area of a parallelogram is the product of of its extents along two orthogonal directions one of which is parallel to one of the sides. The radial and tangential directions are used in (F-6) the latter of which is parallel to the isodels.)

[†] With relativistic effects considered the isodels become ellipses with eccentricity $\varepsilon = \sqrt{1-\beta^2}$, $\beta = v/c$. (See [23]).

From (F-7), $dr = h \sec^2 \theta \, d\theta$, and from (F-1)

$$d(\cos \phi) = - \sin \phi \, d\phi = \frac{\lambda \, df}{2v \sin \theta}$$

Since

$$|\sin \phi| = \sqrt{1 - \cos^2 \phi} = \sqrt{1 - \left(\frac{\lambda f}{2v \sin \theta}\right)^2} \,,$$

we have

$$dA = 2h^2 \tan \theta \sec^2 \theta \, d\theta \, |d\phi|$$

$$dA(\theta, f) = \begin{cases} \dfrac{2h^2 \tan \theta \sec^2 \theta \, d\theta \, df}{\sqrt{(2v \sin \theta / \lambda)^2 - f^2}} & \text{if} \quad |f| \leq 2v \sin \theta / \lambda \\[4mm] 0 & \text{if} \quad |f| > 2v \sin \theta / \lambda \end{cases} \qquad (F-8)$$

The scattering function $\sigma(\theta, f)$ (instead of $\sigma(\tau, f)$ because of (F-5) is given by

$$\sigma(\theta, f) \, d\theta \, df = \frac{G^2(\theta) \lambda^2 \sigma_o(\theta) \, dA(\theta, f)}{(4\pi)^3 R^4(\theta) L} \qquad (F-9)$$

where $G^2(\theta)$ is the two-way antenna gain and $\sigma_o(\theta)$ is the average backscatter cross section per unit area as a function of the incidence angle. As in Appendix R-2 of 13 we shall assume that $G^2(\theta) \sigma_o(\theta)$ is Gaussian in θ with effective beamwidth θ_e. Since $\theta_e \ll 1$ in practice, we may use the small angle approximation in reverse to write

$$G^2(\theta) \sigma_o(\theta) = G^2 \sigma_o e^{-(\theta/\theta_e)^2} \approx G^2 \sigma_o e^{-\left(\frac{\sin \theta}{\theta_e}\right)^2} \qquad (F-10)$$

(Indeed, using sin θ instead of θ is probably a better approximation since most antenna patterns actually are expressible as functions of sin θ)

Substituting (F-4), (F-8), and (F-10) into (F-9) yields the scattering function

$$\sigma(\theta, f) = \begin{cases} \dfrac{2G^2\lambda^2\sigma_o \sin\theta \cos\theta \, e^{-\left(\frac{\sin\theta}{\theta_e}\right)^2}}{(4\pi)^3 h^2 L \sqrt{(2v\sin\theta/\lambda)^2 - f^2}} & \text{if } |f| \le \dfrac{2v\sin\theta}{\lambda} \\[4ex] 0 & \text{if } |f| > \dfrac{2v\sin\theta}{\lambda} \end{cases} \qquad \text{(F-11)}$$

It follows that

$$\sigma(f) \triangleq \int_0^\infty \sigma(\tau, f)\, d\tau = \int_0^{\pi/2} \sigma(\theta, f)\, d\theta \qquad \text{(F-12)}$$

$$= \frac{G^2\lambda^2\sigma_o}{(4\pi)^3 h^2 L} \int_{\frac{\lambda|f|}{2v}}^{1} \frac{e^{-\left(\frac{\sin\theta}{\theta_e}\right)^2}}{\sqrt{\left(\frac{2v\sin\theta}{\lambda}\right)^2 - f^2}}\, d(\sin^2\theta), \quad |f| \le 2v/\lambda$$

Changing variables to

$$z = \left[\left(\frac{2v\sin\theta}{\lambda}\right)^2 - f^2\right]^{1/2} \qquad \text{(F-13)}$$

yields the result

$$\sigma(f) = \begin{cases} \left(\dfrac{G^2\lambda^4\sigma_o}{2(4\pi)^3 h^2 v^2 L}\right) e^{-(\lambda f/2v\theta_e)^2} \displaystyle\int_0^{\sqrt{(2v/\lambda)^2 - f^2}} dz\, e^{-(\lambda z/2v\theta_e)^2} & \text{if } |f| \le 2v/\lambda \\[4ex] 0 & \text{if } |f| > 2v/\lambda \end{cases} \qquad \text{(F-14)}$$

which appears as (F-12) in the text.

APPENDIX G

SOLID-STATE MICROWAVE POWER SOURCES

J. T. Zimmer

G-1 Classification of Sources

Solid-state microwave power device technology is a rapidly changing field, undergoing continuous and intense development. The proliferation of devices and techniques makes it helpful to divide microwave power sources into three basic categories for discussion: 1) amplifiers, 2) harmonic generators, and 3) oscillators. Each of these is examined with respect to the state-of-the-art power capability and their applicability to the IFF application is described.

G-2 Amplifiers

We are concerned primarily with transistor amplifiers here, although various types of diodes which operate as negative resistance amplifiers must also be included.

Transistors have advanced dramatically in power-frequency capability during the past decade. This is illustrated by Figure G-1, which is derived from a 1965 publication[24]. The figure also shows that the rate of advance has slowed appreciably in recent years. The additional 1968 power-versus frequency curve indicates a five dB improvement over the 1965 state-of-the-art in the UHF range, as compared to about a 15 dB improvement in the preceding three year period. Fundamental physical limitations on frequency and power for transistors have been identified[25] which make it difficult to advance much further. The earlier advances were due to improvements in semiconductor junction fabrication technology. These developments were mostly in the formation techniques and the metallurgy of the junction itself, but have reached the point now where increased power capability is obtained primarily by increasing the junction area or by paralleling junction elements.
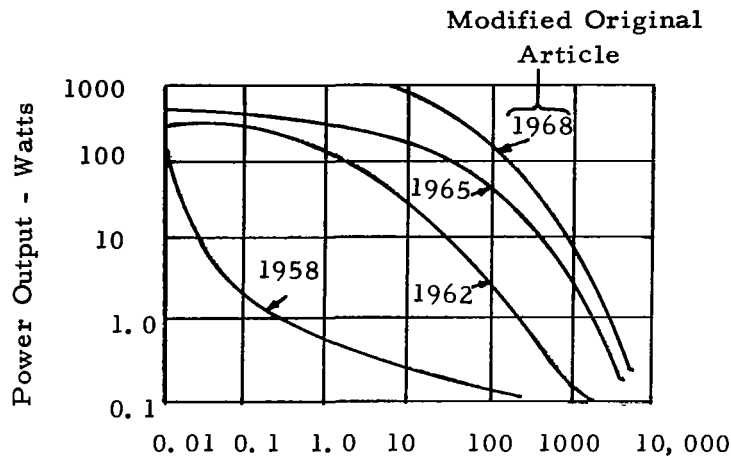
Figure G-1.   Progress in Transistor Power Output as a Function
of Frequency

Increased power capability will now require substantially more complicated
fabrication techniques to be used.   The unit cost of these transistors will
remain higher, by comparison with present day transistor types, and the
reliability lower, so that it will be attractive to obtain higher power by
paralleling the simpler types.

The ratio of peak power to average continuous wave (CW) power
obtainable with a transistor amplifier is much less than that of a vacuum
tube.   This difference exists because a transistor is a current-amplification
device.   A vacuum tube will perform over a wide range of applied current
and voltage conditions, provided that the average power dissipated does not
exceed a maximum value which is related to the size of its' elements.   Under
CW conditions, the vacuum tube is customarily operated at a much lower
average current than the peak values possible for the pulsed mode.

Transistors, however, tend to be operated in the CW mode at current
and voltage levels which are close to their absolute limits, as determined
by internal thermal dissipation and second breakdown capabilities.   At duty
cycles of 10 percent or so, and for pulse lengths of 10 microseconds or less,
it is possible to operate RF power transistors at peak-power levels which
are typically only about twice as high as their rated CW power.

During the time period of this study (1968), the maximum CW power capability of transistors available at 1000 MHz was 10 watts. In 1969, a transistor having a 20 watt capability at this frequency became available.

Semiconductor diode oscillators, particularly the avalanche type, have been operated as amplifiers[26]. Since the power output performance achieved is directly related to that possible for the individual semiconductor device operated as an oscillator, this type of amplifier is a special case of the oscillator class. The main attraction of several of these amplifier arrangements is that they use multiple devices arranged to operate in a phase-locked or traveling wave mode, so as to sum the power from a number of identical devices. This is a special form of power combiner which intimately combines the device and the combiner circuitry.

G-3 Harmonic Generators

Varactor diode harmonic generators can be used to convert power obtained at lower frequencies into microwave energy with remarkably good efficiencies. Varactors of the step-recovery (or "punch-through") type have provided excellent performance in simple multiplier stages without the use of idler circuits. Efficiencies greater than 60 percent have been obtained with triplers of this type providing power outputs in excess of 20 watts at 1000 MHz when driven by transistor amplifiers at a lower frequency. For frequency doublers with output at 1000 MHz, efficiencies in excess of 70 percent for power outputs of around 30 watts are obtained from readily available devices. The power output capability of single-diode frequency multipliers using varactor diodes available in 1968 is shown in Figure G-2.

As in the case of transistors, varactors are normally operated in the CW condition at (RF) voltage levels which are close to their maximum ratings, so that there is little difference between their peak and average
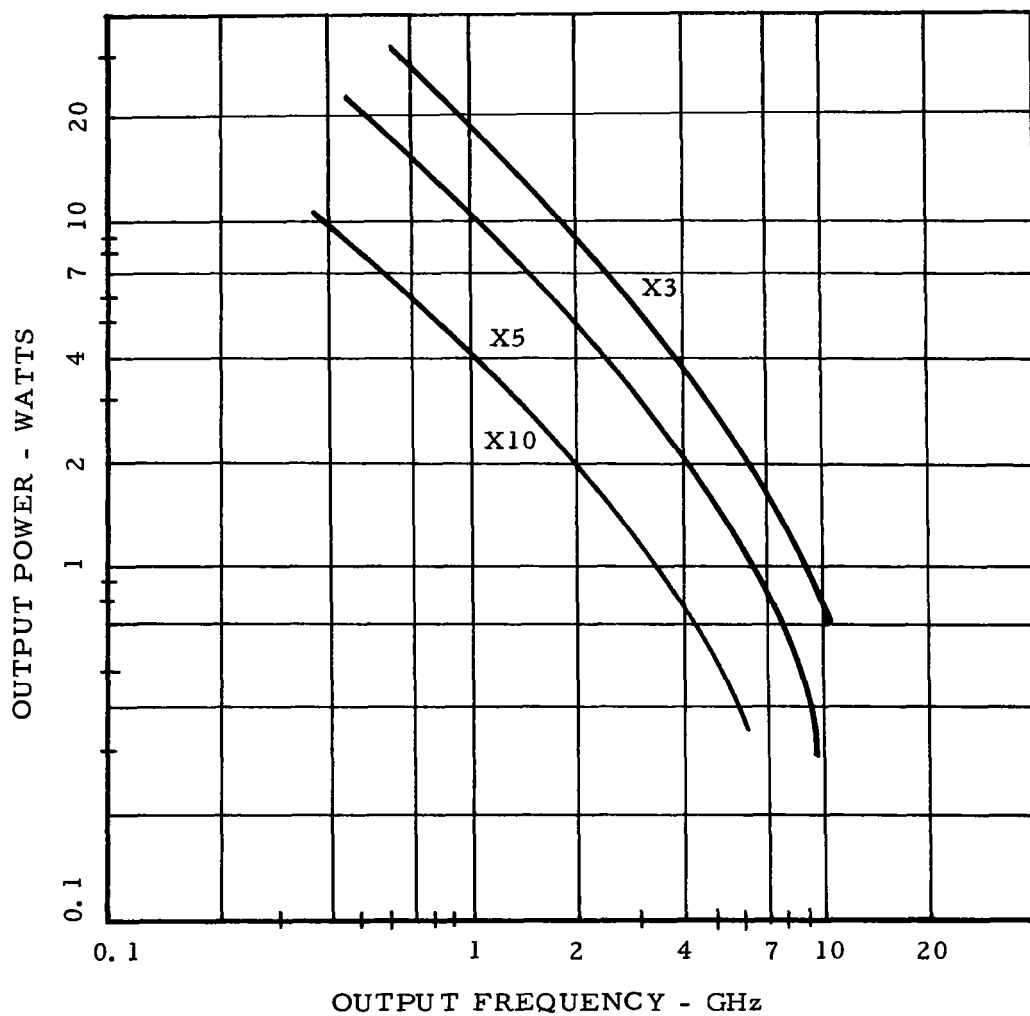
Note: Curves represent best results reported by various workers
using varactor diodes of the step-recovery or punch-through
type available in 1968.

Figure G-2. Output Power Capability of Single-Diode Frequency
Multiplier for Various Multiplication Ratios

power ratings. It is relatively easier, however, to connect diodes in series and parallel arrangements to increase the power capability. A series arrangement of varactor diode elements is particularly effective since the net peak RF voltage level which can be handled is directly increased and the circuit impedance levels are not reduced to awkward levels (as is frequently the case for a parallel network of semiconductors). During 1968, step-recovery diode units have become available which consist of two or three varactor elements mounted in series within a single, standard package. Heat removal from the semiconductor elements is more of a problem for this arrangement (due to the difficulty of heat-sinking each of the elements), but for pulsed operation this is not a serious limitation since the average power incident on each element is lower for this mode. It is feasible to operate at least five varactor diode elements in series to give a peak-power capability of at least five times the best average power performance. At L-band, this indicates a peak-power output capability of 100 to 200 watts from a single, multiple-diode device.

Certain types of transistors have been demonstrated to perform as frequency multipliers with gain. These transistors combine a nomal transistor power-amplifier design with a collector junction capable of varactor-type harmonic generation. Their power output capability does not approach that of the varactor frequency multiplier, however. The transistor harmonic generators are useful mainly for exciter applications.

G-4 Oscillators

The most dramatic progress in solid-state microwave power generation currently being made is in the oscillator area. There are a number of new devices which offer the advantages of simplicity and higher peak power. Since they are fundamental-frequency power oscillators, their frequency stability is relatively poor by comparison with the amplifier-multiplier device techniques.

The high-power, semiconductor oscillators being developed are diodes
belonging to two classes of devices: avalanche (or IMPATT) and transferred
electron. The avalanche diodes are junction devices (usually silicon) whereas
the transferred electron oscillators use bulk gallium arsenide material.
Actually, there are several modes of oscillation possible in each class for
which significant results have been obtained. In the avalanche class, there
are the normal and anomalous modes, and in the transferred electron class
there are the Gunn, Gunn-domain, and LSA modes. Pulse powers which
have been achieved for these devices at various frequencies are shown in
Figure G-3[27].

Efficiencies of 40 to 60 percent have been achieved for anomalous
mode avalanche devices in L-band and efficiencies of 10 to 20 percent, with
peak powers of several kilowatts, have been predicted for the near future
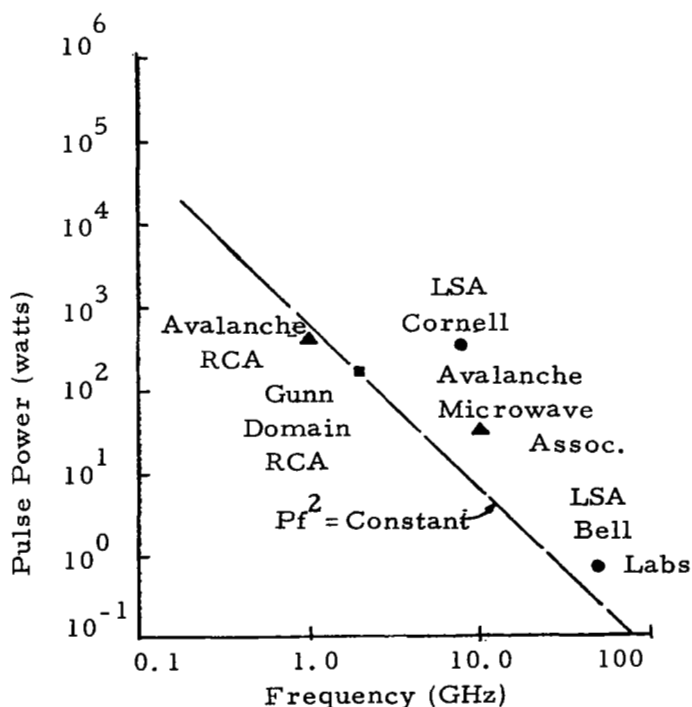for LSA devices at X-band.

Figure G-3. Peak Power Outputs Achieved for Various
Types of Avalanche and Transferred-
Electron Oscillators

Considerable work remains to be done before the operation of these devices will be fully understood and their potential more fully realized. In particular, their pulse length and duty-cycle capabilities require improvement. It is reasonable to expect, however, that these devices will soon replace small vacuum tube and magnetron oscillators for many pulse applications.

APPENDIX H

RANGE SIDELOBES FOR PULSE COMPRESSION WAVEFORMS IN SATELLITE ALTIMETRY

T. Berger

H-1. Introduction

In this appendix the question of errors that arise from the sidelobes of a compressed pulse are examined to establish whether bias or ambiguity erros of sufficient size to effect the conclusions of the study exist. In this study it is assumed that the returned signal is detected in a square law detector and processed through a double differencing processor. For the case where Taylor weighting is applied to the returned signal it can be concluded that

    a.   There are no ambiguity errors of concern

    b.   Bias errors for the noise free clutter free case are less than 0.05 meters.

    c.   The errors introduced by noise and clutter are comparable to those experience by a Gaussian shaped short pulse of length comparable to the compressed pulse.

The unweighted signal return does present a problem and are likely to have both ambiguity errors and bias errors.

Formulas for the ambiguity surfaces of pulse compression waveforms after interaction with the fading dispersive satellite altimetry channel are obtained by applying the theory of radar mapping of distributed targets. (See [28] or [29]. The analysis provides quantitative estimates of the effect of "self-noise" on range sidelobes. Graphs of the average power response vs time are presented for rectangularly weighted and Taylor weighted linear FM signals. Plots of the first and second differences of these power responses in the vicinity of the origin are provided from which the range sidelobe bias error is determined. The generalizations necessary to extend the analysis to account for filter mismatch, antenna stabilization, and sea state are indicated.

H-2. The Ambiguity Surface

A distributed target such as the sea surface is described for radar purposes by a scattering function, $\sigma(\tau, f)$, having the property that $\sigma(\tau, f)$ $d\tau df$ is the average power scattered back to the receiving antenna with delay between τ and $\tau + d\tau$ and frequency shift between f and f + df per unit transmitted power. A radar signal with complex envelope $\mu(t) = |\mu(t)| e^{j\phi(t)}$ has ambiguity function

$$\chi(\tau, f) = \int_{-\infty}^{\infty} \mu(t) \mu^*(t-\tau) e^{j2\pi ft} dt \tag{H-1}$$

A filter matched to this signal save for a doppler frequency shift f_d has a complex impulse response $\mu^*(t) e^{-j2\pi f_d t}$. When this filter is excited by the return from a target with scattering function $\sigma(\tau, f)$ after a signal with ambiguity function $\chi(\tau, f)$ has been transmitted, the power response of the filter output as a function of time t is [†]

$$P(t; \hat{fd}) = \iint_{-\infty}^{\infty} \sigma(\tau, f) |\chi(t-\tau, f-f_d)|^2 d\tau df. \tag{H-2}$$

In particular, setting $f_d = 0$ yields

$$P(t) = \iint_{-\infty}^{\infty} \sigma(\tau, f) |\chi(t-\tau, f)|^2 d\tau df$$

$$= \iint_{-\infty}^{\infty} \sigma(t-\tau, f) |\chi(\tau, f)|^2 d\tau df \tag{H-3}$$

---

† For the derivation of (2), see [28], Section 1-4D, or [29], Chapter 9.

Equation (3) provides the means for assessing the effect of so-called "self-noise" on the time sidelobes (range sidelobes) of the signal. Note from (3) that the frequency spreads both of the distributed target and of the transmitted pulse contribute to the range sidelobes.

If the target is spread significantly in τ but only narrowly in f (deep, nonfluctuating target), then we get

$$P(t) \approx \int_{-\infty}^{\infty} \dot{\sigma}(\tau) \left| \chi(t-\tau,0) \right|^2 d\tau = \int_{-\infty}^{\infty} \dot{\sigma}(t-\tau) \left| \chi(\tau,0) \right|^2 d\tau \qquad (H-4)$$

where

$$\dot{\sigma}(\tau) = \int_{-\infty}^{\infty} \sigma(\tau,f) \, df.$$

That is, P(t) is formed by convolving the square of the sidelobe structure of the filtered signal with the target's average power response to an impulse. If the range length of a deep, nonfluctuating target is much greater than the range resolution of the transmitted signal, then (4) indicates that the resultant range sidelobes are essentially the integral of those of the transmitted signal. Indeed, P(t) of (4) often is referred to as the integrated sidelobe function.

If the target is spread significantly not only in τ but also in f, then (4) no longer is justified. It usually proves necessary to use the more general form of P(t) given by (3) whenever the target is overspread, i. e., whenever LW >1 where L and W are the target's effective width in time and in frequency, respectively. (When LW < 1, the target is said to be underspread. See [28]. Chapter 1, for a detailed discussion of underspread and overspread targets.)

H-2. Underspread and Overspread Altimetry Channels

The time width L of the radar altimetry channel is the round trip delay for a signal returned from the beam edge minus that for a signal returned from the beam axis, namely

$$L = (2h/c)(\sec\theta_e - 1) \approx h\theta_e^2/c \qquad (H-5)$$

where θ_e is the effective beamwidth. (See [3].) The frequency width W of the channel is the peak doppler frequency of target elements within the beam, namely

$$W = (2v/\lambda)\sin\theta_e \approx 2v\theta_e/\lambda . \qquad (H-6)$$

It follows that

$$LW \approx 2vh\theta_e^3/\lambda c. \qquad (H-7)$$

For typical parameter values like v = 7 km/sec, h - 10^3 km, λ = 3 cm, and c = 3 x 10^8 m/sec, we find that LW = 1 for $\theta_e \approx 5°$. Hence, the channel is overspread for $\theta_e > 5°$ with these parameter values. The proposed design value θ_e = 2° yields LW = 0.067. The underspread nature of the channel simplifies the calculation of P(t) as will be illustrated in the next section.

H-3. P(t) for the Underspread Altimetry Channel and Linear FM Signal

In Appendix 2 of [30] we derived the scattering function for the radar altimetry channel, namely

$$\sigma(\tau, f) = \begin{cases} F(\tau) \, (d^2(\tau) - f^2)^{-1/2} & \text{if } |f| \le d(\tau) \\ \\ 0 & \text{otherwise} \end{cases} \qquad \text{(H-8)}$$

where

$$d(\tau) = \frac{2v \sin \theta(\tau)}{\lambda} = \text{peak doppler of target elements with delay } \tau \quad \text{(H-9)}$$

$$\theta(\tau) = \sec^{-1}\left(1 + \frac{c\tau}{2h}\right) \approx \sqrt{c\tau/h} \qquad \text{(H-10)}$$

$$F(\tau) = \begin{cases} K_1 \cos^3 \theta(\tau) \, e^{-\left(\frac{\sin \theta(\tau)}{\theta_e}\right)^2} & , \quad \tau \ge 0 \\ \\ 0 & , \quad \tau < 0 \end{cases} \qquad \text{(H-11)}^{\dagger}$$

and

$$K_1 = G^2 \lambda^2 \sigma_o c / (4\pi)^3 h^3 L . \qquad \text{(H-12)}$$

The parameters appearing in (9) - (12) are defined in [30].

The ambiguity function of an amplitude weighted linear chirp of duration T and bandwidth B is

$$\chi(\tau, f) = \int_{-T/2}^{T/2} a(u) \, a(u-\tau) \, e^{j\pi k [u^2 - (u-\tau)^2]} \, e^{j2\pi fu} \, du$$

$$= e^{j\pi k\tau^2} \int_{-T/2}^{T/2} a(u) \, a(u-\tau) \, e^{j2\pi (f + k\tau)u} \, du \qquad \text{(H-13)}$$

---

† In writing (11) we have included a multiplication by $d\theta/d\tau$ in order to convert the scattering function of [30] from θ to τ.

where $k = B/T$. From (3), (8), and (13) we get

$$P(t) = \int_0^\infty d\tau\, F(\tau) \int_{-T/2}^{T/2} du_1 \int_{-T/2}^{T/2} du_2\, a(u_1)\, a(u_2)\, a(u_1 - t + \tau)\, a(u_2 - t + \tau)$$

$$\int_{-d(\tau)}^{d(\tau)} df\, \frac{e^{j2\pi(f + kt - k\tau)(u_1 - u_2)}}{(d^2(\tau) - f^2)^{\frac{1}{2}}} \qquad \text{(H-14)}$$

Performing the integral over f yields

$$P(t) = \pi \int_0^\infty d\tau\, F(\tau) \int_{-T/2}^{T/2} du_2\, a(u_1)\, a(u_2)\, a(u_1 - t + \tau)\, a(u_2 - t + \tau)$$

$$e^{j2\pi k(t - \tau)(u_1 - u_2)}\, J_o(2\pi(u_1 - u_2)\, d(\tau)) \qquad \text{(H-15)}$$

where $J_o(\cdot)$ is the zeroth order Bessel function.

The following argument shows how (15) can be significantly simplified for the underspread altimetry channel and typical signal parameters. (The argument amounts to a specific demonstration of how (3) simplifies to (4) under appropriate conditions.) First note from (11) that $F(\tau)$ is small for $\sin \theta(\tau) > \theta_e$. This means that the largest argument of the J_o function in (15) that contributes significantly to the integral is

$$2\pi(u_1-u_2)\, d(\tau) = 2\pi(u_1-u_2)\,\frac{2v\,\sin\theta(\tau)}{\lambda} \leq 2\pi\, T\,\frac{2v\,\sin\theta_e}{\lambda} = 2\pi TW \quad\text{(H-16)}$$

where we have used (6) and the fact that $|u_1-u_2| \leq T$ in the range of integration.

Now the uncompressed pulse duration T for a deep target typically is chosen to be of the order of the target depth L of (5). Specifically, $T = 1\mu s$ has been suggested for the altimetry problem whereas L for the parameter values cited above is $4\mu s$. Hence, $2\pi TW \sim 2\pi LW$. If the channel is sufficiently underspread, then the argument of J_o will be small enough over the significant range of integration that we may safely replace J_o by unity. For example, with the proposed design values of $T = 1\mu s$ and $\theta_e = 2°$, we get $2\pi TW \approx 0.1$ in (16). Since $J_o(0.1) = 0.9975$, the approximation is justified.

Upon replacing $J_o(\cdot)$ by 1, we find that (15) collapses to

$$P(t) = \pi\int_0^\infty d\tau\, F(\tau)\left|\int_{-T/2}^{T/2} du\, a(u)\, a(u-t+\tau)\, e^{j2\pi k(t-\tau)u}\right|^2. \quad\text{(H-17)}$$

This agrees with (4) since the term in the integrand multiplying $F(\tau)$ is seen from (13) to be $|\chi(t-\tau,0)|^2$, and

$$\sigma(\tau) = \int_{-\infty}^\infty df\, \sigma(\tau,f) = \int_{-\frac{2v\,\sin\theta(\tau)}{\lambda}}^{\frac{2v\,\sin\theta(\tau)}{\lambda}} df\,\frac{F(\tau)}{\sqrt{\left(\frac{2v\,\sin\theta(\tau)}{\lambda}\right)^2-f^2}} = \pi F(\tau).$$

In Figure H-1 we show P(t) for an unweighted linear chirp with $T = 1\mu s$ and B = 100 MHz. P(t) for the same chirp with 35 dB Taylor weighting[31]
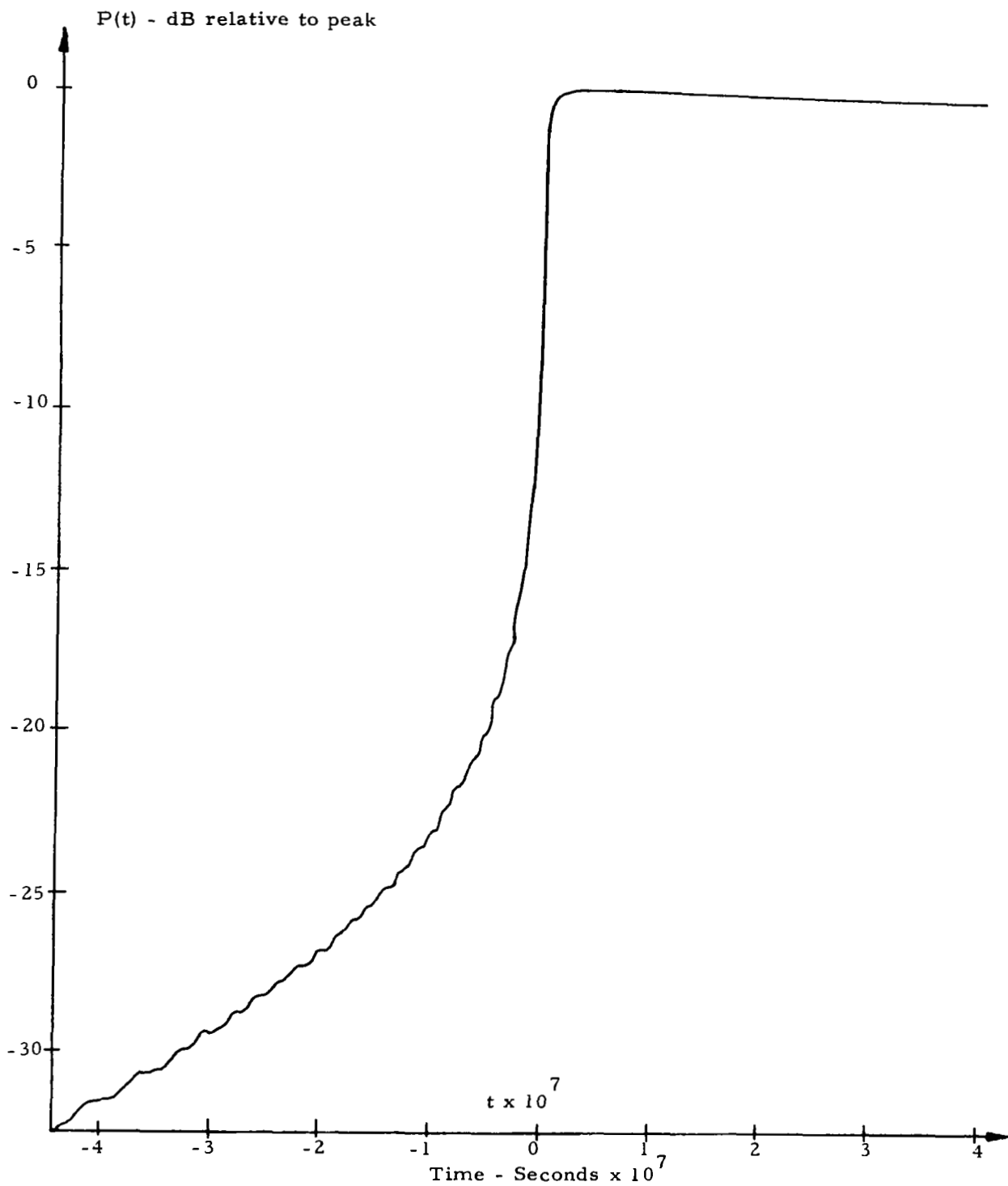
Figure H-1. P(t) for Unweighted Chirp, $T=10^{-6}$, $B=10^8$

is shown in Figure H-2. The time origin in both cases is located at B^{-1} seconds after the first return would be received from a perfectly flat sea. Figure H-3 shows the first and second differences of the P(t) curve of Figure H-1. The first difference at time t* was calculated from samples of P(t) taken at $t* \pm \frac{1}{2B}$, and the second difference from samples taken at t* and $t* \pm \frac{1}{2B}$. Figure H-4 is similarly related to Figure H-2.

Note that in both cases the second difference is zero essentially at t = 0 (i. e., at B^{-1} seconds after the first return from a flat sea) indicating effectively zero range error bias. In this regard it is important to stress that the matched filtering results in an output point target response of total width $2B^{-1}$. This makes the zero of the second difference of the deep target response occur at $t = B^{-1}$, so that one should extrapolate back B^{-1} seconds from the zero crossing in order to estimate the target range. This differs from the backward extrapolation by only half a pulsewidth that one would employ for a simple pulse and an infinitely wideband receiver as discussed in [13]. In general, the effect of the receiver response must be carefully considered when determining how far back from the zero crossing of the second difference one should extrapolate when estimating the time of the first return from a flat sea.

We see from Figure H-3 that spurious zeros of the second difference occur fairly near the origin for an unweighted pulse. The proper zero crossing is easily recognized, however, by the requirement that the first difference must simultaneously exceed an appropriate threshold. From Figures H-2 and H-4 it is clear that Taylor weighting results in markedly lower integrated sidelobes, smoother first and second differences, and no ambiguous zero crossings of the second derivative. The vertical scales of Figures H-2 and H-4 were adjusted for equal peak transmitted power in order to permit meaningful comparison of the sensitivity of the zero crossing time to noise and clutter both with and without weighting. The slope of
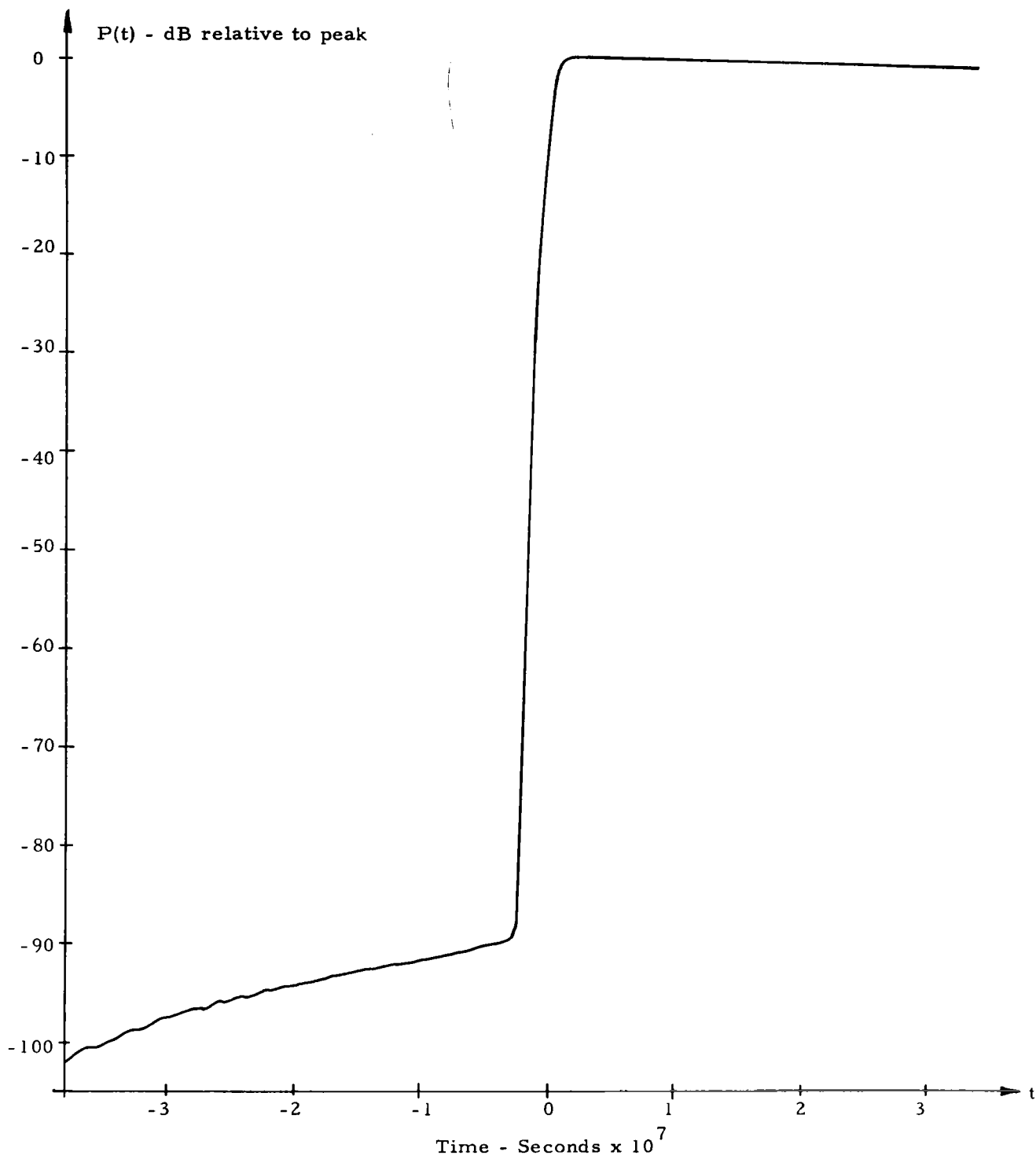
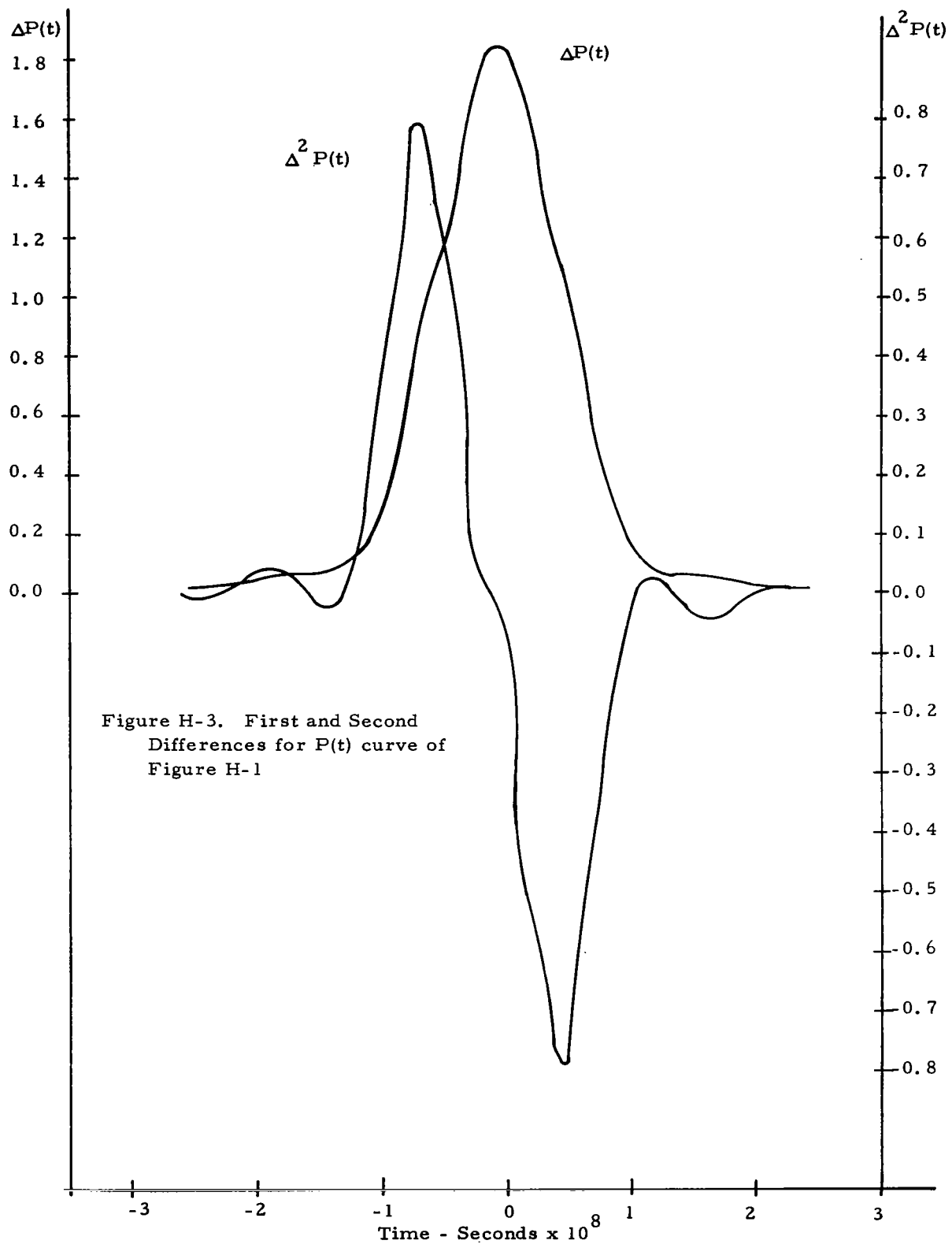Figure H-2. P(t) for 35 dB Taylor-weighted chirp, $T-10^{-6}$, $B=10^8$

Figure H-3. First and Second
Differences for P(t) curve of
Figure H-1
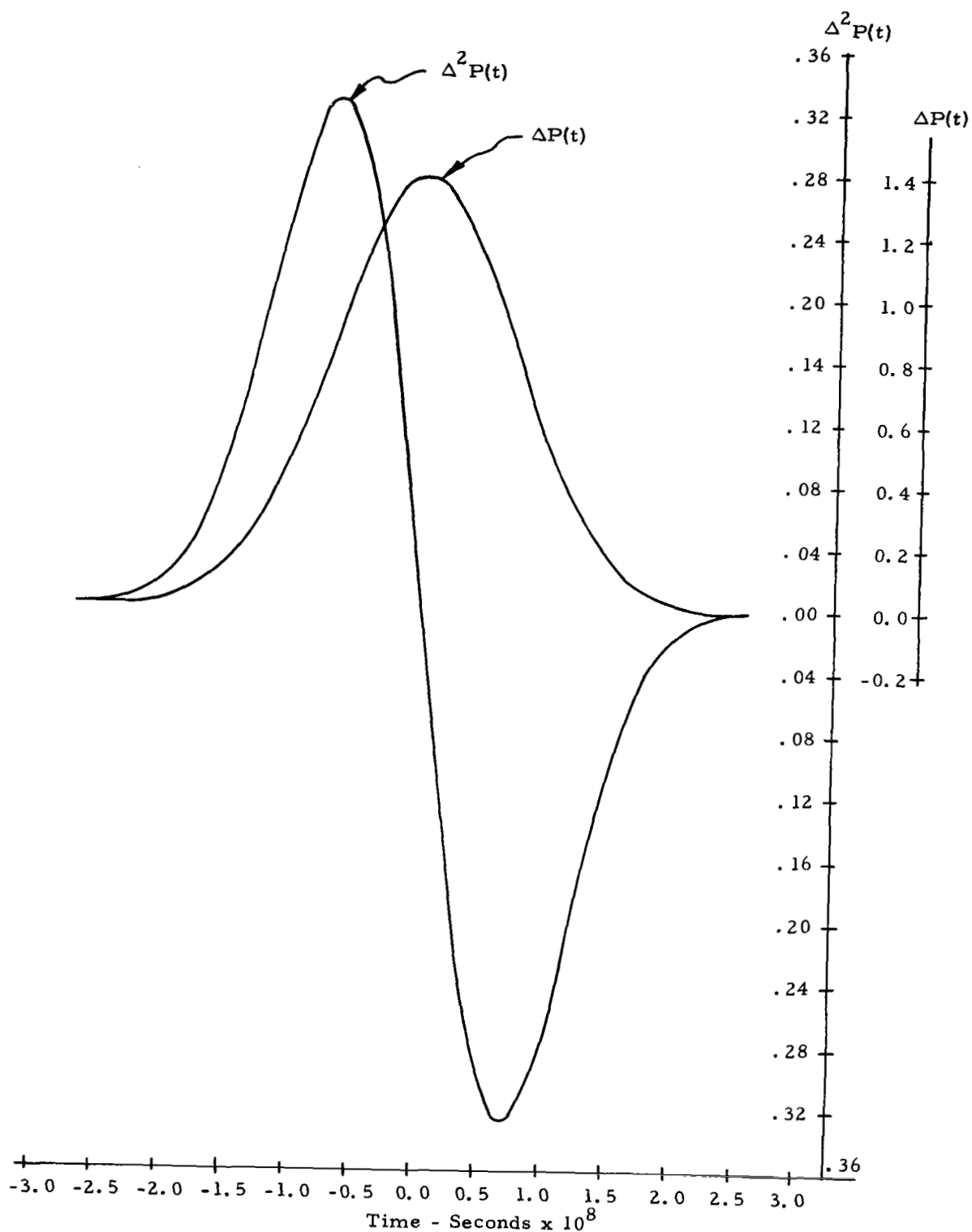
Figure H-4. First and Second Differences for P(t) curve of Figure H-2

the second difference was found to be about 2 times greater with the weighting than without, suggesting an improvement in range accuracy by roughly the same factor.

H-4. Some Practical Considerations

There are several factors that were not considered above that affect $P(t)$ in practice. One of these is that the transmitting and receiving filters generally are not perfectly matched. Both phase mismatch and amplitude mismatch prevail in most instances. If only amplitude mismatch is significant, then (17) gets replaced by

$$P(t) = \pi \int_0^\infty d\tau \, F(\tau) \left| \int_{-T/2}^{T/2} du \, a_1(u) \, a_2(u-t+\tau) \, e^{j2\pi k(t-\tau)u} \right|^2 \tag{H-18}$$

where $a_1(t)$ and $a_2(t)$ are the transmitter amplitude weighting and the envelope of the complex impulse response of the receiver, respectively. Phase mismatch imposes further modifications that will not be considered here.

If the antenna is not pointing directly vertically, then a slightly different form of $P(t)$ results. Formula (3) and simplifications thereof where applicable still apply provided one adjusts the scattering function to account for nonvertical incidence. Departure of the satellite attitude from the horizontal is handled similarly. To account for sea state it is necessary to consider the return signal as a random process and to analyze it accordingly. An attempt at such an analysis may be found in [32].

Finally, it should be pointed out that this analysis has not provided any direct assessment of the relationship between the form of $P(t)$ and the range accuracy achieved by the system. Naturally, the details of this relationship depend on the particular form of range estimator employed, e. g. , three-gate leading edge detection, matched filtering, etc. Roughly speaking, though, the most critical factor for range estimation purposes is the ratio, call it β, of the slope of the second derivative of $P(t)$ at the zero crossing to the RMS power of the second derivative of the noise out of the dechirp filter. However, it should be remembered that the range accuracy attainable with a single received pulse is limited principally by clutter (i. e. , Rayleigh fading), and not by the form of $P(t)$. The form of $P(t)$ will become the limiting factor only if enough pulses with independent clutter can be averaged to make the signal-to-clutter ratio greater than β .

REFERENCES

1.   Marcum, J. I., "A Statistical Theory of Target Detection
      by Pulsed Radar, " IRE, Vol. IT-6, No. 2, April 1960

2.   Frey, Harrington, and Von Arx, " A Study of Satellite
      Altimetry for Geophysical and Oceanographic Measure-
      ment"

3.   Barton, D., "Radar System Analysis, " Prentice-Hall
      Inc., 1965, Chapt. 15

4.   Handbook of Geophysics, Chapt. 9

5.   Thayer, G. D., Atmospheric Effects on Multiple Frequency
      Range Measurements ESSA Technical Report IER-56-ITSA 53

6.   Berkowitz, R. S., Modern Radar, Wiley, pp 368 -369

7.   Elliott, R. S., "Pulse Waveform Degradation due to
      Despersion in a Wave Guide, " IRE Trans., MTT-5
      October 1967, pp 254 - 257

8.   Trancell, R. H., Schulz, M. B., Barrett, H. H., Davis, L., Jr.,
      and Holland, M. G., "Dispersive Delay Lines Using Ultrasonic
      Surface Waves, " Proc IEEE, Vol. 57, page 1211, 1969.

9.   Cook, C. E. and Bernfeld, M., Radar Signals, Academic Press,
      New York, 1967

10.   Goblick, T. J., Jr., Multiple measurement ranging systems
      approximate theoretically ideal performance.   Presented
      at IEEE International Symposium on Information Theory,
      Ellenville, N. Y., January 1969.   Submitted to IEEE Trans-
      actions on Information Theory

11.   Shannon, C. E., Coding theorems for a discrete source
      with a distortion measure. Information and Decision Pro-
      cesses, edited by R. E. Machol, McGraw-Hill: New York,
      1060, pp. 93-126.

REFERENCES (Cont'd.)

12. Shannon, C.E. and Weaver, W.W., The Mathematical Theory of Communication. Univ. of Illinois Press: Urbana, Ill., 1949

13. Raytheon Company, Space Geodesy Altimetry Study NASA Contract NASW-1709, NASA CR-1298, March 1969

14. Helstrom, C.W., Statistical Theory of Signal Detection, Section VIII. 2, Pergamon Press: London, 1960

15. Price, R.and Green, P.E., Jr., Signal processing in radar astronomy--communication via fluctuating multipath media, Lincoln Laboratory, MIT, Tech. Rept. 234, DDC No. 246782 (1960)

16. Price, R., and Green, P.E., Jr., Chapters 1 and 10 of Radar Astronomy, edited by John V. Evans, McGraw-Hill: New York, 1968

17. Gallager, R.G., Information Theory and Reliable Communication, Wiley: New York, 1968

18. Collins, J.H., Gerard, H.M., and Shaw, H.J., "High performance lithium niobate acoustic surface wave transducers and delay lines," Appl. Phys. Lett., Vol. 13, pp 312-313, November 1968 and references therein

19. Rowen, J.H., U.S. Patent 3-289-114, November 29, 1966

20. Klauder, J.R., Price, A.C., Darlington, S., and Albersheim, "The Theory and design of chirp radars," Bell Sys. Tech. J., Vol. 39, pp 745-808, July 1960

21. Sittig, E.K., and Coquin, G.A., "Filters and dispersive delay lines using repetitively mismatched ultrasonic transmission lines," IEEE Trans. Sonics and Ultrasonics, Vol. SU-15, pp 111-119, April 1968

REFERENCES (Cont'd.)

22. Tseng, C. C., "Frequency response of an interdigital transducer for excitation of surface elastic waves, " IEEE Trans. Electron Devices, Vol. ED-15, pp 589-594, August 1968

23. Langer, R, B., Isodops and isodels for satellite radar altimetry system. Raytheon Technical Memo RBL-4, July 22, 1969

24. Sterger, Fred, "Progress in Solid State Microwave Power Sources, " IEEE Transactions on Microwave Theory and Techniques, Vol. MTT-13, No. 6, November 1965

25. Johnson, E. O., "Physical Limitations on Frequency and Power Parameters of Transistors, " RCA Review, June 1965

26. William Crowe and John Sie, "The Use of Avalanche Diodes in an Amplifying Mode to Increase Source Output Power, " The Microwave Journal, February 1969

27. Kennedy, W. K., Jr., and Eastman, L. F., "High Power Pulsed LSA Devices, " MEREM Record, 1967

28. P. E. Green, Jr., Chapter 1 of Radar Astronomy, edited by J. V. Evans, McGraw-Hill, New York, 1968.

29. A. W. Rihaczek, Principles of High Resolution Radar, Chapter 9, McGraw-Hill, New York, 1969.

30. T. Berger, Theoretical Accuracy Limits for Satellite Altimetry, Raytheon Tech. Memo TB-96, 21 July 1969.

31. T. T. Taylor, Design of Line Source Antennas for Narrow Beamwidth and Low Side Lobes, IRE Trans. on Antennas and Propagation, Vol. AP-3, January 1955, pp. 16-28

32. T. Berger, "A Theory of Ocean Backscatter of Radar Pulses," Raytheon Technical Memo TB-98, August 1969.